Supernovae with IceCube: Direction and Average Neutrino Energy Determination

Dissertation
zur Erlangung des Grades
«Doktor der Naturwissenschaften»
am Fachbereich Physik, Mathematik und Informatik
der Johannes Gutenberg-Universität
in Mainz

Benjamin Eberhardt
geb. in Mainz

Mainz, den 12.07.2017

Supernovae with IceCube:
Direction and Average Neutrino Energy Determination

Dissertation

Tag der Einreichung: 12.07.2017
Tag der mündlichen Prüfung: 27.10.2017

Benjamin Eberhardt
Johannes Gutenberg-Universität (D77)
Institut für Physik / ETAP
Staudingerweg 7
D-55128 Mainz
eberhabe@uni-mainz.de

Abstract

Supernovae explosions are among the most powerful events known to occur in the universe. They are also to date the only known source of extrasolar neutrinos. Observing such an explosion in the neutrino sector would provide valuable information about the explosion mechanism of the star, as well as properties of the neutrino.

The IceCube neutrino telescope monitors the Antarctic glacier for neutrino induced Cherenkov photons. Even though it was designed to detect high energy neutrinos, IceCube can detect large numbers of MeV neutrinos by observing a collective rise in all photomultiplier rates. This feature enables IceCube to detect outbursts of neutrinos from core collapse supernovae within the Milky Way.

In case of a supernova in the centre of the galaxy, IceCube would be able to provide the highest statistics of all experiments world-wide, recording $\approx$40.000 times more neutrino events than recorded for the last observed supernova in 1987. The collective photomultiplier rate, however does not carry information about single neutrinos making it e.g. impossible to determine the energy and direction. Part of this thesis was dedicated to developing new methods to remedy this situation.

In the course of this thesis, major contributions have been made to extend the functionality, increase the reliability and to improve the monitoring of the data acquisition system to detect core collapse supernovae. A newly introduced storage system of all recorded photons for an adjustable time in case of an alert opened new analysis opportunities.

The passage of the neutrino wave front through the detector can in principle be monitored by triangulation even in the presence of a dark rate background, whenever the flux changes abruptly. This is, e.g., the case for large progenitor stars that end up in a black hole, shutting down the neutrino flux almost instantaneously. By using a proper likelihood description, a method has been developed that estimates the supernova direction with 20 degree uncertainty, if the effect of neutrino masses can be neglected and the flux ceases sufficiently fast at the time of black hole formation.

The coincidence probability for observing Cherenkov light from $\mathcal{O}(10\,\mathrm{cm})$ long positron tracks in the 17 m spaced light sensors lies only in the percent range. Nevertheless, given the large signal on top of the background, one can estimate the fraction of coincidences and thus determine the average neutrino energy.

Contents

Introduction

In the first chapter a general overview of the relatively new field of neutrino astronomy will be given as well as the detection method of low energy supernova neutrinos in IceCube. An introduction of supernovae will mainly focus on type-II core collapse supernovae which are detectable by IceCube and highlight two different development possibilities for the star to result in a black hole. We conclude with a discussion of the expected total rate of supernovae in the galaxy and the fraction wich produces a black hole as the final state. Chapter two presents a brief overview of IceCube and its construction. Different neutrino signatures and background sources are being discussed. A description of the technical components of IceCube is followed by an overview of other current and future neutrino detectors.

The major part of this work is detailed in chapter 3. Many technical improvements have been implemented into IceCube's supernova data aquisition system (SnDaq) in the course of this work, mainly concerned with automatic and manual data quality control, data acquisition uptime, and information delay. SnDaq's logging mechanism has been rebuilt and the software has been integrated into a global control and monitoring system named IceCubeLive, thus improving its usability by detector operators and winter personnel. Physics data and status-information are being automatically categorized on site and transmitted via different satellite systems, thus decreasing the overall delay times bewteen the South Pole and experts in the collaborating institutes. Hereby realising alert transimission to a world wide, inter experiment supernova early warning system, as well as sms notifications, both within a matter of seconds. Other new features are a more robust handling of corruption errors in data and timestamps as well as support for leap seconds when converting from detector internal timestamping into UTC. Most importantly, a new data aquisition component, the hitspooling system[1], was connected to the SnDaq system in order to produce high time resolution datasets in case of a supernova alert.

The analysis chapter 4 is based on noise datasets being harvested with the hitspooling system, combined with simulated signal data produced with a new supernova simulation framework. The combination of these newly developed, high-resolution datasources opens up new analysis opportunities in the previously inaccessible sub millisecond regime of individual hit time differences. The use of real noise data from the detector minimizes the overall systematical error which is forcibly intruduced by simulation. We attempt to reconstruct the direction of a black hole forming supernova based on triangulation of its rapidly decreasing neutrino signal inside IceCube's very large volume. The possibility of measuring the average energy of the supernova neutrinos is explored by analysing coincident hit patterns in the $\mathcal{O}(10\text{ ns})$ regime.

Chapter 1

Theory

This chapter covers the essential theoretical background for this thesis. It introduces the neutrios in the Standard Model of particle physics as well as in the context of astronomy. The main focus is put on supernova explosions, the role of the neutrinos during the explosion and their detection with IceCube. The chapter concludes with an overview of past supernova explosions in the Milky Way and their expected rate.

1.1 Neutrinos in the Standard Model

The Standard Model of particle physics describes the interactions of elementary particles. There are twelve elementary particles, called fermions, three of which are the neutrinos. They have a low mass, are chargeless and interact weakly. A graphical representation of the standard model particles is show in Fig. 1.1.

Interactions between particles are mediated by vector bosons which correspond to the generators of the local symmetry groups SU (3) $\otimes$ SU (2) $\otimes$ U (1), the basis of the Standard Model. The former describing the strong force with eight generators, the gluons and the latter two describing electroweak interactions with four generators in total, two charged ($W^{\pm}$) and two uncharged (Z^0 and γ).

The uncharged photon γ, mediator of the electromagnetic force, does not carry mass and is therefore unlimited in reach. The weak force can only be carried over a relatively short distance by the heavy bosons $W^{\pm}$ and Z^0 and therefore effectively appears weak. The gluon, mediator of the strong force, is again massless but carries strong color charge which enables it to interact with other gluons. This restricts the reach of the strong force to the order of the size of a nucleus. The relative strengths of electromagnetic- weak- and strong-force are $10^{-2} : 10^{-5} : 1$. With a relative strength of 10^{-38} gravity does not play a role in the interaction of fundamental particles.

Due to their chargeless and weakly interacting nature, neutrinos offer new disovery opportunities in astronomy. They might help to prove the existence of massive weakly interacting dark matter particles or deliver information from within the core regions of exploding stars, hence giving insight into the explosion process.

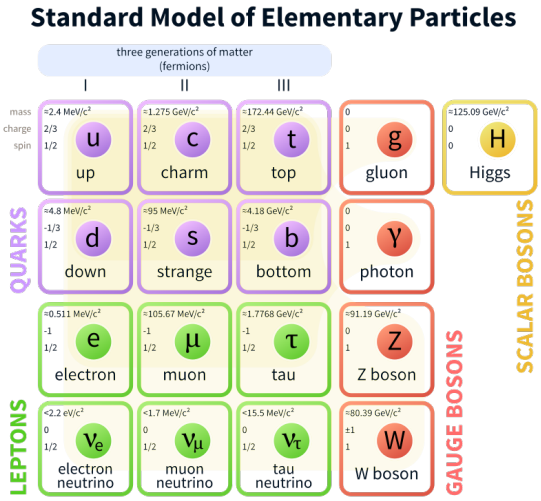

Figure 1.1: The Standard Model of particle physics including the 12 fermions and the force mediating bosons. The fermions are arranged in three families with one neutrino belonging to each. Figure taken from [2].

1.2 Neutrino astronomy

Whenever astronomy explored new regions of the electromagnetic spectrum, spanning 18 orders of magnitude in wavelength from radio-waves to GeV gamma rays, plenty of new discoveries were made. The observed photon spectrum of conventional astronomy extends to energies in excess of 10 TeV, perhaps as high as 50 TeV [3]. When looking into options for additional messengers from the Universe beyond the electromagnetic spectrum, few usable options remain. The majority of Standard Model particles (or their composits) which arrive on earth are charged and therefore affected by interstellar magnetic fields. It is therefore impossible to determine the source of these cosmic rays except at very high energies exceeding 100 EeV. At such energies, their gyroradii exceed the size of our galaxy. The energy range in between had been left unexplored before the neutrino astronomy was established.

As illustrated in Fig. 1.2, neutrinos are not charged and thus not affected by magnetic fields. As they only interact weakly with other matter, they are also able to travel through interstellar dust clouds and other obstructions. This makes them ideal messengers to be used in astronomy and to explore new energy regions. The energy spectrum of cosmic neutrino fluxes is shown in Fig. 1.3.

The neutrino's small crossection with matter makes it necessary to compensate with a large detector volume in order to achive an acceptable detection rate and to contain high energetic events [6]. IceCube is the largest neutrino detector to date, instrumenting a volume of 1 km^3 with ≈5000 optical sensors. After the first discovery of high energetic cosmic neutrinos in 2013 [7] a 10 km^3 extension called IceCube-Gen2 has been proposed [8] which would enable to indentify the respective sources.

A review of the energy dependent neutrino-matter cross sections from sub-eV to EeV is given in [9]. This cross section can be translated into an in-

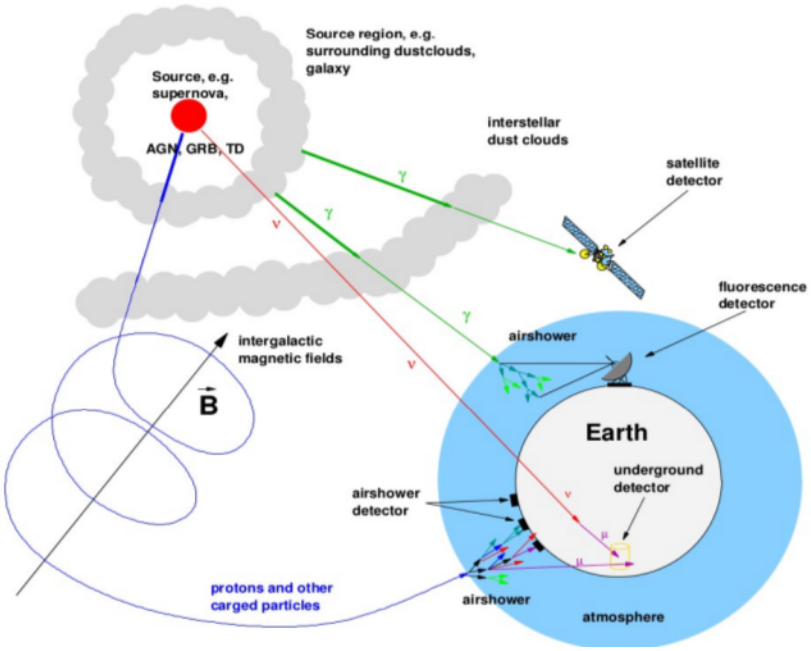

Figure 1.2: Schematic overview of common cosmic messengers and their propagation. Neutrinos offer certain advantages as they are not deflected by cosmic magnetic fields or absorbed by dust clouds. During supernova explosions, they transport information from inside the star. The Figure was taken from [4] and also illustrates typical detector locations as well as the neutrino production in the atmosphere which produces background events.

teraction length [10]. Neutrinos as high energetic as 1 TeV would on average travel through 2.5 million kilometers of water before interacting. The interaction length becomes of the order of earths diameter only for neutrinos with energies exceeding 100 TeV. In this thesis, however, we will concentrate on MeV neutrinos, whose interaction cross section, which will be described in the next section, is much smaller.

1.3 Neutrino detection in IceCube

Due to the low energy of supernova neutrinos, secondary particles heavier than electrons or positrons cannot be produced. The dominant effect in water is the inverse beta decay which is responsible for >90% of the total rate:

$$\bar{\nu_e} + p \rightarrow n + e^+. \tag{1.1}$$

Further reaction channels involve electron scattering as well as reactions with the oxygen nucleus. They each participate to the total rate with about 1%. A detailed overview of all reaction channels is given in [12] Tab. 1. and is presented in Fig. 1.4. The angular distribution of the reaction products is almost uniform in the regime of MeV neutrinos. They are producing very localized, spherical

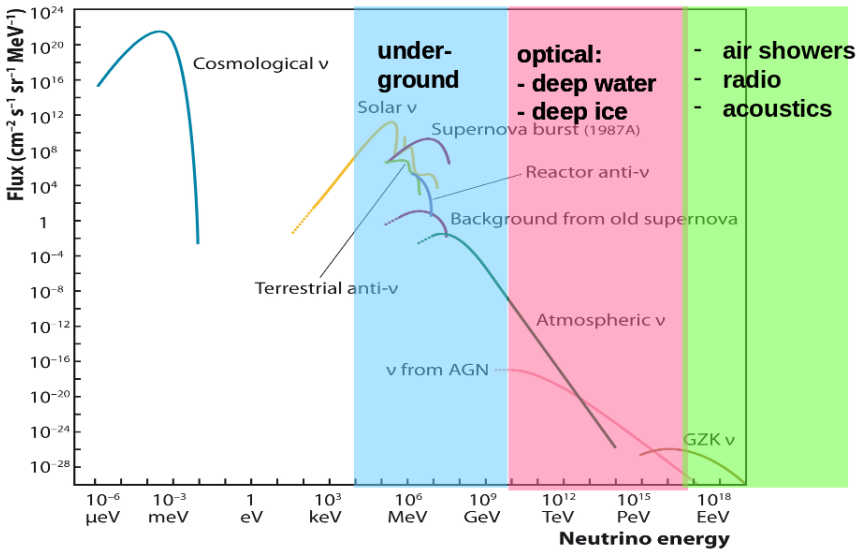

Figure 1.3: Fluxes of cosmic neutrinos covering more than 24 orders of magnitude and corresponding detection technologies. Low energy ($\mathcal{O}$(MeV)) neutrinos are mainly detected in underground laboratories which are entirely human built and shielded by rock. For higher energies, as the interaction events extend to larger dimensions and occur less often, the approach is to instrument large volumes of natural transparent medium such as ice or water. The detection mechanism is outlined in the next section. Neutrinos with $\mathcal{O}$(keV) energies or smaller are currently undetectable. The figure was taken from [5] with detection technologies added.

light depositions in IceCube which do not allow for a directional resolution of single neutrino events.

The energy dependent neutrino cross section for the inverse beta decay is given in [13], which also provides a simplified approximation for neutrino energies <300 MeV with an uncertainty smaller than 1%

$$\sigma(E_\nu, E_e) = 10^{-47} |\vec{p}_e| E_e E_\nu^{-0.07+0.02 \ln E_\nu - 0.002 \ln^3 E_\nu} m^2 \quad . \tag{1.2}$$

The proportionality on E^2 as well as the lower reaction threshold

$$m_e + m_n - m_p = 1.806\text{MeV} \tag{1.3}$$

are responsible for the large contribution of the inverse beta decay to the total supernova signal. The differential form of the cross section is needed to derive the detection rate

$$\frac{\mathrm{d}}{\mathrm{d}E_e}\sigma(E_\nu, E_e) = \sigma(E_\nu, E_e)\delta(E_e - \langle E_e \rangle) \quad . \tag{1.4}$$

The detection of the neutrino happens indirectly via its charged reaction products. Charged particles, exceeding the speed of light native to the detector medium, will emit Cherenkov light along their trajetory until energy loss effects slow them down below the threshold speed. Photomultipliers, which have been

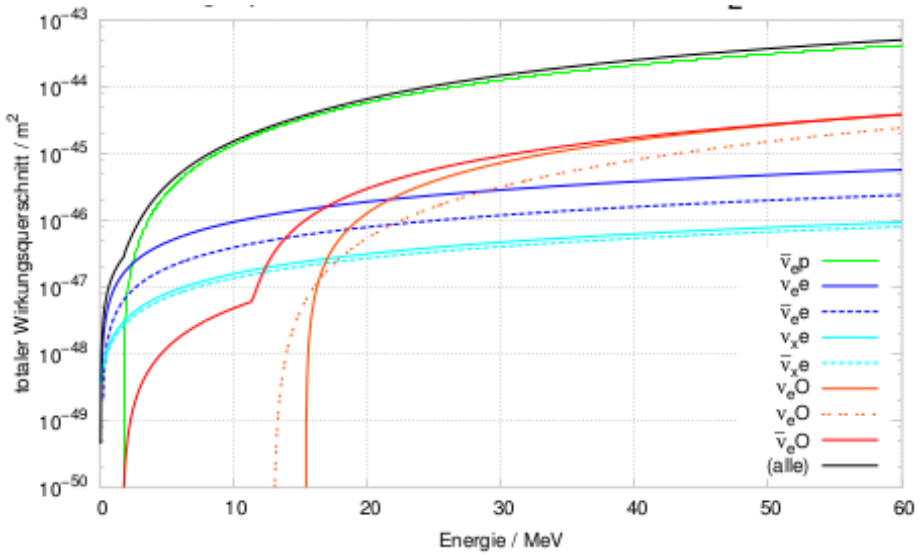

Figure 1.4: Comparison of all neutrino cross sections with the H_2O-molecule [11] (Fig. 1.2). The main contribution comes from inverse beta decay mainly because of its proportionality to E^2. The natural isotope composition of oxygen is also considered. It causes a shoulder in the ν_e-reactions at lower energies as the reaction threshold energy is lower for ^{18}O than for the more abundant ^{16}O.

lowered into the ice, are used to detect the arrival time and number of the Cherenkov photons.

For $\mathcal{O}$(MeV) leptons travelling through the ice, the dominant energy loss mechanism is ionisation. The leptons (only $e^{\pm}$ are produced) elastically collide with electrons of the water molecules. Bremsstrahlung on the molecules' Coulomb field becomes linearly more important with increasing energy [14]. Allthough relativistic pair production is possible based on the bremsstrahlung, the majority of the detected photons originate from the Tscherenkov effect. The number of detected photons therefore mainly depends on the duration of time the lepton is travelling the detector medium above the threshold speed. Based on the two dominant energy loss mechanisms, the corresponding average track length has been determined in simulations [15]. Assuming $E_e < 100$ MeV it increases linearly with energy:

$$\bar{x}(E_e) = (0.579 \pm 0.017)\text{cm} \cdot E_e/\text{MeV} \quad . \tag{1.5}$$

1.4 Neutrino mixing

The three known neutrinos, each of which belong to a specific lepton generation are ν_e, ν_μ and ν_τ. They are partners of the charged leptons in charged current reactions like the beta decay. The neutrinos travel in their mass eigenstates ν_1, ν_2 and ν_3 according to their masses. Unlike the leptons, neutrinos can only be detected indirectly in weak interaction processes and always carry the flavour of their leptonic reaction partner. It is therefore not necessary that neutrinos

of a specific flavour also carry a specific mass. This implies that the individual neutrino flavour eigenstates are a linear combination of the three available mass eigenstates:

$$|\nu_\alpha\rangle = \sum_i U^*_{\alpha i} |\nu_i\rangle \,, \tag{1.6}$$

where $U^*_{\alpha i}$ is the PMNS-matrix element which describes the translation between flavour and mass eigenstates. This matrix works in analogy to the CKM matrix in the quark sector. It was introduced in 1962 by Ziro Maki, Masami Nakagawa and Shoichi Sakata, to explain the neutrino oscillations predicted by Bruno Pontecorvo and it is commonly named after all of them. The translation is a rotation based on three Euler angles and one phase angle and can e.g. be written as:

$$U = \begin{pmatrix} 1 & 0 & 0 \\ 0 & c_{23} & s_{23} \\ 0 & -s_{23} & c_{23} \end{pmatrix} \begin{pmatrix} c_{13} & 0 & s_{13}e^{-i\delta} \\ 0 & 1 & 0 \\ -s_{13}e^{i\delta} & 0 & c_{13} \end{pmatrix} \begin{pmatrix} c_{12} & s_{12} & 0 \\ -s_{12} & c_{12} & 0 \\ 0 & 0 & 1 \end{pmatrix} \quad . \tag{1.7}$$

The abbreviations c_{ij} and s_{ij} stand for $\cos\theta_{ij}$ and $\sin\theta_{ij}$, respectively.

1.4.1 Vacuum oscillation

When propagating through empty space, the time development of the neutrino mass eigenstates can be obtained by applying the Hamilton operator. The phase of the oscillation depends on the travelling time and the neutrino's mass and energy as follows [11]:

$$L_{ij} = \frac{4\pi E}{\Delta m^2_{ij}} \approx 2.48\text{m} \frac{E}{\text{MeV}} \frac{\Delta m^2_{ij}}{\text{eV}^2} \quad . \tag{1.8}$$

The width of the energy spectrum of the emitted neutrinos smears the oscillation length L_{ij} which leads to a reduction of the oscillation amplitude. As the distance of a supernova can be assumed to be much larger than the oscillation length, the oscillation probability converges, time averaged, to:

$$\bar{P}(\nu_\alpha \to \nu_\beta) = \sum_i |U_{\alpha i}|^2 |U_{\beta i}|^2 \quad . \tag{1.9}$$

This leads to the following survival probabilities per lepton flavour:

$$\bar{P}(\nu_e \to \nu_e) = 53.8\%, \bar{P}(\nu_\mu \to \nu_\mu) = 40.3\%, \bar{P}(\nu_\tau \to \nu_\tau) = 43.0\% \quad . \tag{1.10}$$

1.4.2 Matter oscillation

When moving through matter, neutrinos experience an effective potential due to scattering effects with electrons and nucleons which significantly modifies the oscillation phenomena. This behaviour is called the *MSW-Effect* after Mikhejew, Smirnow und Wolfenstein and has been a key factor in explaning the solar neutrino problem [16]. Due to the absence of muon and tau leptons in normal

matter the effective potential can be described [17] for the electron density n_e as:

$$V_{\text{eff}} = \pm\sqrt{2}G_F n_e \quad , \tag{1.11}$$

where G_F is the Fermi-constant and the potential is positive for electron neutrinos and negative for its anti neutrino. Electron- and anti-electron neutrinos have a higher cross section, their mass eigenstates become "heavier", so that the may reach the same mass or even exceed the mass of heavier neutrinos. If the density changes slowly (i.e. adiabatically), particles can "flip" completely into a different mass eigenstate. A two neutrino case is considered. With $\Delta m^2 \approx \Delta m^2_{21}$ and $\theta \approx \theta_{12}$, the oscillation length in matter modifies to

$$L_m = \frac{4\pi E}{\Delta m^2} = \frac{L}{\sqrt{(\xi - \cos 2\theta)^2 + \sin^2 2\theta}} \quad , \tag{1.12}$$

to simplify the discussion, where

$$\xi := \frac{2EV_{eff}}{\Delta m^2} \tag{1.13}$$

is a local density parameter. It can be seen that, depending on the size of the star, up to two resonances exist in matter for $\xi = \cos 2\theta$, which correspond to a density of

$$\rho_{\text{res}} = \frac{\Delta m^2 \cos 2\theta}{2\sqrt{2}G_F E} \quad . \tag{1.14}$$

In analogy to the vacuum oscillations, a modified mixing matrix translates between flavour and mass eigenstates. The mixing angle and mass difference are replaced by θ_m and Δm_m, which are the respective effective and position dependent values in matter. If a constant electron density n_e can be assumed along the trajectory of the neutrino, the two-neutrino flavor transition probability in matter is given by

$$P(\nu_\alpha \to \nu_\beta; x) = \sin^2 2\theta_m \sin^2\left(\frac{\Delta m^2_m x}{4E}\right) \quad . \tag{1.15}$$

A constant n_e can be assumed for neutrinos crossing the earth's mantle [18]. In stellar matter the density profile is inhomogenious, which leads to a transition probability of the form [11]:

$$P(\nu_e \to \nu_\mu; x) = \frac{1}{2} - \frac{1}{2}\cos 2\theta_c \cos 2\theta_m + P(\nu_1 \to \nu_2; x)\cos 2\theta_c \cos 2\theta_m \quad , \tag{1.16}$$

where θ_c stands for the mixing angle for neutrinos produced at $x = 0$, the center of the star. It can be seen that in case of a non-homogeneous density profile even the mass eigenstates can mix. Considering the mass effects at production and detection site, the total survival probability per neutrino flavour can be derived.

1.5 Supernovae

Supernovae [19] are spectacular explosions, accompanying the death of a massive star. They are among the most brightest and most energetic events in the universe. There are different types of supernovae which will be mentioned in this chapter. Two distinct mechanisms, thermonuclear and gravitational core collapse, have been identified to date as cause for supernova explosions. Both types are interesting for cosmology, astro- and particle physics for different reasons and will be discussed. The most interesting for this thesis is the core collapse supernova which is caused when the star has used all the nuclear power in its core and it collapses due to its mass with no radiation pressure left. When this happens, huge amounts of gravitational binding energy are released, almost all of it in the form of neutrinos. This makes galactic core collapse supernovae ideal events to be studied with neutrino telescopes. Even though only a small fraction of the energy is released in the electromagnetic spectrum, the exploding star can reach very high apparent magnitutes in the sky, outshining whole galaxies.

The first and only observation of such an event in the neutrino sector happened in 1987, when the blue supergiant *Sanduleak* in the Large Magellanic Cloud[1] exploded, marking it the beginning of neutrino astronomy. Allthough very common in the universe, supernovae are quite rare within our single galaxy. Numbers are estimated to range between one and three events per century, making it necessary to be well prepared and to monitor the sky around the clock.

1.5.1 Star formation and burning stages

Astronomical observations indicate [20] that stars are born in giant molecular clouds extending their dimensions up to several light years. This so called interstellar medium (ISM) mainly consists of molecular hydrogen H_2 and helium. It is possible for such a cloud to collapse, if its gravitational energy exceeds the thermal energy of its constituents. The criterion for this collapse to happen depends on a minimal total mass and is parameterized in the so-called Jeans criterion:

$$M \geq \frac{2kTR}{G\bar{\mu}m_H} \quad . \tag{1.17}$$

Here, $\bar{\mu}$ is the average atomic mass number of the cloud, T the temperature, R the radius, k the Boltzmann-constant and G the gravitational-constant. It can be seen that low temperatures and a low spatial spread of the cloud favour collapse. One possibility to trigger a collapse could be the shock wave of a former explosion [21] which could lead to a compression of the ISM above the critical density.

While the cloud collapses, density and pressure in its interiour increase. At a density of $\rho \approx 10^{-13}$g cm^{-3}, the cloud becomes opaque to photons and the potential contraction energy can no longer be cooled off via radiation. The compression becomes adiabatic and the temperature inside the cloud rises which in turn slows down the collapse. At this point, a so-called *proto-star* has formed which continously accretes matter from the surrounding ISM. At a temperature of 1800 K, the molecular hydrogen starts to dissociate. As this process costs

[1] The LMC is a dwarf galaxy orbiting the Milky Way

energy, the collapse accelerates again until the dissociation is complete and the collapse comes to another halt. Continous matter accretion leads to a further increase in density and temperature. At approximately 6000 K the hydrogen atoms start to ionize and the collapse contiues until all atomic hydrogen is dissociated and the so-called *young stellar object* (YSO) is in hydrostatic equilibrium. The YSO accretes additional matter over the next millions of years until the core temperature exceeds $3.5 \cdot 10^7$ K which is enough for hydrogen to fuse into helium.

Hydrogen burning starts as the first burning stage of the newborn star. Its life is then dominated by an equilibrium between the inward gravitational pressure and the outward thermal pressure which is given by the virial theorem:

$$\langle E_{kin} \rangle = -\frac{1}{2} \langle E_G \rangle \quad , \tag{1.18}$$

where $\langle E_{kin} \rangle$ and $\langle E_G \rangle$ are the average kinetic and gravitational energy for one atom in the star. If the star contracts, $\langle E_G \rangle$ will get more negative increasing $\langle E_{kin} \rangle$ on the other hand.

The star looses energy by emitting photons and neutrinos. To compensate for this loss, the star burns an equivalent amount of fuel in order to keep its equilibrium. When the hydrogen fuel is depleted in the now helium dominated core, the fusion stops. The star contracts until pressure and temperature are again high enough to start the helium burning at around 10^8 K. During the helium burning stage, the so-called triple-α-process fuses three ^{4}He into ^{12}C. Due to the high temperature gradient, the hydrogen fusion process continues in the separated surrounding layer. If the star is relatively light, such as our sun, this is the last burning stage that reacts. If the helium is exhausted, fusion stops and the star collapses into a so-called white dwarf.

The mass of a star mainly determines its fate. Three examples of star development based on different initial masses are shown in Fig. 1.5 (right). Other factors, like the mass ratio of hydrogen and helium to heavier elements (the so-called metallicity of the star) can also affect the development [23].

If the mass of the star exceeds eight solar masses, it can produce heavier elements from the ashes of the previous burning stages [24]. This chain of successive burning stages can not continue indefinitely, however. As the core gets denser and hotter, the reaction rate increases and burns more and more fuel in shorter times. Electron neutrinos continue to carry away energy and the energy gain per fusion reaction decreases until the last burning stage produces elements of the iron group. These elements have the highest binding energy per nucleus thus fusion towards heavier elements would *cost* energy and is therefore disfavoured. All nuclear fusion stops and the star collapses due to its own gravity. The following compression leads to a core collapse supernova.

1.5.2 Supernova classification

The supernova classification is historically based on a spectral analysis of the light curve near maximum luminosity. The spectral features can be linked to a physical explosion process. The main feature are the identification of hydrogen spectral lines (Type II) or their absence (Type I) [25]. Type II supernovae are gravitational core collapse supernovae (CCSN) which will be discussed further in the next section. Type I supernovae can be further separated into subgroups.

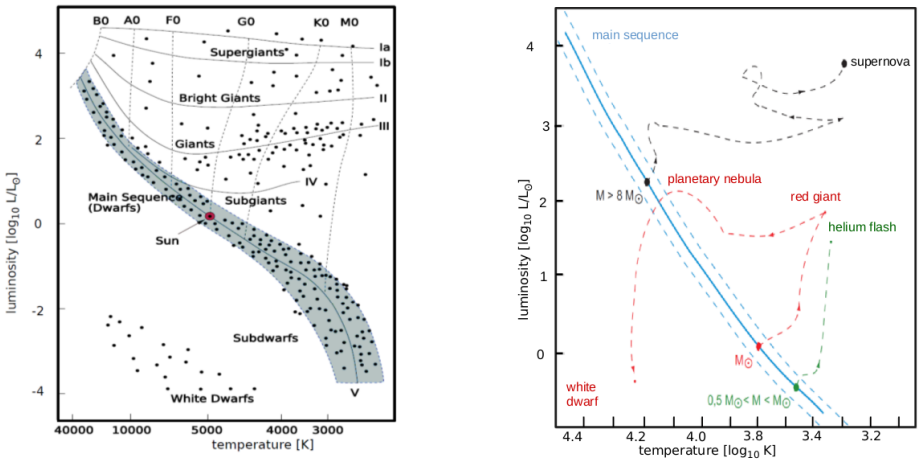

Figure 1.5: The Hertzsprung-Russel Diagram (left) displays the luminosity of stars (in units of solar luminosity $L_\odot$) in dependence of their surface temperature. It can be used to categorize the different burning stages of a star. Stars being in the hydrogen burning stage are arranged in the so-called main sequence, depending on their mass. The sun is in the centre, heavier stars are hotter and brighter. The right plot shows three exemplary star evolutions, our sun, a lighter star and an 8 solar mass star which ends up in a core collapse supernova. The plots have been taken from [1, 22].

If the spectrum contains silicon lines, the explosion has a thermonuclear cause. If no silicon lines can be identified, the cause is a CCSN which can be subdivided into further categories [26]. Fig. 1.6 shows a mass dependent overview of the different supernova types which also includes the influence of the stars' metallicity.

Thermonuclear or type Ia supernovae are of particular interest to astrophsics and cosmology as they are both the brightest of supernova explosions and very homogeneous in their mass and their energy release. This makes them ideal so-called standard candles which are used to determine distances in cosmology [27]. To achieve their brighness, type Ia supernovae combine two available energy sources: the gravitational energy due to collapse and the nuclear fusion energy from the core. They result e.g. from white dwarfs situated in a binary star system [28]. If the second star is close and in its early burning stage, hydrogen can be transferred onto the white dwarf where it will eventually ignite hydrogen and helium burning. This will increase the mass of the white dwarf. Once the Chandrasekhar mass limit of $\approx 1.4 M_\odot$ [29] is exceeded, the star collapses until the rising temperature initiates the explosive fusion of the core into elements of the iron group, the star is completey destroyed in the process. This type of supernova only produces a very low rate of neutrinos and is hence not detectable with IceCube [22] except for very close events.

1.5.3 Core collapse supernovae

The main feature of CCSN, on the other hand, is their immense neutrino signature. CCSN gain most of their energy from the gravitational collapse of which

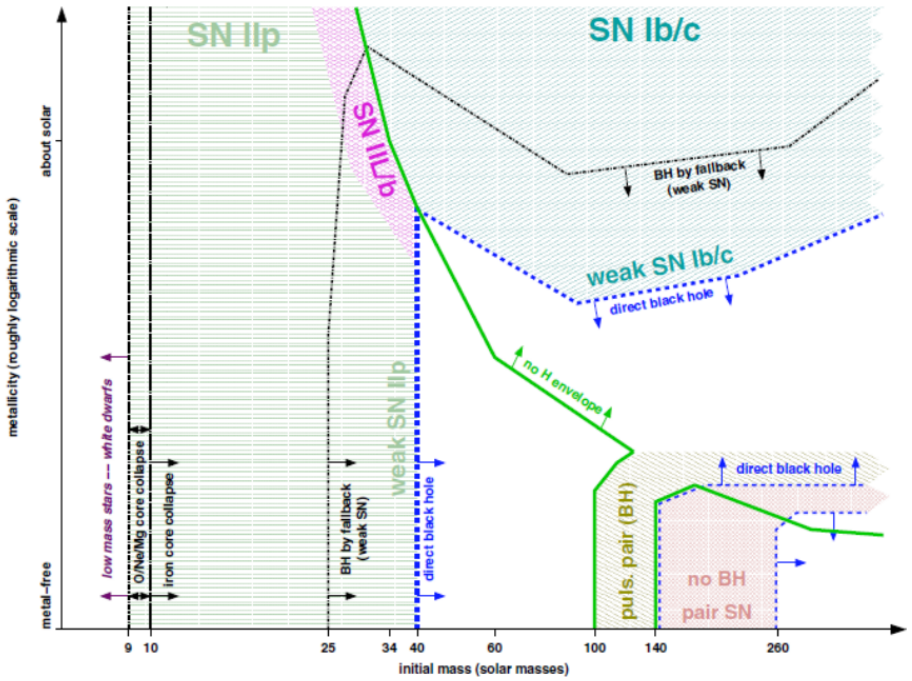

Figure 1.6: Supernova types of non-rotating stars depending on their mass and metallicity [23]. Rotation can enhance mass loss and smear out the transition regimes. The green horizontally hatched area indicates where type II supernovae can occur. For very massive stars $>100 M_\odot$, pair-instability can occur. In this case, thermal pressure is dissipated into electron-positron pair production which accelerates the contraction and in case of stars $>140 M_\odot$, can lead to an explosion with no remnant at all.

99% are carried away by neutrinos. Approximately 1% is ejected as matter and only 0.01% in form of photons [30]. This makes them ideal events to be studied with neutrino detectors such as IceCube. Progenitors of these events are heavy stars with at least 8 $M_\odot$. When the star runs out of fuel in its last burning stage, the equilibrium between thermal and gravitational pressure can no longer be maintained. The star collapses. Unlike the supernova Ia scenario, the heavy star already has produced an iron core and cannot gain further energy by fusion. The star hence collapses until it reaches nuclear density. The development of the CCSN is shown in Fig. 1.7 in a sequence of sketches.

First, at densities of $\rho \approx 10^{13}$ kg m^{-3} and temperatures of $T \approx 10^{10}$ K, the radius of the core is as small as a few thousand kilometers. The core matter, still composed of iron atoms, is in hydrostatic equilibrium. This means that electromagnetic and weak-interaction rates are at their maximum. The energy gained by the contraction and the resulting temperature rise enables endotherm reactions like

$$\gamma + {}^{56}\mathrm{Fe} \rightarrow 4n + 13\alpha \tag{1.19}$$

which cost approximately 124 MeV. This energy loss further reduces the thermal pressure and the star continues to contract. Then electron capture on

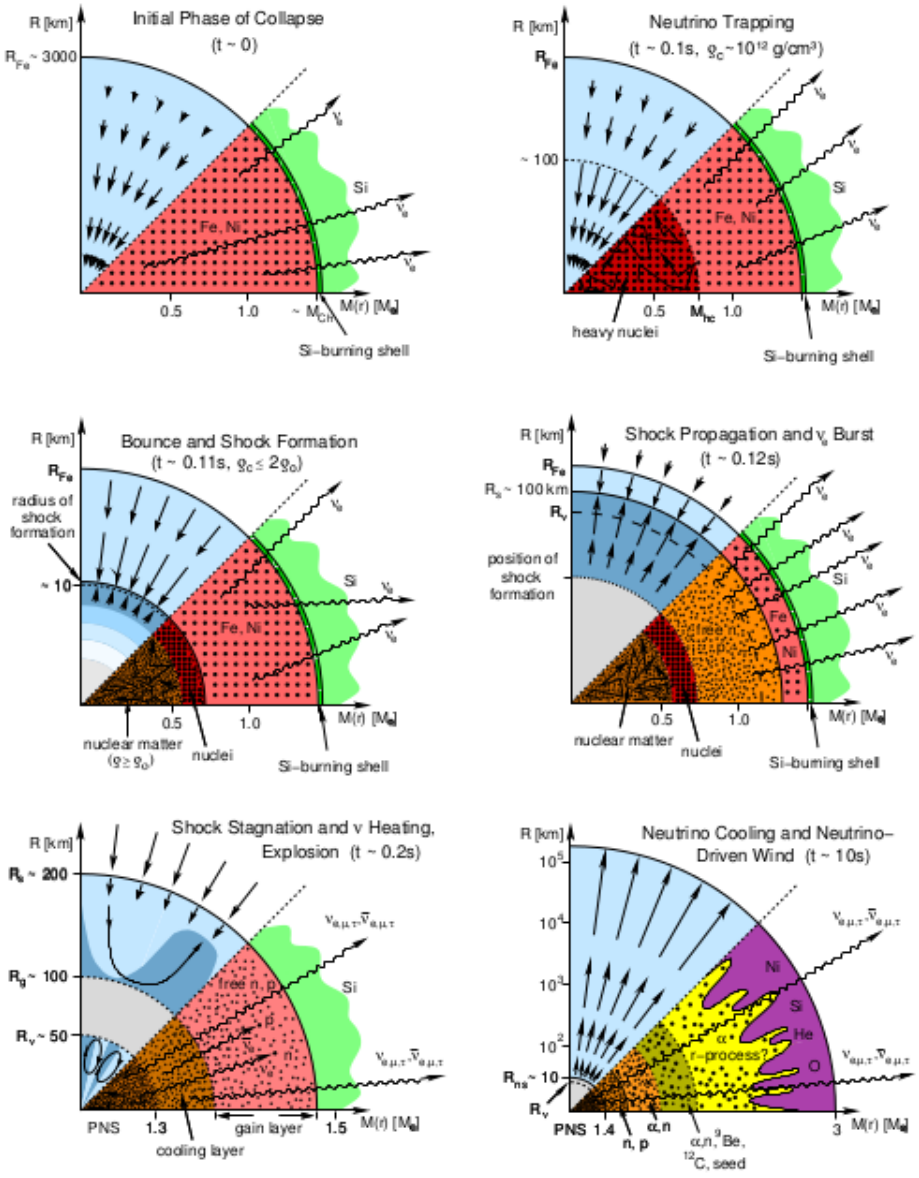

Figure 1.7: Core collapse supernova stages as described in the text. The right part of each graphic show the radial matter composition of every phase, whereas the left side of the figure displays the corresponding velocity vectors. The images are based on [31].

protons and nuclei

$$e^- + p \rightarrow n + \nu_e; \quad e^- + N(Z, A) \rightarrow N(Z-1, A) + \nu_e \tag{1.20}$$

becomes possible and reduces the electron density. Neutrinos can freely leave the core and carry away energy. This process is called deleptonisation as it reduces the number of electrons in the core and hence the ratio of electrons to barions $Y_e = n_e/\rho N_A$. As the formerly introduced Chandrasekhar mass limit depends on the electron density and is proportional to Y_e^2, the limit reduces simultaneously. The core eventually collapses by exceeding the mass limit [32]. As more and more electrons occupy the same volume, as they are fermions, their energy level rises due to the Pauli exclusion principle. Continouing compression increases electron degeneracy pressure. With sufficient compression, electrons are forced into nuclei in the process of electron capture.

When reaching densities of $\rho \approx 10^{15}$ kg m^{-3}, neutrinos can no longer escape the core. Scattering on protons and neutrons as well as scattering on infalling nuclei becomes dominant. This is called neutrino trapping. Minimal neutrino emission continues in a layer around the core which is called the neutrinosphere, allthough the largest fraction of neutrinos is being pulled toward the core along with the infalling matter. The continued conversion of electrons into neutrinos in the core further accelerates the gravitational collapse. This process happens in a fraction of a second.

At $\rho \approx 10^{17}$ kg m^{-3}, the core reaches nuclear density and cannot be compressed any further. The collapse comes to a very abrupt halt. Infalling matter bounces back and builds an outward shock wave colliding with the infalling plasma. The collision converts kinetic into thermal energy which is enough to disassociate nuclei into free nucleons and slows the shock wave. The increasing amount of free protons capture electrons and produce neutrinos at a high rate. The outward shock wave reaches less dense regions which enables these neutrinos to escape and to further slow it down due to energy loss. This phenomenon is called the deleptonisation neutrino burst. The shock wave eventuall stalls [33] and the resulting core object is called a proto-neutron-star (PNS).

The PNS accretes mass from infalling matter and continues to convert gravitational into thermal energy. Thermal neutrino production happens through nucleon-nucleon bremsstrahlung

$$N + N' \rightarrow N + N' + \nu + \bar{\nu} \tag{1.21}$$

as well as paiproduction due to annihilation electrons and positrons

$$e^- + e^+ \rightarrow \nu + \bar{\nu} \quad . \tag{1.22}$$

These processes create (anti-)neutrinos of all different flavours [34] and cool the PNS. Within 10 s, 99% of the gravitational binding energy are carried away by neutrinos. As the photon cross section is much larger and their interaction length inside the core is much smaller, they only escape into interstellar space some hours after the neutrinos.

It was long speculated what eventually causes the explosion of the star and the revival of the stalled shock wave. A possible mechanism has been found by accident. It is said that Jim Wilson of the Lawrence Livermore National Laboratory forgot to turn off his simulation before the weekend. When he

returned to his computer on monday he found that the model had exploded, but at a much later time than ever expected and simulated [35]. In the so-called delayed explosion model it was found that a fraction of the neutrinos escaping from the PNS would eventually revive the shock wave.

This fraction of neutrinos is absorbed by protons and neutrons in the stellar matter between the PNS and the stalled shock front, depositing energy and effectively heating this matter. This so-called neutrino heating expands said regions of the star, forming hot bubbles of stellar matter with decreased density. The expansion also delays the rate of infalling matter causing further energy deposition and heating of the bubble. Convection also plays an important role in the delayed explosion process [36]. Cooling matter moves towards the PNS where it is either absorbed and adds to neutrino emission or it is heated and rises again. If enough energy has been deposited, the shock front is reactivated and driven through the infalling stellar matter, the star explodes.

Due to the very high neutron flux, the explosion region is an ideal candidate for rapid-neutron-capture (or *r-process*) which creates most of the heavy elements beyond the iron group [37]. The remaining objects are a diffuse nebula and a solid core object which are further cooled by emmiting neutrinos, resulting in a neutron star.

Neutrino emission stages and energy spectrum

The neutrino emission during a core collapse supernova event can be divided into four different stages which are similar in current models. An exemplary neutrino light curve and neutrino energy development throughout the explosion process are shown in Fig. 1.8. The underlying *Lawrence Livermore model* is based on observational data from the last supernova SN1987A. As the neutrino emission follows the physical processes outlined in the previous section, observation of the neutrino light curve with IceCube would allow one to verify current explosion models with high statistics. It would be particularly interesting to resolve differences between the accretion and cooling phase. The neutrino emission profile during the cooling phase would give insight into neutrino transport in hot stellar plasma, whereas the variations in the accretion phase would provide information about the importance of convection before the explosion.

- **Neutrino-Trapping** occurs at the first stage of the collapse prior to the explosion. When the collapsing core reaches densities of 10^{15}kg m^{-3} neutrino-nucleon scattering dominates and neutrinos are pulled back toward the core along with infalling matter. This reduces neutrino luminosity at this point.

- The first remarkable feature after the core bounce is the **deleptonisation peak**. Behind the shock wave, free protons and neutrons are capturing electrons. The resulting electron neutrinos eventually clear the neutrinosphere and produce a visible peak in electron neutrino luminosity for several milliseconds. As the PNS always has the same initial mass, the total energy of the peak of $\approx 10^{44}$J and its width of 5-7 ms is independent of the supernova model or the total mass of the progenitor.

- During the **accretion** phase, neutrinos of all lepton families are being produced by neutrino-pairproduction via electron-positron annihilation.

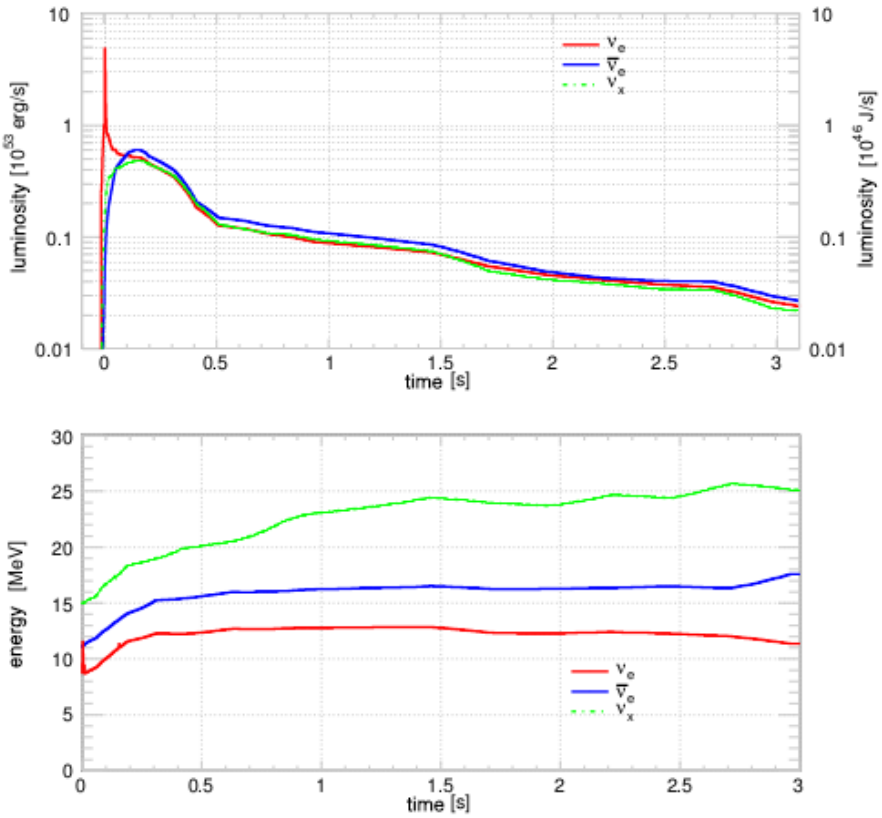

Figure 1.8: The energy spectra and neutrino light curves have been created with the *Lawrence-Livermore* model [38] and taken from [22]. It shows all known characteristics of CCSN neutrino emission and is one of the few model which simulates the cooling phase up to a time of 15 s.

Nucleon-bremsstrahlung further creates thermal neutrinos of all flavours. The production of ν_μ and ν_τ is usually summarized as ν_x due to their common different behaviour in matter as opposed to the ν_e. As ν_x production usually happens in deeper layers, their luminosity is reduced by a factor of up to two and their average energy is higher than that of ν_e and $\bar{\nu_e}$. The reactions are kept alive by the continued infall of matter and contributes to the heating of the stellar matter.

- **Cooling** of the PNS starts right after the core bounce, however the initial part is superimposed by the previous phases. The cooling phase dominates from 0.5 s and can last several tens of seconds depending on the size of the PNS. During the cooling phase, 90 % of the stars' gravitational binding energy are being carried away by neutrinos of all flavours. The PNS cools from the inside to the outside, and the main production channel is pairproduction. The neutrino luminosity and energy of the neutrinos contineously decreases during the process, reducing the flux similar to black body radiation. The cooling phase is completed when the core tem-

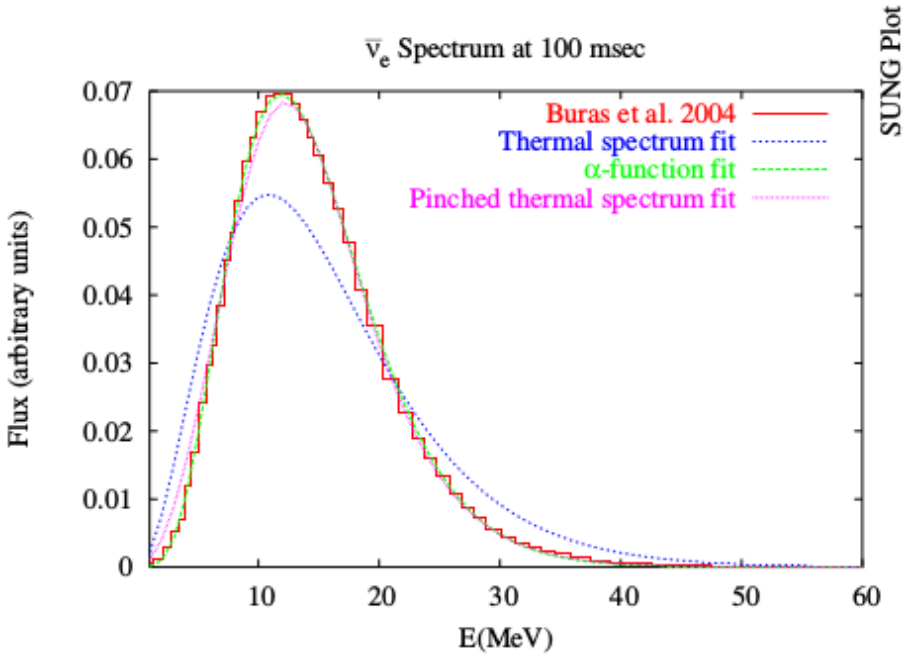

Figure 1.9: Core collapse supernova neutrino energy spectrum as compared to the expectation of a thermal spectrum. Plot taken from [39]. The modified spectrum can be fitted by adding a "pinch-factor" or by the *α-function*-parametrisation developed in [40].

perature drops below 10^{10}K and the core matter becomes transparent to neutrinos.

Neutrinos trapped inside a supernova core region are exchanging energy with electrons and protons through elastic scattering processes and are hence kept in thermal equilibrium with the surrounding plasma. It can therefore be expected that the neutrinos are being emitted with the spectral temperature of the region at which they energetically decouple. Their energy spectrum would then follow a Fermi-Dirac-distribution. This basic energy spectrum is modified by different factors.

For electron neutrinos, charged current reactions (β-processes $ep \leftrightarrow n\nu_e$, $e^+n \leftrightarrow p\bar{\nu_e}$) dominate the transport in the core. The neutrinos diffuse outwards until they reach the neutrinosphere and their reactions freeze out. As the cross-sections of the β-processes are energy dependent, the neutrinosphere radius and hence the thermal temperature of the neutrinos also differ with energy. High energy neutrinos are preferably released from larger radii with lower temperatures, whereas low energy neutrinos are radiated from lower radii and higher temperatures. This causes a depletion of the neutrino energy distribution's high and low energy tails. The spectrum appears to be "pinched".

As the surface of the PNS is more neutron rich than lower layers, it is more opaque for electron neutrinos. The majority of anti-electron neutrinos hence originate from deeper layers and are released at higher energies. The spectra modifications for the heavy neutrinos is very complex and described in [40] in

full detail. The average neutrino energies eventually follow a hierarchy of

$$\langle E_{\nu_x} \rangle > \langle E_{\bar{\nu_e}} \rangle > \langle E_{\nu_e} \rangle \quad . \tag{1.23}$$

The modifications of the neutrino energy spectrum as compared to a Fermi-Dirac distribution are shown in Fig. 1.9. It can be described by applying a *pinching factor* on the thermal spectrum or by the α-*function*-parametrisation developed by Keil et. al [40]. The Keil two-parameter distribution will be used in the analysis. It describes the energy dependent neutrino flux based on the average neutrino energy $\bar{\epsilon}$ an the parameter α which varies between 2.5 and 5:

$$F_\alpha(E, \bar{\epsilon}, \alpha) = N(\bar{\epsilon}, \alpha) \left(\frac{E}{\bar{\epsilon}} \right)^\alpha \exp(-(\alpha + 1)\frac{E}{\bar{\epsilon}}) \quad , \tag{1.24}$$

where the normalisation constant is given by

$$N(\bar{\epsilon}, \alpha) = \frac{(\alpha + 1)^{\alpha+1}}{\Gamma(\alpha + 1)\bar{\epsilon}} \quad . \tag{1.25}$$

1.5.4 Neutron stars and beyond

For very heavy stars it is possible to further collapse into an even denser state eventually resulting in a black hole [35]. An upper mass limit of neutron stars of $\approx 0.7 M_\odot$ has first been formulated by Oppenheimer and Volkoff in 1993 [41] based on the work of Tolman. The so-called Tolman-Oppenheimer-Volkoff-limit (TOVL) works in analogy to the Chandrasekhar mass limit for stable white dwarf stars, which describes the mass needed for the gravitational energy to overcome the electron pressure and enable further collapse. Neutron stars exceeding the TOVL will gravitationally overcome the quantum degeneracy pressure of neutrons. Modern and more realistic models concerning structure and composition of neutron stars lead to a current estimation of the mass limit of 1.5 to 3.0 $M_\odot$ [42]. This leads to an initial mass of the main sequence star of $\approx$ 15 to 20 $M_\odot$. The great uncertainty of the TOVL value is based on poor knowledge of the equation of state of cool high dense handronic matter which cannot be produced in laboratories. The current empirical lower limit of the TOVL is set by the mass measurement of the PSR J0348+0432 pulsar [43] with 2.01 $M_\odot$.

A lower mass limit of neutron stars is determined to be $\approx$ 0.2 $M_\odot$ [44]. The simulation assumes a sudden mass loss of the neutron star which is then destroyed by a massive explosion. This hypothetical mass loss is assumed to be possible in double neutron star systems when matter is transferred from the lighter to the heavier star.

The observed mass distribution of neutron stars is shown in Fig. 1.10. The basis of most neutron star mass estimates is the analysis of binary motion, and the mass distribution differs depending on the type of the companion. Measurements based on double neutron star (DNS) systems show a narrow mass distribution with an average of 1.33 $M_\odot$. Considering a white dwarf companion (NS-WD system), measurements show a broader distribution with an average neutron star mass of 1.55 $M_\odot$ [45]. In the latter case it is assumed that the neutron star continously accretes matter from the white dwarf which additionally spins it up to rotational periods of milliseconds. Such fast rotating neutron stars are a likely candidate for millisecond pulsars [46].

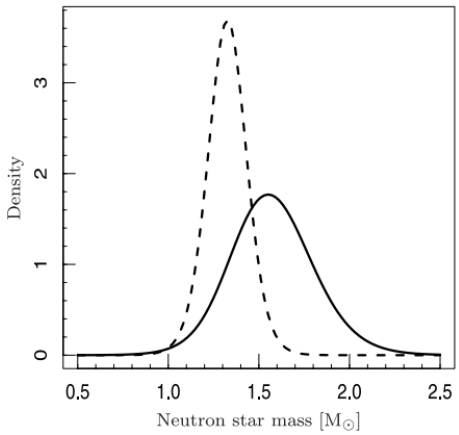

Figure 1.10: Observed neutron star mass distribution based on double neutron star systems (dashed line) and neutron star- white dwarf systems (solid line). Mass densities have respective peaks at 1.33 $M_\odot$ and 1.55 $M_\odot$ [45].

Neutron stars exceeding the TOV-mass-limit are speculated to form a new matter state in their interior. Under sufficient gravitational pressure the neutrons are hypothesized to break down into free quarks [47]. The resulting so-called quark matter would then be stabilized against gravity by quark degeneracy pressure. Such stars might then be difficult to distinguish from ordinary neutron stars. It is further speculated that so-called quark-stars which are composed entirely by quark matter would only be stable if a sufficient number of u and d quarks are converted into strange quarks [48].

Generally it is assumed that a star exceeding the TOVL collapses indefinitely at an asymptotically slowing rate forming an object of infinite density and zero radius, a black hole. The collapse of a hot neutron star, which has just undergone a supernova explosion, into a black hole is simulated in [49]. It is shown that the formation of the black hole can be observed in the neutrino sector by a sudden decrease of all neutrino fluxes. When the surface of the collapsing star reaches the event horizon the neutrino fluxes cease within a fraction of a millisecond.

1.5.5 SN1987A

On Feb 23rd 1987 astronomers on earth were able to observe the explosion of the $\approx 20\ M_\odot$ blue supergiant *Sanduleak* in the Large Magellanic Cloud (LMC) [51, 52]. This historic event which happened about 168 000 years ago at distance of 51 kpc, was the first supernova visible to the naked eye since more than 400 years and hence the brightest supernova observed since the invention of the telescope. It is also the only identified source to date of low energy extrasolar neutrinos. High energy extrasolar neutrinos were discovered in 2013 by IceCube [7], but their origin also remains unclear to date.

The remnants of SN1987A[2], as shown in Fig. 1.11, are the most intensively

[2]Supernovae are named by a combination of the two letters "SN", the year in which they were observed followed by a letter from the latin alphabet. The first 26 observed supernovae in a year are assigned letters from A to Z, the following supernovae will carry two letter starting with "aa" and so on.

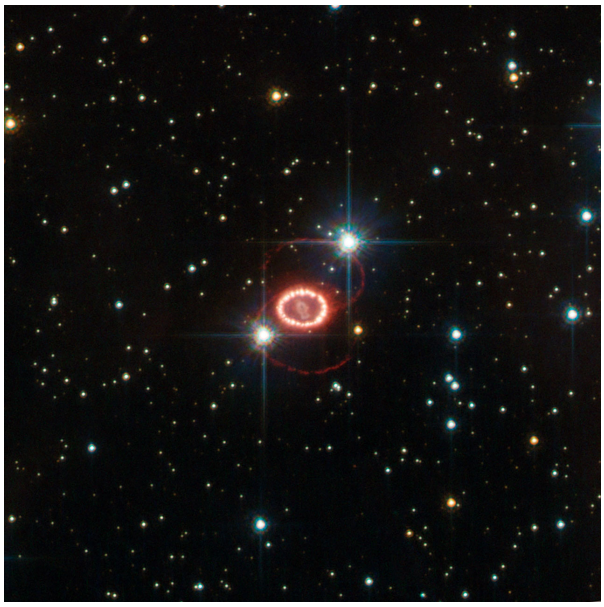

Figure 1.11: A Hubble image of SN1987A. Dominating this picture are two glowing loops of stellar material and a very bright ring surrounding the dying star at the centre of the frame [50].

studied objects in the history of astronomy being visible to a broad range of telescopes from γ to radio wavelengths. Soon after the explosion it was found, that neutrinos associated with the event were already registered an hour earlier by at least two underground neutrino observatories. At 7:35 universal time, both the IMB [53] and the Kamiokande-II [54] detector observed about a total of 20 of the 10^{58} neutrinos emitted by SN1987A.

Measurements the Balmer absorption lines by optical telescopes later confirmed the presence of hydrogen in the optical spectrum and hence classify the event as a type-II supernova. Even though the number of observed neutrinos was low, it was still possible to draw basic conclusions about the explosion mechanism and the nature of the neutrinos. A 1-dimensional numerical model was developed, which simulates the average energy and luminosity of the emitted neutrinos from collapse onset until 18 seconds after core bounce. The present work is mainly based on this so-called *Lawrence Livermore* model [38]. It differs from more modern simulations and the simulation methods are no longer considered optimal, but it is sufficient to explore the capabilities of the detector and contains all of the explosion features as discussed earlier.

In addition it was possible to draw some particle physics specific conclusions based on the detection of the few supernova neutrino events, such as the lifetime of the anti-electron-neutrino, its charge and mass [16]. It was found with 90% C.L. that

$$m_{\bar{\nu_e}} < 13\text{eV}, \quad \tau_{\bar{\nu_e}} \geq 2.5 \cdot 10^5 s \frac{\mathrm{m}_{\bar{\nu_e}}}{\mathrm{eV}}, \quad Q\bar{\nu_e} < 10^{-18}\mathrm{e} \quad . \tag{1.26}$$

One important question still to be answered about this supernova is the fate of its remaining core object. As it has still not been directly observed it could

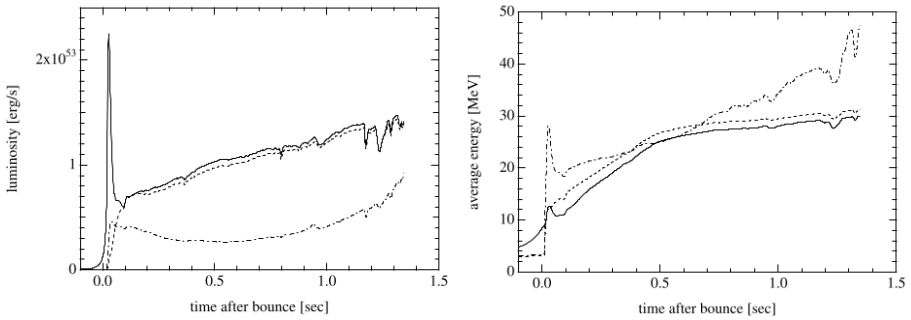

Figure 1.12: Luminosities and average energies of ν_e (solid lines), $\bar{\nu_e}$ (dashed lines), and ν_x (dot-dashed lines) as a function of time after core bounce for a failed supernova model [56].

be a neutron star which is hidden by dust and fragments from the explosion. Another explanation for its unobservability would be the formation of a black hole [55] as described in the previous section.

1.5.6 Failed supernovae

It is also being discussed that stars exceeding 15 to 20 $M_\odot$ might be too heavy to revive the shockwave and skip the delayed explosion [56, 57]. This process is called rapid black hole formation. If the iron core of the PNS is sufficiently large, the shock wave cannot propagate outward, and comes to a halt above the proto-neutron star. As the material of the outer layers continues to fall down, the mass of the PNS increases toward the maximum mass and the dynamical collapse to the black hole takes place. Accordingly, no optical explosion is associated with this type of collapse.

There is multiple evidence for the occurance of failed supernovae which are summarized in [58]. An upper mass limit of $\approx$18 $M_\odot$ for observed SNII progenitors for example leads to the conclusion that something else than a supernova might be happening to super massive stars. Another discrepancy lies in the formation rate of massive stars which exceeds the observed supernova rate. One option to search for failed supernovae is to repeatedly compare optical records of the sky with previous versions. Disappearing stars which cannot be associated with a regular supernova are failed supernova candidates. One example is N6946-BH1 which is a disappearing red supergiant in galaxy NGC 6946[3]. The star was 25 times the mass of the sun and disappeared from optical view by 2015 [58].

Failed supernova events should be well visible in the neutrino sector as shown in Fig. 1.12. Around the core bounce (t $<$ 0.1 s), the time profiles of average energies and luminosities are similar to those for ordinary supernovae. There is a distinctive peak due to the neutronization burst in the luminosity of ν_e. The rise of the luminosities of $\bar{\nu_e}$ and ν_x right after bounce occurs owing to the

[3]Galaxy NGC 6946 is a medium-sized, face-on spiral galaxy about 22 million light years away from Earth. In the past century, nine supernovae have been observed to explode in the arms of this galaxy[59], giving it the nickname *Fireworks Galaxy* [60]. NGC 6946 is categorized as a so-called starburst galaxy for its relatively high star formation rate (SFR).

thermal production of neutrinos. The peak of average energies around the core bounce appears as a result of heating by the passage of the shock wave. As there is no explosion, the PNS continues to accrete matter which leads to continouous contraction and heating. The average energies are reflecting the temperature increase and increase toward black hole formation.

Different estimates exist concerning the timescale of the neutrino signal drop due to the black hole formation. Naively, an instantaneous drop can be assumed [61] whereas other sources report that the neutrinosphere will be swallowed by the horizon in a fraction of a millisecond and the major neutrino emissions cease at this point [56]. There is also a time smearing due to the macroscopic size of the black hole progenitor.

1.5.7 Galactic inital mass function

The initial mass function (IMF) is an empirical function which describes the distribution of initial masses for a population of stars. The term initial refers to the time at which the star begins hydrogen burning and enters the main sequence. The IMF can be derived from the present day mass function by observation of the stellar mass-luminosity relation in combination with a model of how the star formation rate varies with time [62].

The IMF is often specified as a probability distribution function which describes the number of stars with a specific mass $\xi(m)$ in relation to the solar mass. Multiple models exist which mainly differ at the low mass region $m < M_\odot$. For heavier stars the IMF generally takes the following form for the Milky Way (e.g. [63])

$$\xi(m) = k \left(\frac{m}{M_\odot} \right)^{-\alpha} \quad \text{with} \quad \alpha = 2.3 \pm 0.3 \quad . \tag{1.27}$$

Considering the above mentioned lower initial mass limits of stars of 8 $M_\odot$ for a supernova and 15 $M_\odot$ for a black hole formation, the IMF can now be used to determine the fraction of black hole formation events in relation to all supernovae

$$\frac{\int_{15}^{\infty} \xi(m)}{\int_{8}^{\infty} \xi(m)} = 0.44 \quad . \tag{1.28}$$

This leads to the estimation that ≈44% of the stars which will end in a supernova are likely to produce a black hole. A 20 $M_\odot$ lower limit for black hole formation changes the estimate to ≈30%.

1.5.8 Galactic supernova rate

Supernova explosions are very common considering the whole universe. Multiple events happen every second, two thirds of which are type II supernovae [64]. The majority of observed explosions though are of the optically extremely bright type Ia. The supernovae rate in the Milky Way, on the other hand, is very small, even in a timeframe of hundreds of years.

Determining the galactic supernova rate is therefore a difficult task and based on a combination of different kinds of observations. One option is to compile a list of every optical supernova observation worldwide of the past 1000 years.

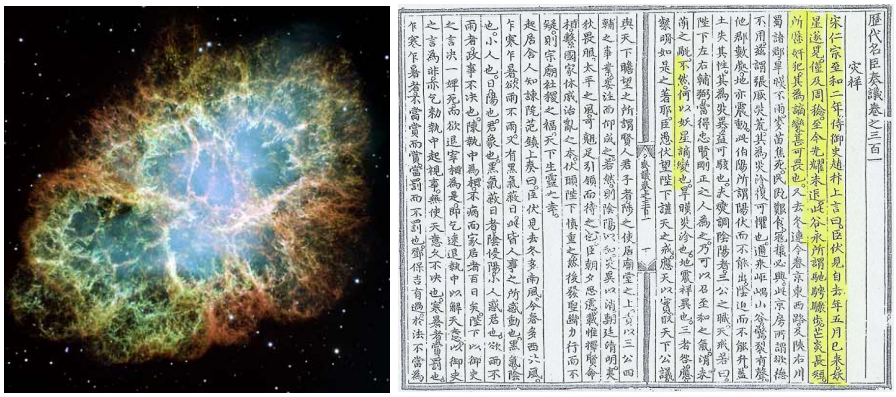

Figure 1.13: A recent image of the Crab Nebula made by The Hubble Space Telescope (HST) and historic detection notes of the corresponding SN1054 in a Chinese document. Images taken from [66] and [67]

An example is shown in Fig. 1.13 for a supernova having been first observed on 4 July 1054 and described in a Chinese document as a *guest star*, which remained visible for around two years. Based on these notes, the supernova can be matched to its remnants still visible today in form of the crab nebula. For some of these historical events it is additionally possible observe the optical *echo light curves* which have been reflected by gas- and dust-clouds hence taking a longer time to reach earth [65]. This allows one to learn about the type of the event hundreds of years of after its original observation.

With this list containing less than 10 entries during the past millenium, the rate is very low and likely underestimated. Since all of these past observations are based in the optical regime, the list does not account for failed supernovae or optically hidden events by e.g. dust clouds oder nebulae. Neutrino detectors that overcome this limitation only existed for 30 years.

Another approach is to investigate the supernova rate in a large number of different distant galaxies. This, on the other hand, introduces a selection factor as different galaxy types are producing different supernova rates. Supernovae are e.g. more common in spiral galaxies than in elliptic ones [68]. One can also look at the rate of star formation in the Milky Way, since fate and lifetime of the star is mainly determined by its mass.

Many other approaches exist, like the systematical survey of the sky for supernova remnants or the ratio of specific radioactive isotopes in the ISM which are typically produced by supernovae [65]. All of these methods introduce different uncertainties.

In summary, on average two to three supernovae are expected to happen in the Milky Way within a century. The last galactic supernova was observed optically in the 1870s and no supernova has been observed since the construction of the first neutrino telescopes approximately 30 years ago[4], which have a detection capability of galactic supernovae of 100 % [22].

[4]With the exception of the above mentioned SN1987A, which occurred in the Large Magellanic Cloud, a dwarf galaxy orbiting the Milky Way.

Chapter 2

The IceCube detector

This chapter describes the setup of the IceCube neutrino telescope, the world's largest neutrino observatory to date. IceCube was primarily built to detect and learn about the most high energetic cosmic neutrinos and its origins. As the detector also allows to search for low energy galactic supernova neutrinos a separate data acquisition stream has been established. The chapter begins with a technical overview of the instrument.

2.1 Construction

IceCube is a water (ice) based Cherenkov neutrino detector [69] in a so-called long string configuration. IceCube consists of 5160 optical modules on 86 strings covering one cubic kilometer of ice at depths between roughly 1.5 and 2.5 km. After six years of construction, the last IceCube string was deployed in Dec 2010. A schematic view of the setup can be found in Fig. 2.1.

Modules are positioned at vertical distances of 17 m to each other. The strings are configured in an hexagonal arrangement ensuring a distance of 125 m between each string. Additional surface stations containing two modules each at the top of each string enable for muon veto capabilities and cosmic ray research.

Two different kinds of drills were used in order to deploy the IceCube strings, both using hot water in order to melt the antarctic glacial ice and snow. The enhanced hot water drill (EHWD) uses a high pressure water jet of 14 bar and takes about 30 h to drill a hole of the required 2.5 km of depth.

The independent firn drill (IFD) is a separate drill which is used to drill a hole up to the depth of 60 m. This upper region mainly consists of porous snow where free flowing water would just seap away. The IFD therefore implements a cone-shaped drillhead which consists of thin copper tubing from which the drilling fluid cannot escape. A heated mixture of glycol and water is then pumped through the tubing under high pressure while the cone is slowly lowered into the compacted snow.

As the EHWD and the IFD are two separate drills, the construction crew was able to work on two holes simultaneously allowing for a maximum deployment rate of 20 strings per season. IceCube has already been taking data in its partial configuration and is expected to run at least 15 years with all 86 strings.

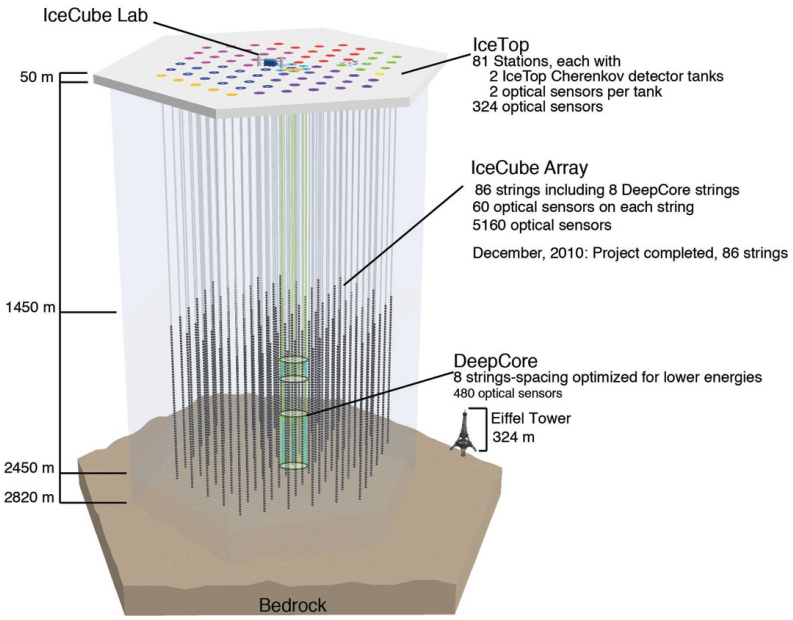

Figure 2.1: Schematic view of the IceCube detector [69]. The IceCube detector consists of 86 strings that have been lowered into the ice in order to instrument about 1 km^3 of pure and highly transparent ice. The different construction stages are color coded onto the surface stations of the strings. Each color corresponds to the year of deployment of the string.

2.2 Scientific goals

The IceCube project aims at a large variety of physics goals a few of which are discussed in the following paragraphs. The main focus of the experiment lies on the discovery of high energetic astrophysical neutrinos but it also enables to explore e.g. cosmic rays, neutrino oscillations, galactic supernovae, and particles beyond the Standard Model.

Cosmic neutrinos. The main goal of IceCube is the search for high energetic neutrinos of cosmic origin. Two approaches are used in this search, namely the point source search and the diffuse search.

The point source search aims at discovering transient sources such as gamma ray bursts as well as permanent sources such as e.g. active galactic nuclei. A variety of so called cosmic accelerators are expected to be the source of high energetic cosmic neutrinos and have yet to be discovered. The background for extraterrestial neutrino signals are atmospheric muons and neutrinos. In order to exclude the muon background from the analyses, it is possible to only look at neutrinos coming from the northern hemisphere, effectively using the earth as a filter against muons. An additional likelihood analysis on the directions of the incoming netrinos helps to reveal point sources in the directionally homogenous

atmospheric neutrino background.

The diffuse search looks into the energy spectrum of cosmic neutrinos which is expected to decrease with energy according to the powerlaw $\sim E^{-2}$. As the atmospheric neutrino spectrum falls as rapidly as $\sim E^{-3.7}$, these analyses mainly focus on measuring an excess in neutrino count at very high energies on the order of TeV.

Cosmic rays. IceCube, together with its 2D surface grid of optical modules, is also used to investigate cosmic rays and their secondaries. IceTop modules mainly observe electromagnetic shower components such as photons, electrons and positrons. As IceCube observes the muonic component of the showers, the combination of both detectors can be used to gain knowledge about the ratio of the electromagnetic and muonic component thus providing insight about the composition of cosmic rays.

Neutrino osciallations. Earth matter induced neutrino oscillation effects can be studied at energies around 25 GeV. Cosmic rays are reaching earth isotropically from every direction producing neutrinos in air shower processes in the athmosphere. Depending on the source of the shower neutrinos travel varying distances through the earth before reaching the detector. This enables IceCube to measure θ_{23}, the "athmospheric" mixing angle and additionally provides a rough matter density profile of our planet.

Dark matter and exotic particles. The IceCube detector can also be used to uncover deviations from the standard model. Various groups are investigating the possibility of observing neutrinos from magnetic monopoles or weakly interacting massive particles (WIMPs) which are a candidate for dark matter, or are testing non-standard neutrino oscillation models.

Galactic supernovae. An additional data aquistion system aims at detecting low energy neutrinos from galactic supernovae. These neutrinos are well below the detector's energy threshold and can only be detected in a collective fashion. This method therefore needs a minimum neutrino flux reaching the detector which is only satisfied for events at relatively close ranges not exceeding the Milky Way [12]. The supernova analyses aim at discovering properties of the star as well as the neutrino itself. In particular, the average energy of supernovae neutrinos is of interest as it links the detected hit rate to the actual neutrino flux. Learning about the time dependent neutrino flux of a supernova explosion, the so-called neutrino light curve, would enable to learn about explosion mechanisms in the star. Under some constraints IceCube is also able to narrow down the direction of a galactic supernova, allthough it needs to rely on optical follow up to determine the distance. More details on direction and energy reconstruction of supernova neutrino events are discussed in the analysis chapter.

2.3 Detection method and neutrino signatures

A neutrino telescope such as IceCube indirectly detects neutrinos by observing Cherenkov radiation from neutrino reaction products. This mainly happens via

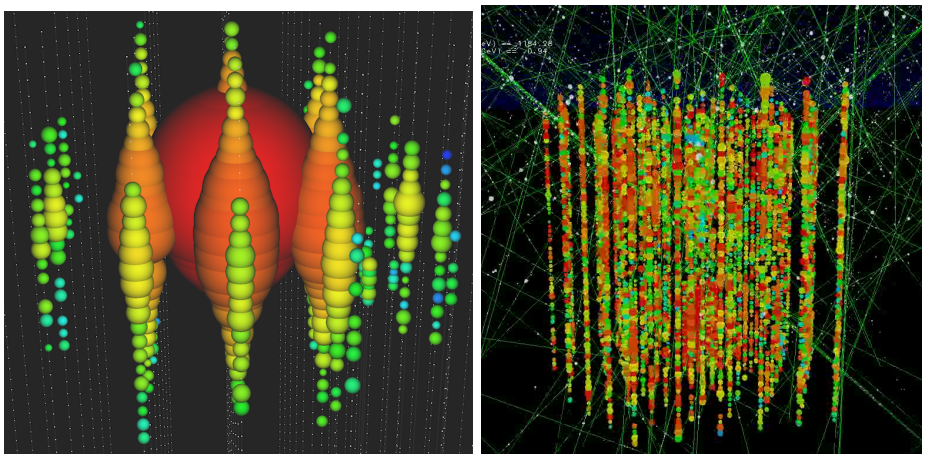

Figure 2.2: Neutrino and background signatures in IceCube. Left: The 2 PeV high energetic electron neutrino event *Big Bird* [70]. Right: Background/ noise hit simulation including the influence of 800 low energetic atmosperic muons. Supernova neutrinos with an average energy of $\mathcal{O}(10\ \text{MeV})$ are almost undistinguishable from this backgound.

charged current reactions between the neutrino and the detector medium which produces charged leptons of all kinds:

$$\nu_l + N = l + X \quad \text{with} \quad l = e, \mu, \tau \quad . \tag{2.1}$$

In order to compensate for the very small neutrino cross sections, the reactive detector volume has to be very large[1]. In case of a telescope based on the detection of Cherenkov light, the detector medium additionally needs to be transparent. Cosmic radiation also creates charged particles in the atmosphere which can reach the detector and create additional Cherenkov light. Shielding from cosmic radiation is realised by constructing the detectors at great depths. Using a natural detector medium enables one to reduce the construction costs which mainly leaves two options for potential construction sites: very deep water bodies like oceans or lakes, or deep ice layers. In case of IceCube, as much as 1 km^3 of south polar glacier ice has been instrumented with optical sensors ranging as deep as 2.5 km.

In IceCube, the optical sensors are a combination of a photo multiplier tube and sophisticated digital data aquisition components [69]. The so-called digital optical module, or DOM, is discussed in the following section.

Two different examples of a detector response of the optical modules are shown Fig. 2.2. The left image shows a reconstructed high energy shower event [7, 71] caused by an electron neutrino depositing ≈2 PeV of energy. High energy muon neutrinos create muons which cause longer, track like, signatures in the ice. Along with their energy, the direction of these events can be reconstructed and matched against known optical events in order to obtain information about their source. A recent development in IceCube is an automatic online reconstruction of high energetic events. The reconstructed directional information is

[1] For a more detailed relation between detected Cherenkov photons and the neutrino flux see A.1

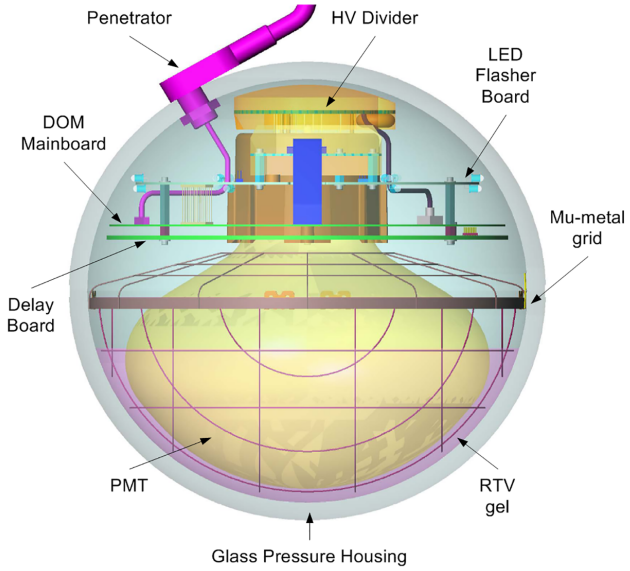

Figure 2.3: Schematic view of a digital optical module as described in [72]. The DOM is a combination of a photo-multiplier and digital data acqusition electronics housed in a high pressure glass sphere. It additially contains test intruments to measure the ice properties of the south polar glacier at great depths.

immediately made available to optical follow-up. This offers a *multi messenger* approach on the most intriguing questions: The origin of the cosmic radiation and the nature of cosmic particle accelerators.

The right picture in Fig. 2.2 illustrates the situation in the very low energy domain. The 10 ms snapshot of a Monte Carlo simulation shows mainly noise hits and 800 muons across the whole detector. Supernova neutrino events with an average energy of $\mathcal{O}(10\,\mathrm{MeV})$ can not be easily distinguished. The supernova analysis hence aims at resolving collective background rate changes in all modules.

2.4 Digital Optical Module

The main data taking components are the IceCube digital optical modules (DOMs) [72] as shown in Fig. 2.3. The quality demands on the DOM are very high. Once frozen into the ice, it can never be recovered or repaired. It consists of a 10" diameter photo multiplier tube, associated circuit boards, data acquisition, control, and calibration units.

Due to largely different energies and distances of the potential signals, the PMT is designed to measure a wide variety of pulse widths and amplitudes with nanosecond time resolution. It contains multiple digitizers with overlapping dynamic range and different sampling speeds. The DOM can be configured from the surface and then almost autonomously collects the data. Approximately every second, the digitized data is sent to the surface.

Every DOM detects single photons which trigger the PMT waveform digitization process forming a so-called hit. Multiple digitizers are being run in parallel to reduce deadtime. The hit time and waveform are saved for later analysis. The DOM additionally registers the hit rate in a separate datastream.

Whenever a certain voltage threshold is exceeded at the PMT's anode, the detection of one or multiple photons is assumed and the signal is forwarded to the different processing chains:

- The **Scaler** is a simple 16 bit hit counter based on a 40 MHz clock leading to a binning of 1.6384 ms. It is used exclusively in the supernova analysis as a collective rate increase in all DOMs could indicate the detection of many low energy supernova neutrinos.

- With a sampling rate of 290 MHz the costum built Analog Transient Waveform Digitizers or **ATWD**'s can store up to 426 ns of data in 3.3 ns resolution. Two ATWDs are built onto the DOM's mainboard in order to reduce deadtime during the readout periods. This fine binned data are only kept if the next or next-to-next DOM has also been hit during a time window of 1 μs. This is called the *hard local coincidence* (HLC) criterion. If it is not fulfilled, the ATWD digitization process is aborted which further reduces the deadtime.

- The **fADC** continously samples the PMT data at 40 MHz and has a total storage capacity of 6.4 μs. In case of an initial HLC condition, the full low resolution waveform is saved, otherwise only three values surrounding the first peak are stored with the hit data.

The HLC criterion is determined by each optical module autonomously for every hit. Additional *LC-wiring* connect each module to its neighbours and enable each DOM to independently decide which waveform information to keep. If the HLC criterion is not met, the DOM immediately discards both ATWD and fADC waveforms and only sends a condensed dataset to the surface data acquisition.

The calibration tools of the DOM consists of multiple LED light sources which can be used for multiple purposes such as measuring the exact location of the DOM in the detector or measuring the properties and impurities of the ice at different locations. They can also be used to monitor timing and reconstruction capabilities throughout the analysis chain.

Time synchronisation between all modules is performed using the RAPcal[2] method [72]. In between data transmission cycles, the surface station sends periodic messages to every DOM which respond with timestamped replies. This method enables the main data acquisition system to keep track of every DOMs clock and translate individual DOM times to a global data acquisition time and eventually to universal time using GPS receivers.

2.5 Surface data acquisition

The surface data acquisition components are housed in the IceCube laboratory (ICL), a two story building located at the centre of the detector surface. One

[2]Reciprocal Active Pulsing calibration

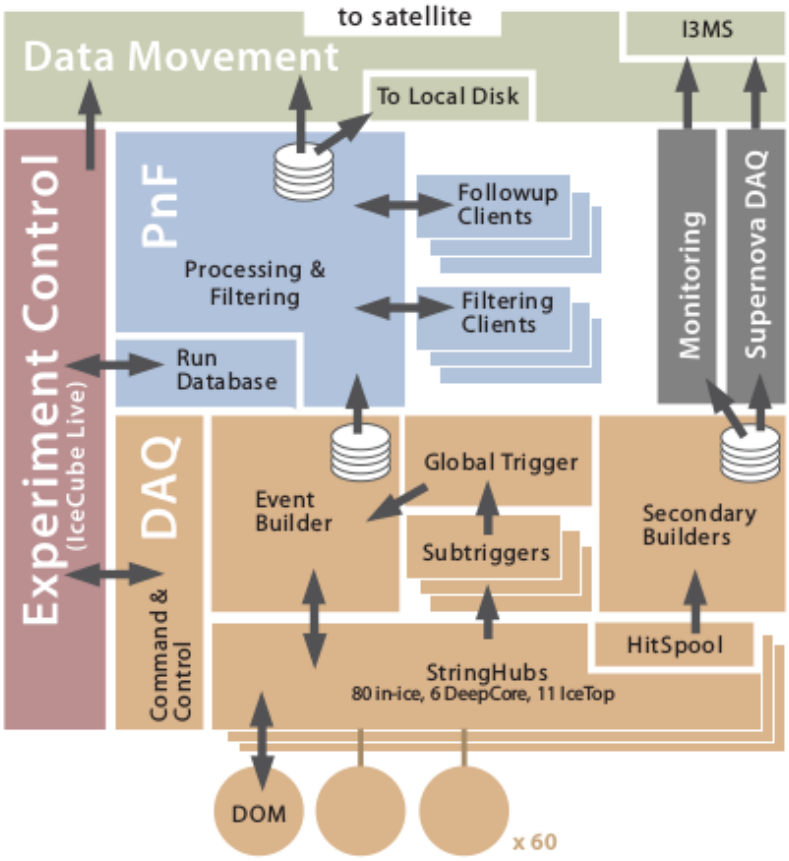

Figure 2.4: IceCube data acquisition dataflow from the optical modules (bottom) through the triggering and filtering stages to the satellite transmission of the condensed data (top). The control components are illustrated on the left side of the graphic, whereas the supernova scaler data (or secondary data) flow is shown on the right. Figure taken from [69].

cable from every string leads to the ICL and is connected to one server each, called the *DomHub*. Every hub provides power to the individual DOMs and caches and relays the data it recorded via a software package called *StringHub*. The IceCube data flow is shown in Fig. 2.4.

As mentioned before, the main goal of IceCube is the analysis of high energetic neutrino events by reconstructing the track of the neutrino and its deposited energy. Digitized hit and waveform information is passed through various triggers and filters in order to select interesting events and to identify background induced from atmosperic muons. As IceCube has a limited satellite data transfer quota per day, a first analysis is already performed on site in the ICL. This is realized in the Processing and Filtering (PnF) section of the online system which then submits the resulting data to the satellite transfer queues.

The scaler data (or secondary data) from all DOM's are also first collected on each DomHub and then made available as combined datasets on a dedicated

server. The supernova analysis synchronises these data in 2 ms bins accross all DOM's for its own online analysis which is fundamentally different from the previously described event analysis (see Chap. 3). In case the supernova analysis detects an interesting event it can request additional unfiltered hit data from the DomHubs (see Chap. 3.5.1). This allows a subsequent analysis of the interesting time region to overcome the 2 ms resolution limit of the original supernova online analysis.

2.6 Monitoring and control

The IceCube data acquisition system (DAQ) needs to control and monitor a cluster of more than one hundred data hubs and servers. This task is split into two levels. The *Command and Control* (CnC) server handles all control communication and directly controls all low level components of the surface DAQ system. The CnC system can stop data taking if problems are detected and it is notified whenever a component is started. It also manages the components during run transitions. The messaging protocol in use is based on XML-RPC.

The IceCube Live system (I3Live) offers a user control and monitoring interface including a convenient web service. The CnC server as well as all secondary subsystems regularly report the status of all components to I3Live. This mostly Python-based project is also responsable to collect log messages from the DAQ system and to generate and transmit alerts from the subsystems, for example via e-mail to the responsable experts. The web based user interface provides a convenient way for operators to observe the current state of all DAQ components or to browse respective log files. Control commands can also be entered and are relayed to the CnC system.

As there is no continouous internet connection between the experiment site and the various operators and experts around the globe, two instances of the I3Live system have been established. An on-site "southern" instance of I3Live directly interacts with the DAQ as described using gigabit ethernet connections. All monitoring and log messages are additionally synchronised to a "northern" I3Live server which is fully available via the internet. Control commands which are entered into the northern I3Live instance are transmitted south vice versa and executed at the experiment site. This message exchange happens in JSON[3] format via the ZeroMQ[4] message library. The data is then transmitted via different commercial satellite streams based on predefined message categories. Messages with a higher priority are reflected more quickly on the northern mirror server whereas low priority messages may use a different stream with a higher bandwidth and higher latency.

2.7 Related noise sources

Multiple independent factors contribute to the pool of noise sources. They are originating from within the optical modules or the glass pressure sphere without being triggered by an external (e.g. Cherenkov) photon. This so-called dark noise rate of the standard optical modules is 540 Hz on average.

[3] The JavaScript Object Notation is a language independent text format

[4] ZeroMQ (also spelled ØMQ, 0MQ or ZMQ) is a high-performance asynchronous messaging library, aimed at use in distributed or concurrent applications. See www.zeromq.org.

- **Thermal noise** from the electronics is identified as Johnson-Nyquist noise [73] which is inherent to any electronical system due to thermal disturbance of electrons and is temperature dependent.
- **Thermionic noise** originates from the photomultiplier tube and is caused by the emission of electrons from (hot) metal surfaces. Both thermal and thermionic noise increase quadratically with temperature following a Richardson-type law on thermal emission. They are responsible for <10 Hz of the total dark noise rate.
- **Afterpulsing** occurs when residual gas in the photomultiplier tube is ionised by accelerated electrons between the dynodes. The resulting ions are then also acellerated and cause an additional delayed electron cascade. This effect is estimated to be responsible of ≈30 Hz of the dark noise rate.
- **Triboluminsecence** is light emission caused by the application of mechanical stress [74]. This process is associated with the so-called *freeze-in* process of the drill hole. The pressure which is created during the re-solidification of the water in the drill hole causes molecular bonds to break in the ice and causes light emissions. For the first couple of weeks this noise effect is orders of magnitude higher than all other noise sources. Triboluminsecence is affecting the sensitivity of the DOM for supernova analysis of the first couple of years after deployment [75].
- **Radioactive decay in the PMT and glass pressure sphere** is believed to be responsable for the vast majority of the dark noise. A feature of this noise contribution are hit bursts lasting up to several milliseconds which have not yet been fully understood. Sources are Potassium (^{40}K) and decays from Uranium to Thorium [12].
- **Atmospheric muons** are produced in the atmosphere by charged cosmic rays. If their energy is sufficient, they can penetrate the IceCube detector and contribute to the noise rate with up to 16 Hz depending on the depth of the optical module and the surrounding ice properties [1].

Fig. 2.5 illustrates the total dark noise time difference distribution at different temperatures. An abundance of short time intervals is observed which is more prominent at lower temperatures and cannot be explained by afterpulses alone. An additional process must be responsible for the increase in the noise rate for temperatures lower than 260 K [76]. The rate increase with lowering temperature can be experimentally fitted [77] and is more prominent for a photomultiplier which is inside a glass pressure sphere. It is currently speculated that luminosity effects are triggered by the above mentioned radioactive decay processes and that these effects get more efficient at lower temperatures. Fig. 2.6 shows an example of this corellated noise in form of a burst of hits following a large pulse. The IceCube supernova online analysis removes most of the corellated noise background by introducing an artificial deadtime of 250 μs [22].

The atmospheric muon background component is small compared to the total noise rate of the module. It is still an important background for the supernova analysis which assumes each optical module to be an independent counting experiment. Atmospheric muons on average create hits on multiple optical modules when passing through the detector. This will produce a higher

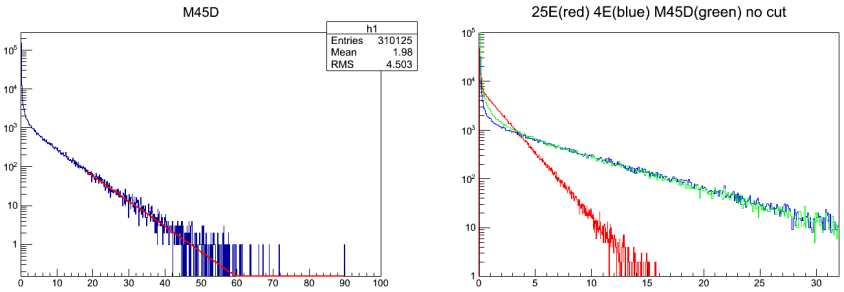

Figure 2.5: Distribution of time differences (in ms) between hits in a DOM and the exponential expectation for a Poissonian process fitted in the range of 20 to 60 ms (left, red curve). The contribution of corellated noise hits is visible from the excess in hit time differences <6 ms. The left dataset has been taken at a temperature of -45 °C and with the bare PMT without the glass pressure sphere. The three datasets on the right have been taken at three different temeperatures of 25 °C (red), 4 °C (blue), and -45 °C (green). For higher temperatures, the thermal hit rate increases leading to a lower time difference between hits and hence to a steeper curve. For lower temperatures, the effect of the corellated noise hits becomes more and more prominent for small hit time differences.

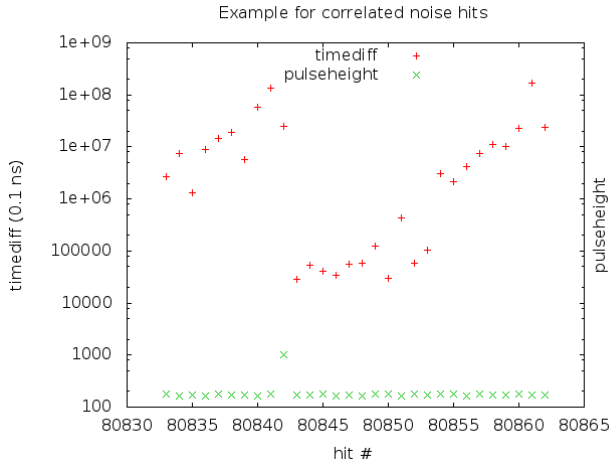

Figure 2.6: Data taken from an optical module test setup. Hits are arranged in sequential order displaying the time difference to the previous hit on the ordinate axis. The green curve shows the intensity of the hit. The data extract shows that large pulses are followed by a number of high frequency afterpulses.

Table 2.1: Current and a selection of proposed or planned supernova detectors [11, 80]. The four different detection technologies employed are: Water Cherenkov (WCh), Scintilator (Sc), Liquid Argon (LAr), and Lead. The detector volume is given in 10^6kg, the number of events refers to a supernova at a distance of 10 kpc and the mass is specified in megatonnes.

Detector	Type	Location	Mass	Events	Status
IceCube	WCh	South Pole	3000	$8{\cdot}10^5$	running
Super-K	WCh	Japan	32	8000	running
LVD	Sc	Italy	1	300	running
KamLAND	Sc	Japan	1	300	running
Borexino	Sc	Italy	0.3	100	running
Baksan	Sc	Russia	0.33	50	running
Mini-BOONE	Sc	USA	0.7	200	running
Daya Bay	Sc	China	0.33	100	running
HALO	Lead	Canada	0.079	20	running
NOνA	Sc	USA	15	3000	running
Icarus	LAr	Italy	0.6	60	running
MicroBooNE	LAr	USA	0.17	17	running
SNO+	Sc	Canada	1	300	construction
LENA	Sc	Europe	50	15000	future
Hyper-K	WCh	Japan	540	110000	future
LBNF	LAr	USA	40	?	future

than expected number of DOMs over a certain threshold, hence artificially increase $\Delta\mu$ in Eq. (3.4) and subsequently broaden the significance distribution of supernova events. Several techniques have been developed to identify and filter out the atmosperic muon background in the online analysis [78, 79] as well as in the high resolution datasets [1] which are used in this work.

2.8 Supernova neutrino detectors

Four different detector technologies [80] are currently being used to detect low energy supernova neutrinos. Each detection method and detector material allows for different neutrino properties to be explored. An overview of present and future detectors implementing these technologies is given in Tab. 2.1.

Water Cherenkov detectors, such as e.g. Super-K, use water as interacting medium and exploit the Cherenkov effect to indirectly observe the neutrino. Detectors like IceCube or the planned KM3NeT [81, 82] are exceeding the size of what can possibly be built artificially. In their so-called *longstring* configurations, they instrument very large natural bodies of water or ice. In case of IceCube this is the South Polar glacier ice which offers the clearest and most transparent natural medium on earth. Water Cherenkov detectors are in general not primarily dedicated to supernova detection. IceCube's large volume makes it also sensitive to supernova events via the main neutrino reaction channel of inverse beta decay (IBD). The Super-K detector is substancially smaller but has a very low energy threshold of $\mathcal{O}(5\text{ MeV})$ which enables it to observe more reaction channels. Based on the directionality of elastic scattering processes of

electron neutrinos on electrons, it is able to exploit the high number of neutrinos originating from the deleptonisation peak and to determine the direction of a supernova to $\approx 10°$ [83]. Via the positron energy of the IBD, Super-K is able to determine supernova neutrino energies with a resolution of 15% at 10 MeV [84].

Scintillator detectors also indirectly observe neutrinos via their charged reaction products which deposit energy in the hydrocarbon based detector material. The relaxation of its molecular energy levels produces detectable light. The *Large Volume Detector* (LVD) [85], which is dedicated to supernova searches is one example of this type. As the light emission from de-exitation of the scintillating material is fairly isotropic, it provides little direction information. LVD expects an energy resolution of $\sigma_E/E = 0.3/\sqrt{E}$ [86] and can set a limit on the galactic supernova rate of < 0.1 per year with 90% C.L. [87]. The main detection channel is again inverse beta decay but scintillator detectors can additionally measure the low recoil energy protons from neutral current elastic scattering processes which enables them to gain information about the heavier neutrino flavours as well [88].

Lead based detectors offer interesting possibilities to observe supernovae neutrinos as they are primarily sensitive to ν_e and ν_x reactions. Anti neutrino reactions are suppressed by Pauli blocking due to the excess of neutrons in lead. Due to high neutrino cross sections and high density, lead detectors can be build very compact at a low cost. *The Helium and Lead Observatory* (HALO) implements this technology [89] and is also dedicated to detect supernova neutrinos. The main channels are based on the reaction of $\nu + {}^{208}\mathrm{Pb}$ producing either one or two neutrons which can subsequently be detected in the surrounding ${}^{3}\mathrm{He}$ chambers. The ratio of the single- to double-neutron ejections can be used to derive a neutrino energy spectrum. Supernova direction reconstruction is not possible.

Liquid argon detectors also offer a relatively high cross section for neutrinos a low energies < 20 MeV. This makes them ideal instruments to e.g. perform oscillation studies or to observe supernova neutrinos. One example is the *Icarus* experiment which uses a large time projection chamber filled with 600 kt of liquid argon (LAr-TPC) [90]. The dominating interaction ($\nu_e + {}^{40}\mathrm{Ar} \rightarrow e + {}^{40}\mathrm{Ar}^*$) enables the observation of the deleptonisation peak. Similar to Super-K, pointing potential is given via direction sensitive elastic scattering processes on electrons.

Chapter 3

Supernova Data Acquisition

This chapter describes IceCube's supernova data aquisition system (SnDaq), its control and monitoring components, low and high level data quality surveillance tools, and the respective improvements which have been implemented. A new data aquisition component, called hitspooling has been developed [1], and is connected to SnDaq. The main goal of the work presented in Chapter 3.6 is to improve the data taking uptime of IceCube's supernova data acquisition system to exceed 99%. By the time of writing this chapter, this goal was exceeded and the average system online coverage was $\approx$ 99.7%. An overview of data acquisition uptime between 2012 and 2016 along with additional measures is summarized in [79]. Furthermore, SnDaq is integrated into a new IceCube-wide experiment control and monitoring system called IceCube-Live.

3.1 Supernova detection method

IceCube's primary task is to detect high energy cosmic neutrinos in the $\mathcal{O}$(TeV) to $\mathcal{O}$(PeV) energy range. Neutrinos of this high energy produce charged leptons in the ice which travel up to hundreds of meters emitting detectable UV Cherenkov light. The spacing between IceCube's optical sensors has thus been arranged to be on the order of tens to hundreds of meters, covering a total of $\approx$1 km^3.

The average energy of neutrinos originating from supernovae is $\mathcal{O}$(10 MeV). The respective positrons, which are produced through inverse beta decay only show a travel length of a few centimetres in the ice. It is therefore unlikely, with a chance of only a few percent, that light emitted from one positron is detected by multiple modules. Modules also show an average noise rate of $\approx$540 Hz making it impossible to distinguish indiviual supernova neutrino hits within IceCube.

IceCube, however, has another handle on detecting supernovae events. As $\approx$99% of the gravitational binding energy of the dying star is emitted in form of neutrinos, the respective flux is very high within a relatively close region of the cosmos. Due to the number of optical modules and the scale of IceCube, it has been shown [12] that a significant rise in the detector backgound noise rate can be observed for supernovae in the Milky Way. For a supernova happening in the centre of the galaxy, IceCube is expected to observe the combined effect of 40,000 times more neutrinos than were detected from SN1987A.

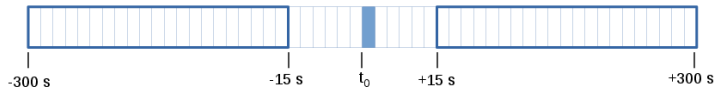

Figure 3.1: During one SnDaq analysis cycle, the noise rate of the centre bin is compared to the average noise rates in the two 5 min sidebands. An additional 30 s exclusion zone around the centre bin prevents the supernova signal from shifting into the sideband region. SnDaq performs analyses in four different time binnings of 0.5 s, 2 s, 4 s and 10 s. As each analysis is shifted only by 0.5 s after each analysis cycle, this results in 1+4+8+20=33 concurrent realtime analyses.

A separate data acquisition software, which is described in the next section, monitors the noise rate of all IceCube optical modules. If the software detects a significant increase of the combined noise rate an alert is issued and further automated and manual steps are performed depending on the significance of the increased rate.

3.2 Supernova data acquisition system - SnDaq

The IceCube supernova data aquisition (SnDaq) system is designed to contineously monitor module noise rates for significant rate changes. The optical modules have an internal hit counter based on an ≈1.6 ms clock. This data are called scaler data. SnDaq synchronises the scaler data over all modules using a GPS clock and organises it in time bins of 2 ms. In a second step, the data are rebinned to 500 ms, defining the base binning for each of SnDaq's realtime sliding window analyses. Based on expected signal durations on the order of 10 s and to account for model uncertainties four analysis time windows of 0.5, 2, 4 and 10 s are defined. Each sliding window is shifted by 0.5 s throughout the analysis process resulting in a total of 33 concurrent realtime analyses.

The scheme of each of SnDaq's analysis is shown in Fig. 3.1 in their respective bin size. As the analysis progresses, the centre bin is compared to the average rate of two surrounding 5 min sidebands defining the current background rate of the detector. Two regions of 15 s each directly surrounding the centre bin are excluded from the background definition in order to prevent a broad signal from shifting into the sideband region.

The most likely collective rate deviation $\Delta\mu$ of all DOM noise rates r_i from their individual $\langle r_i \rangle$'s, assuming the null hypothesis of no signal, is obtained by maximizing the likelihood

$$\mathscr{L} = \prod_{i=1}^{N_{DOM}} \frac{1}{\sqrt{2\pi}\sigma_i} \cdot \exp\left(-\frac{(r_i - (\mu_i + \epsilon_i \Delta\mu))^2}{2\sigma_i^2}\right) \quad . \tag{3.1}$$

The factor ϵ_i contains a correction for module and depth dependent detection probabilities. An analytic minimization of -ln($\mathscr{L}$) leads to

$$\Delta\mu = \sigma_{\Delta\mu}^2 \sum_{i=1}^{N_{DOM}} \frac{\epsilon_i (r_i - \mu_i)}{\sigma_i^2} \tag{3.2}$$

with an approximate uncertainty of

$$\sigma^2_{\Delta\mu} = \left(\sum_{i=1}^{N_{DOM}} \frac{\epsilon_i^2}{\sigma_i^2} \right)^{-1} \quad . \tag{3.3}$$

The significance

$$\xi := \frac{\Delta\mu}{\sigma_{\Delta\mu}} \tag{3.4}$$

should approximately follow a Gaussian distribution with unit width centered at zero if the background is uncorellated and statistics are high. In practice, the width turns out to be larger. This broadening is due a to non-Poissonian influence of hit clusters deposited by atmospheric muons. The online analysis is described in full detail in [91].

An online muon subtraction algorithm has been developed based on binned muon hit rates determined by internal triggers of IceCube's main data acquisition [92]. This feature enables IceCube to reduce the effect of significance broadening in the online analysis. It also reduces the seasonal dependence introduced by the muon hit rate which depends on atmosperic pressure and temperature.

3.3 Supernova alert scheme

In case the SnDaq detects a high significant rate in one its analyses, different actions are being automically performed depending on a corresponding significance threshold. A reason for why a specific threshold was chosen is given below. The significance values appear very large, as they are based on the original corellated noise background. A new set of thresholds were developed in the meantime which are additionally based on the muon corrected noise background [79].

- 6.00: Alert E-Mail to the supernova working group email list, latency: $\mathcal{O}$(min). Transmit alert data to the IceCube Live monitoring and control system and to the IceCube SNEWS[1] gatway as a test message, latency: $\mathcal{O}$(s). A significance of 6.00 would allow for a detection of a SN in the Large Magellanic Cloud. As it happens multiple times a day, it is also an ideal choice to serve as a heartbeat for the alert system(s).

- 7.30: Extract 90 s of fine binned 2 ms data and transfer this data north for immediate inspection. Latency: $\mathcal{O}$(h). Send max one dataset per day.

- 7.65: Transmit alert time to the Supernova Early Warning System. Latency: $\mathcal{O}$(s). One alert is produced in ≈10 days (see 3.5.5).

- 7.65: Extract 90 s of individual hit data with $\mathcal{O}$(ns) precision using the HitSpool interface as described in section 3.5.1. Latency: $\mathcal{O}$(d).

- 8.00: Alert SMS to list of SMS subscribers. Latency: $\mathcal{O}$(s). Allow only ≈ one SMS per month.

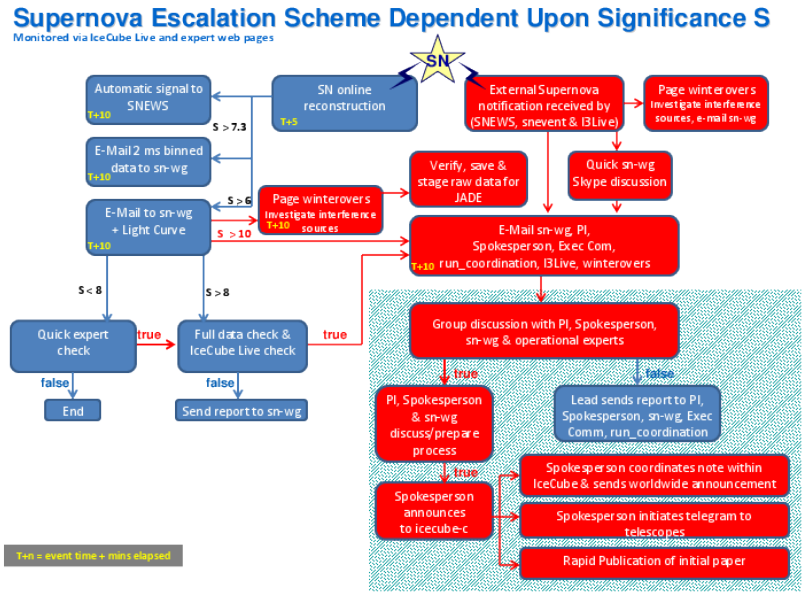

Figure 3.2: The Supernova alert escalation scheme [93] outlines different actions to be taken depending on the significance value of the alert. Significance values >8 result in a full manual data check by experts in the north. Significance values >10 will additionally cause an automated set of instructions to be sent to the winterover personnel on station.

In addition to the automatic alert actions, the supernova working group has derived an alert scheme which covers manual actions linked to certain significance threshold. The supernova escalation scheme dependent upon the significance is shown in Fig. 3.2.

3.4 Data transport and processing

The SnDaq scaler dataflow is shown in Fig. 3.3. Currently, the main data aquisition system pDaq receives both hit and supernova-scaler data. It packages each 60 s of data into one file which is then loaded and processed by SnDaq. SnDaq also currently relies on a helper tool "process_files.pl" which acts as a buffer between the two data aquisition systems in order to ensure that only completed files will be loaded into SnDaq. This procedure causes an additonal data processing delay of up to 1 min.

The "process_files.pl" additionally takes care of moving SnDaq output data and SnDaq logfiles into the appropriate satellite transfer dropboxes. It also maintains a 24 hours backup storage of unprocessed scaler data as well as 7 days of processed data files.

[1] The Supernova Early Warning System is described in 3.5.5.

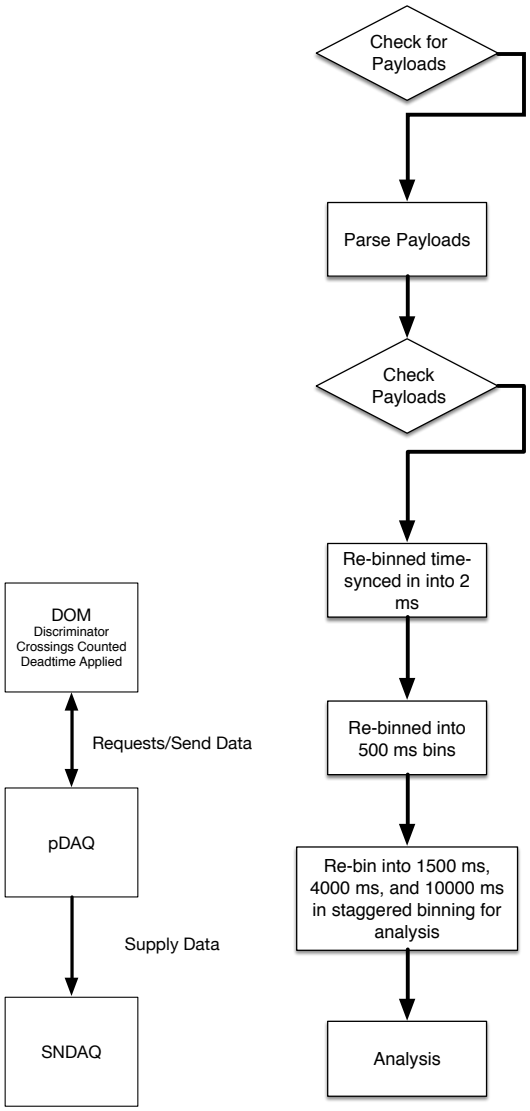

Figure 3.3: The left image ilustrates data transfer from the optical modules to SnDaq. The right image shows the rebinning and processing dataflow within SnDaq. From [75].

Currently a new data collection system named OmicronD is being developed. Its purpose is to decouple data collection and processing. OmicronD would continuously record hit and scaler data into large buffers and make it available to consumers such as both pDaq and SnDaq equally. Data collection would then also become continous over run transitions. SnDaq could then continously consume data from OmicronD without being affected by pDaq special runs or pDaq downtime.

Fig. 3.4 shows in more detail the available dataflow channels for SnDaq on the southpole systems. Endpoint of the data channels can either be user notifications/ alerts, permanent data storage or temporary data storage/ cyclic buffers.

3.5 Technical components

The technical development of IceCube still progresses, new components are being developed aiming at different goals like increasing detector stability and uptime, simplifying monitoring and control mechanisms or minimising data transmission times. Especially the field of broadband communication with the South Pole is difficult as there can be no geo-stationary satellites. Sparse satellite availability is subject to constant change outside of IceCube's influence to which the whole system has to adapt.

In the course of this work, the supernova data aquisition system has been made compatible with e.g. new data aquisition, monitoring and transmission systems. Whereas originally every IceCube component, like SnDaq, had to worry about its own data transmission and monitoring, these processes are now being handled by a central system to which every subsystem can connect. A new on-demand high resolution datastream has been developed which can now be triggered by SnDaq in order to obtain additional information in case of a supernova event.

3.5.1 The hitspooling system

In addition to the scaler data, which are used exclusively by the supernova system, each optical module also stores information about every individual hit it receives with $\mathcal{O}(0.1\ \text{ns})$ precision. These are extracted from the modules and collected on the respective machine responsable for one IceCube string. This machine is called a domhub. The hit data is then processed by IceCube's trigger and filtering chain producing datasets for higher order high enegy neutrino data analyses. The hit data is now additionally forked before the trigger and filter systems and stored up to 48 h on the domhub. This data buffer is called the hitspool buffer.

A newly developed system provides an interface to facilitate an extraction of a specific time range of hit data from the hubs. This interface is called the hitspool interface. Its functionality is outlined in Fig. 3.5.

Whenever SnDaq detects a high significance in one of its analyses surpassing a given threshold, the hitspool interface is tasked to extract 90 s of unfiltered raw hit data from the buffer on the hubs. The hit data is packed and handed to the satellite transfer system for further analysis in the north.

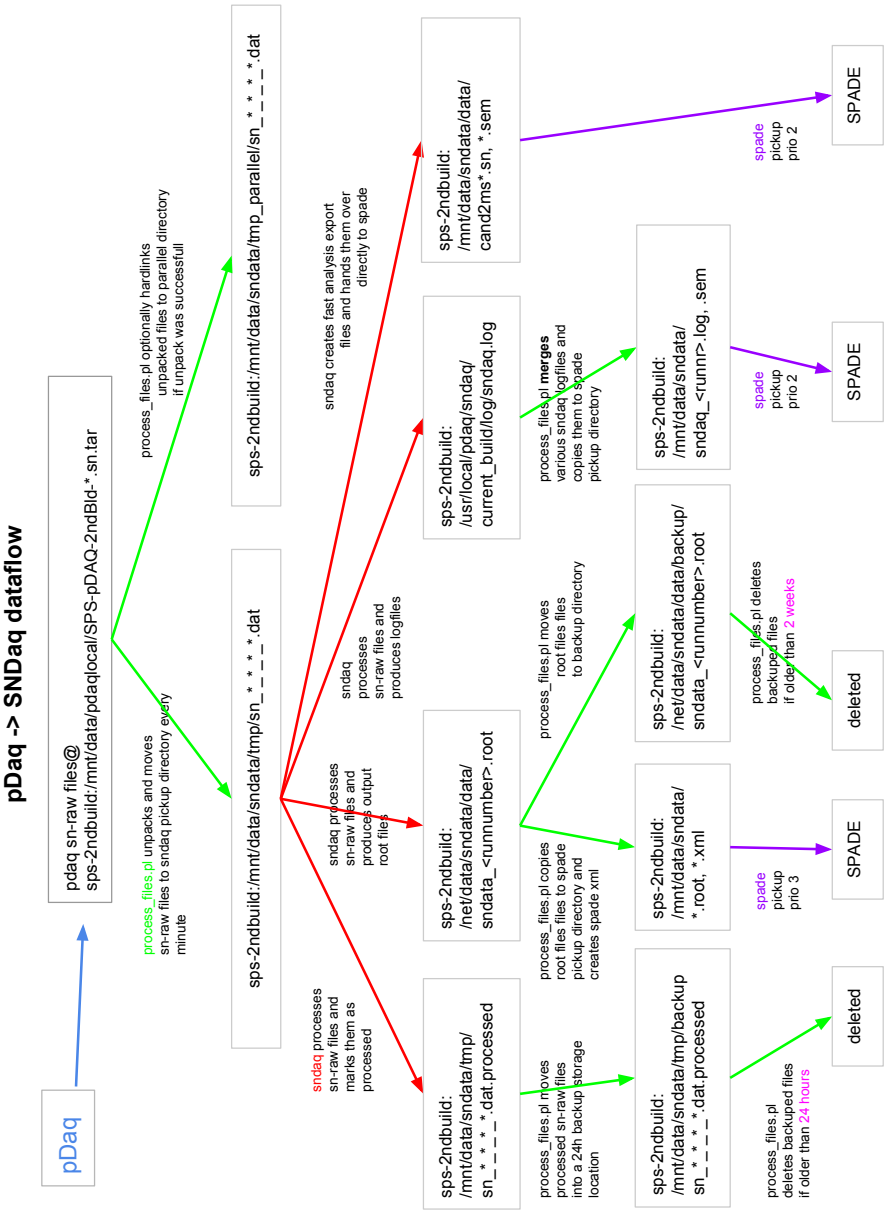

Figure 3.4: This is an almost complete visualisation of the supernova data flow, from recording to alert notifcation and permanent data storage. The blue arrow illustrates data transfer handled by the main data aquisition software pDaq. The green arrows show data being transported by the SnDaq helper tool "process_files". Red arrows show data that is moved by SnDaq itself and the purple arrows indicate that data is picked up by the satellite transfer and archival system.

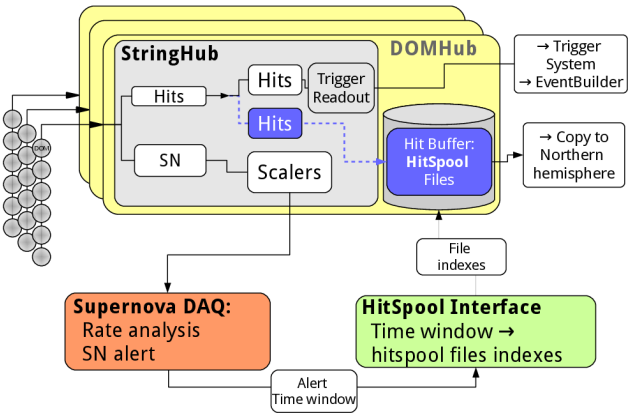

Figure 3.5: This figure ilustrates the two different data streams being extracted from the optical modules [1]. The scaler stream is sent to SnDaq whereas the hit stream is sent to the trigger system. The hit stream is additionally duplicated and stored into a ring buffer with a size of currently 150 h. Based on an alert in SnDaq's scaler analysis, it can then request additonal hit data from the hitspool buffer for a subsequent manual or automatic analysis.

3.5.2 Satellite data transfer channels

The IceCube IT infrastructure at the South Pole is connected to the internet through different satellite providers and technologies which are mainly managed by ASC (Antarctic Support Contract/ Lockheed Martin) for the NSF[2]. This section provides an overview of the channels being primarily used by SnDaq's messaging and data transfer system. Internet connectivity is available 24 h per day but the capabilities of the different satellite channels that are available at different times vary greatly.

Science data is mainly transferred using NASA's tracking and data relay satellite system (TDRSS[3]) which was build to support communication with independent projects like satellites, balloons, aircraft, and the International Space Station. TDRSS increases the usable communication time windows w.r.t. previous ground based communication stations. The South Pole system (SPS) connects to TDRSS through the South Pole TDRSS Relay (SPTR) which was originally built in 1997. SPTR-2 today offers a 150 MBit uplink for science data transfer and a 5 MBit uplink for general user internet access during the TDRS-6 satellite visibility window. IceCube queues about 100 GB/d through the SPTR-2 link.

Furthermore, SPS also connects to the British Nato-4B satellite in the military satellite system SKYNET[4] and to the NASA GOES[5] weather satellite system which provides an uplink of ≈1 MBit. Those systems are mainly used for emailing and user data. An example of the visibility windows of the SKYNET, TDRS and GOES satellites in use can be found in Fig. 3.6. Currently an addi-

[2] National Science Foundation: https://www.nsf.gov/
[3] https://www.nasa.gov/directorates/heo/scan/services/networks/txt_tdrs.html
[4] https://en.wikipedia.org/wiki/Skynet_(satellite)
[5] https://www.nasa.gov/content/goes

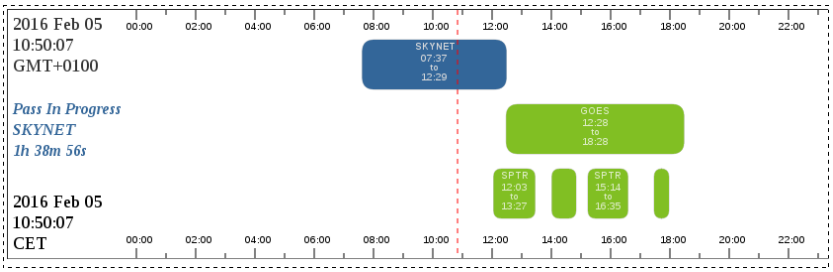

Figure 3.6: Satellite availability display showing the SKYNET, TDRS and GOES usage times for the current day. This display is self updating and available on an IceCube internal website[6].

tional connection is being established to the Defense Satellite Communications System (DSCS) in order to increase usable internet time at SPS by several hours per day.

Additional connectivity but reduced functionality is provided by different products of the commercial Iridium satellite network which all offer a 24 h coverage. The Iridium system consists of 66 operational satellites flying on 6 polar orbits. Satellites can relay signals via their neighbours thus not requiring any ground station between two communicating partners. Given that there are no obstructions, users will always be able to connect to at least one satellite at any time at any place on the planet. Given the polar orbits of the satellites, their density increases towards both poles making them an ideal communications choice in (Ant-)Arctic operations.

The so-called IceCube teleport system (ITS) is an Iridium short burst data (SBD) channel. It supports only up to 1800 characters of ASCII data per message with a message transmission time of only seconds.

The Iridium *icms* system is used to provide the so-called thinlink, a 24 h ssh access to the SPS system which is limited to one person at a time. *icms* also provides an E-Mail service supporting messages on the order of 10 kB in size with delay times of $\mathcal{O}(10)$min.

IceCube currently established its own independent satellite link between the IceCube Lab at the South Pole and the headquarter in Madison using the Iridium *Rudics* product. This will enable 24 h multi user ssh access at improved speed and latency. It also enables round the clock data transmission on the order of 100 kB per message. This data transmission will not be based on E-Mail but on the new IceCube messaging system I3MS. More information on message an data delay can be found in chapter 3.6.6.

3.5.3 IceCube Live monitoring and control

In the course of this work SnDaq has been fully integrated into an online monitoring and control system called IceCube-Live or I3Live. This new system offers realtime data quality monitoring as well as a monitoring and control of all of IceCube's technical systems such as the main data aquisition component pDaq, SnDaq or the trigger and filter system. SnDaq has also been integrated into

[6] https://internal.icecube.wisc.edu/satellite/riseset_table.php

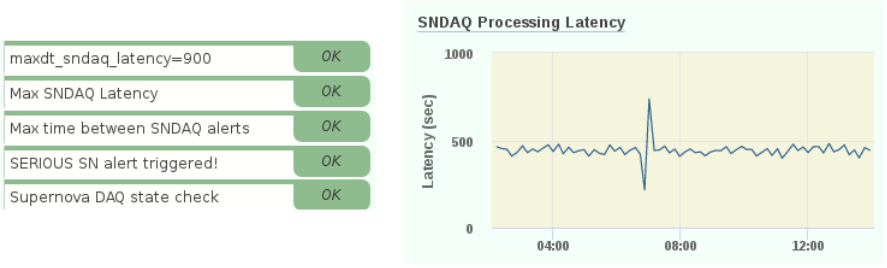

Figure 3.7: On the right, SnDaq's processing latency is displayed over time. The left side illustrates five alert handles which have been attached to SnDaq's monitored status variables. The two upper items, for example, trigger an alert notification in case SnDaq's latency increases over 900 s or if the variable itself has not been transmitted any more for the same time. Alert notifications can be of different types. The state check for example generates a notification email if SnDaq's state is not reported as "running", it then also issues an automatic restart. Subsequently, if restarting fails and SnDaq's processing latency is not reported as mentioned before, a pager-alert to the station personnel is issued. If a serious alert is triggered, all available channels are being notified including text messages to selected cell phones. Compiled from a screenshot of IceCube-Live's main status page[8]. A complete screenshot can be found in [69].

a new extension of I3Live which is called *moni2.0* and provides monitoring of physics variables being collected by IceCube.

A list of quantities, respective transmission frequencies, as well as transmission priorities have been worked out for SnDaq. The aim hereby was to compile a set of quantities that would enable to present an almost complete overview of SnDaq's operational status as quickly as possible to human experts, enable automatic failure detection of the SnDaq system, while simultaneously minimising the overall data transfer amount between the South Pole system and the "northern" I3Live servers. SnDaq's processing latency has been one of the piloting quantities to be displayed on the main overview page of the new IceCube-Live system.

IceCube subsystems in general feed data into the I3Live system at South Pole which is then automatically mirrored onto a server in the North, whenever satellite connectivity permits. Control commands entered into the I3Live system in the North are being transmitted South in the same fashion. I3live offers a convenient django[7] based modular website which combines all of its features into one easy to use web interface.

Components communicate variables and log messages to I3Live using the 0mq[9] messaging library. I3Live monitors these variables and can display them in various ways on its web page such as e.g. text, status indicators or graphical display as evolution of the variable over time (See Fig. 3.7). It also allows for specific tests to be attached to a variable. These can be e.g. simple threshold, rate or timeout tests. If one of these tests fail, I3Live can initiate actions such as to restart a component. As the system is integrated into the station's paging,

[7] Django is a high-level Python Web framework: https://www.djangoproject.com/
[8] https://live.icecube.wisc.edu/
[9] 0mq is a distributed messaging library: http://zeromq.org/

email and phone system it can also notify station personnel and northern experts in different ways depending on the severity of the alert.

All available satellite channels are used by I3Live in order to transfer the information it receives onto to the northern mirror server. When submitting a variable or log message to I3Live, the submitting component specifies which satellite channel the information should use by defining its priority. This directly affects the delay time of the information before it shows up on the northern web pages.

The following priorities and transfer channels are available to be used when submitting information:

- priority 1: High priority via ITS. Message must be < 1800 bytes. As the system does not guarantee reception of the message, priority 1 messages are redundantly sent as priority 2.
- priority 2: Medium priority via *Rudics*. Messages/ datasets may have a size of up to $\approx$350 kB.
- priority 3: Low priority via SPTR. Datasets may have a size of up to $\approx$1 GB.
- priority 4: Datasets/ messages, which are received with a priority of 4, are only stored/ processed and displayed on the southern I3Live server and not transferred to the north.

The data are transmitted from subsystems to I3Live in JSON[10] format using the 0mq protocol. The JSON dictionary can contain various additional metadata describing the data and/ or trigger, as well as additional actions on the I3Live servers. Additonal metadata may be:

- a variable name which can be used to store and display these data in the I3Live system or to attach a test function,
- an email flag, corresponding adress and a subject text which triggers the I3Live server to forward the received dataset by email, as well as
- additional metadata such as the current run number, a timestamp, histogram binning information, etc.

SnDaq currently sends three different types of information to or through I3Live:

- Technical monitoring variables, such as data processing delay, memory consumption and current data processing rate. These data are displayed on the SnDaq technical details page in I3Live. Specific automated alerts have been coupled to these variables which can call for operator attentions should specific thresholds be crossed.
- Physics monitoring quantities such as analysis significances or sn hitrate per dom. These data are presented on a per run basis to the shift personnel. Automated predefined tests are being applied to these quantities in order to highlight irregularities. The monitoring shift is then discussed in a weekly phone call.

[10] JavaScript Object Notation: http://www.json.org/

- Alert messages which directly trigger email messages to different targets. This type of message is used to e.g. notify everybody in the supernova workinggroup of a potential supernova candidate.

Fig. 3.8 shows in detail all control, monitoring, and install components of SnDaq within the IceCube Live experiment control system. It illustrates both user control interfaces as well as automatic control features and monitoring components.

Technical variables and notifications

The following technical monitoring variables[11] are sent to I3Live by SnDaq. It was found that when adding a transmission timeout threshold test to one of the variables it could cover every failure situation in which human intervention is necessary. More details can be found in A.3.

- SnDaq processing latency, every 10 minutes, priority 2: The time difference between the actual time and the time of the current databin being processed is presented as a plot as a function of the actual time. An attached timeout-alert additionally triggers a paging call to the winterovers on station whenever this variable has not been transmitted for >15 min. It is then assumed that the SnDaq software has crashed, is not automatically recoverable, and needs human attention. The processing latency itself was found not to be an ideal criterion to identify a malfunction which needs human interverntion, as occasional data backlogs can occur.

- The value of every supernova alert significance, at every threshold alert, priority 1: A page[12] is also triggered whenever the alert significance >10. This is a very serious supernova candidate alert and requires the station personnel to check for possible sources of interference and to ensure that all systems work reliably.

- SnDaq quantities such as e.g. data processing rate, memory consumption, cpu load, number of scaler files queued to be processed by SnDaq, necessary free disk space, every 10 minutes, priority 2: These variables are transmitted as one dataset and are displayed as graphs and text on the I3Live technical details page.

The following alert messages are triggered to be sent by I3Live to supernova experts in case of supernova alerts, depending on its significance:

- notification to cell phones via short email and text message/ sms,

- notification to snews,

- notification to working group email lists such as sn-wg[13] and sn-urgent[14].

[11] https://live.icecube.wisc.edu/moni/?service=sndaq

[12] Winter personnel on station have pagers, which are wireless telecommunications devices that can receive and display alphanumeric messages. A page in this work generally means an immediate notification of the winter over personnel.

[13] The sn-wg email list contains every member of the IceCube supernova working group.

[14] The sn-urgent email list contains key people within IceCube according to the alert escalation scheme (see Fig. 3.2).

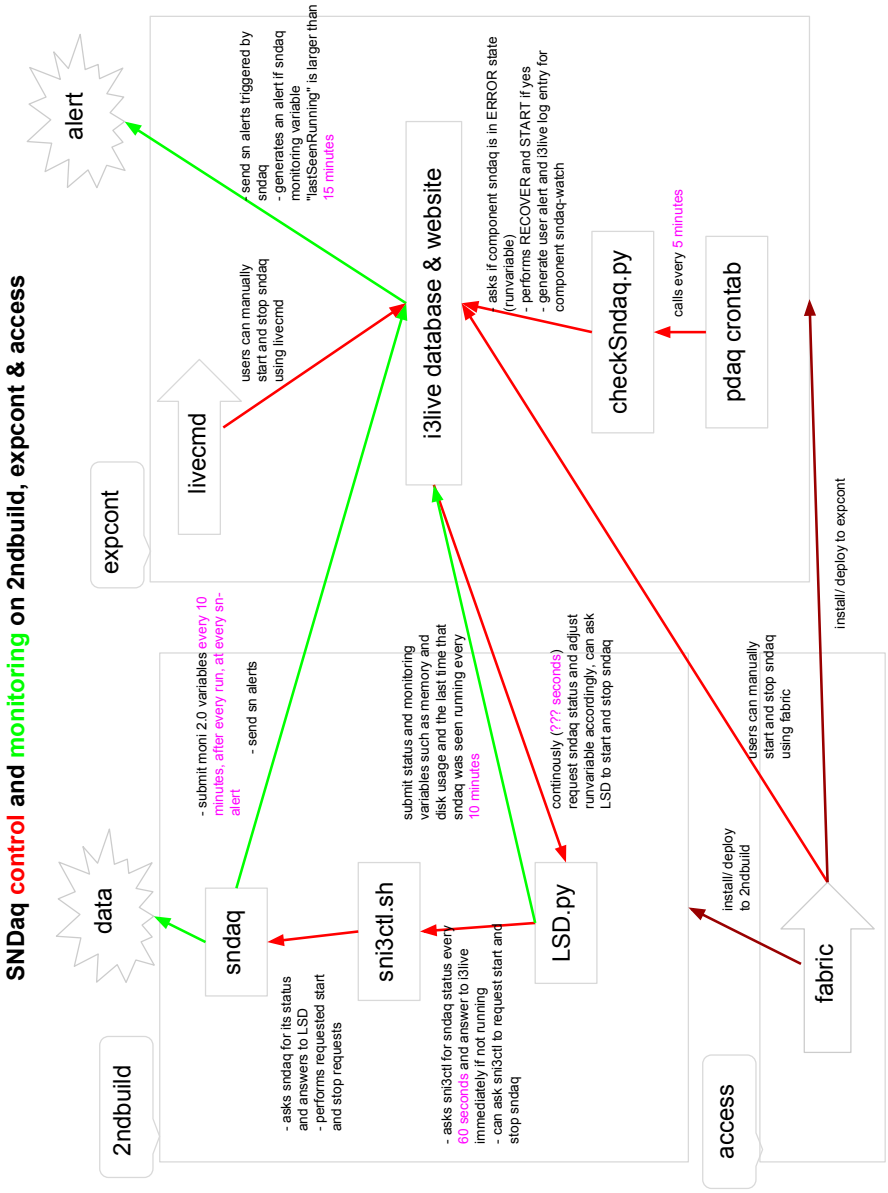

Figure 3.8: This figure shows a subset of the South Pole computing system (SPS) contaning three servers which are the ones mainly used to install, operate, and monitor SnDaq. Due to internet connectivity reasons, all software is downloaded to the *access* server. From *access* modules can then be deployed to the target servers at any time of the day. Deployment is performed using a python method called *fabric*. SnDaq software components are deployed to the *2ndbuild* and *expcont* servers. The *2ndbuild* server runs consumers of the IceCube secondary datastream, the supernova-scaler data. The *expcont* server runs the IceCube Live experiment control sofware and SnDaq control interface components.

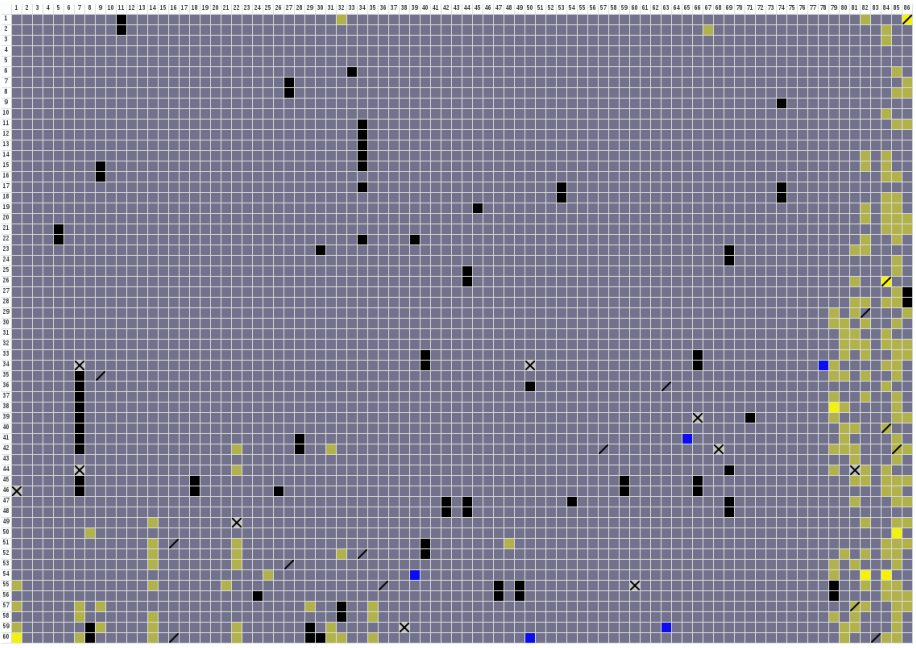

Figure 3.9: This matrix encodes the average supernova scaler rate for every optical module of one run. The modules are arranged per string from left to right and as module per string from top down. Blue color indicates a lower than average rate, yellow color indicates a higher rate which is mostly the case for IceCubes high quantum efficiency sub detector deep-core. If the rate per module differs significantly, its rate during the reference run then the module is flagged with an additional marker to attract the attention of then run shift taker. Black and crossed out modules are dead, modules marked by a single slash are known to be problematic. Based on a screenshot taken from the IceCube-Live monitoring system[15].

IceCube's new run monitoring system - Moni2.0

The Moni2.0 system is the second version of a run-based physics monitoring system within I3Live. The IceCube data aquisition system as well as trigger and filter systems regularly send specific quantities to the moni system such as optical module hit rates, filter or trigger rates or analysis significances. Specific tests are applied to these quantities which are then compared to previous reference runs. Irregularities are automatically highlighted. Per week, one IceCube member reviews the monitoring data of all the runs taken. The resulting report is discussed among experts in a weekly phone call.

Moni2.0 presents one web page per run and can display data in various different ways such as graphs or histograms including fits. The main feature of each moni page ist the so-called dom map, a 2D matrix of IceCube string over dom (see Fig. 3.9).

SnDaq monitoring quantities are displayed essentially in two different ways: quantity as a function of time or as an average value per run for every module

[15] e.g. https://live.icecube.wisc.edu/run/129697/

in the 2D matrix form. In particular, there are quantities that are displayed per 10 min time intervals:

- Minimum active channels (modules) per analysis binning: This is used as a check that the number of minimum active channels inside SnDaq per 10 min is not too low compared to the number of optical modules being active in IceCube's main data aquisition. A mismatch between these two numbers means that SnDaq deactivated some channels based on specific statistical rate tests, some of which will be mentioned later. If the number of minimum active channels drops below the test threshold, this usually hints at a technical problem affecting a larger number of DOMs at once (i.e. problems with a StringHub).

- Supernova scaler hit rate per dom: This quantity provides a count of noise hits in a given length of time. This is all the information from which the supernova hit rate can be derived. The supernova hit rate is the number of hits in a given time which have been seen by each dom including a 250 us non paralysing deadtime which is also applied by each dom individually. Checks for unexpected DOM behaviour are applied by comparing the rate to and average of previous runs.

Some quantities are evaluated on a per run basis as soon as the run has ended:

- Supernova alert rate: The SnDaq analysis bins the dark noise rate of the doms as a function of time in [0.5, 1.5, 4, 10] second bins. These binning values define the four different analyses of SnDaq. A sliding window background level is defined as a mean over five minutes before and after the bin the analysis processes. The value of the current bin is then compared to the background value which defines the significance per time bin. A significance value >= 6 defines a supernova candidate which also generates an alert in I3Live and a sn-wg alert email. This quantity defines the number of times that the significance value has exceeded a given limit (currently 3 and 6)[16] in a given time as a sum over all analyses.

- Status changes per dom: This quantity is send in order to monitor the frequency of (SnDaq-)dom-status-changes for each DOM. Doms are qualified and disqualified based on various data tests, whereby each disqualification or requalification is counted as one status change. SnDaq requires rate-mean, skewness and fano factor[17] of each DOM's rate to be within a certain range in order to qualify.

- Dark noise rate RMS in Hz per dom: Since proper Gaussian behavior of each DOM is necessary to carry out SnDaq's likelihood based significance calculation, it is important to monitor both mean rate and RMS of each

[16]The significance value of 3 (6) indicates the detection threshold for a supernova at the Small (Large) Magellanic Cloud. A value of 6 is also a typical threshold value above which alerts are being forwarded to the IceCube SNEWS gateway. As this happens multiple times a day they serve as test messages for the alert chain. The gateway server then only forwards alerts to the SNEWS coincidence network in excess of 7.65 sigma.

[17]These factors are used for example to detect sudden rate variations. A detailed definition can be found in [11] Chap. 3.1.2.1-3

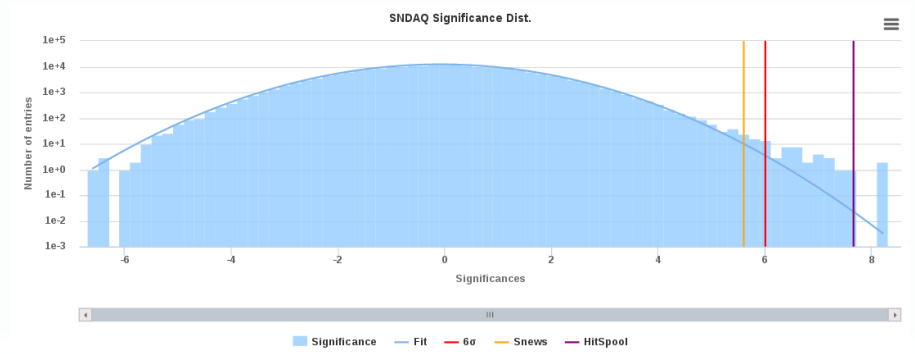

Figure 3.10: Monitoring2.0 SnDaq significance distribution per run as a sum of the significances over all analysis binnings. During this run, one significance value exceeded the current hitspool extraction threshold. Furthermore the *6σ-limit* is shown which is used as a trigger to test the alert message chain. The snews alert threshold was artificially lowered in this run to test a new data aquisition method which reduces the influence of atmosperic muons. Based on a screenshot taken from the IceCube-Live monitoring system.

DOM. The rate RMS is calculated from all 0.5 seconds analysis bins in this specific run.

- Significance distribution per run: The quantities are sent to monitor the quality of the significance distribution, which is a measure of defining a supernova candidate. The histogram will show the whole distribution for the run. This quantity is a sum of the significances over all analysis binnings.

3.5.4 IceCube's satellite transfer system

The majority of IceCube's science and monitoring data ist handled by the Java Archival and Data Exchange system (*JADE*)[18]. It manages the disk archival system on SPS and also offers an easy and transparent way for users to get data transferred from SPS into the northern data warehouse. From there it is available via the internet for further analysis.

Users can create empty folders on any server of the SPS system which produces data. These folders act as dropboxes for the *JADE* system and are continously monitored for new files. Once a data-file has been completely written to disk, the user process creates a so-called semaphore file with the same filename but a different suffix indicating that the data-file is ready for transfer. The semaphore-file can be an empty file or it may contain additional information on the data in xml-format which is then also processed by *JADE*.

Once *JADE* detects a new semaphore-file it is processed and the corresponding data file is transferred onto the *JADE* server which places it into the satellite queue. Both files are then deleted from the user system.

The *JADE* service holds a list of dropboxes and associates them with a specific transfer channel. The following transfer channels are available:

[18] *JADE* is an upgrade of the South Pole Archival and Data Exchange (SPADE).

- priority 2: Medium priority via *Rudics*. Messages up to ≈350 kB may be transmitted. This was formerly realised by sending up to 25 kB e-mail attachments through the Iridium *icms* system.

- priority 3: Low priority via SPTR. The data rate is limited in total to ≈105 GB/d. The processes are queued until SPTR is available for data transfer (see 3.5.2).

- priority 4: Files, which are received with a priority of 4, are written to the archival system's hard drives which are handcarried north once per year.

On the northern end, another server called *ingest* collects the incoming data from the different streams and places the data into the central IceCube data warehouse used by everybody for subsequent reconstructions or analyses. It then sends a receipt confirmation back to *JADE* on an hourly basis for bookkeeping. In the unlikely event of a failed transmission it will be retried. The following transmission latencies have been determined as an average over the 2015 SPADE transmissions:

- The average priority 2 e-mail took ≈16 min to reach the North. In total it took ≈1.3 h for the confirmation checksum to be received back by SPADE at the SPS.

- The average priority 3 file took ≈24.5 h to reach the data warehouse.

3.5.5 SuperNova Early Warning System - SNEWS

World-wide, ∼10 detectors currently running are sensitive to a core-collapse supernova neutrino signal in the Milky Way. New detectors such as Juno, are under construction. The neutrino burst signal emerges promptly from a supernova's core, whereas it may take hours for the first photons to be visible. Therefore, the detection of the neutrino burst from the next Galactic supernova can provide an early warning for astronomers. Requiring a coincident signal from several detectors will provide the astronomical community with a very high confidence early warning of the supernova's occurrence, reducing the false alert rate to approximately one in a century. In addition, a neutrino burst alert may be able to serve as a trigger for detectors that are not able to trigger on a supernova signal by themselves, allowing extra data to be saved.[19]

The SuperNova Early Warning System (SNEWS) project involves an international collaboration of experimenters representing current supernova-neutrino-sensitive detectors. The goal of SNEWS is to provide the astronomical community with a prompt alert of the occurrence of a Galactic core-collapse event.

SNEWS has been running in automated mode since 2005. Currently, as of October 2015, seven neutrino experiments are involved: Super-K (Japan), LVD (Italy), IceCube (South Pole), KamLAND (Japan), Borexino (Italy) Daya Bay (China), and HALO (Canada).

The SNEWS alert mailinglist is publicly subscribable[20] and issues an alert email whenever the following criteria are satisfied [94]:

[19] http://snews.bnl.gov/whatissnews.html
[20] http://snews.bnl.gov/mailinglists.html

- There is a 2 or more -fold coincidence within 10 seconds, involving at least two different experiments. (The time window refers to the maximum separation of any of the alarms in the coincidence.)

- At least two of the experiments involved are at different laboratories.

- Two or more of the alarms in the coincidence are flagged as GOOD or CONFIRMED. Available flags are: GOOD/ POSSIBLE/ TEST and CONFIRMED. GOOD alerts are being sent by IceCube during normal operation. TEST messages are being sent every six hours in oder to monitor functionality of the alert mechanism. The POSSIBLE flag could be used during special runs e.g. calibration runs, but in this case IceCube currently is inhibited not to send any alerts at all. IceCube also currently has no procedure implemented to send CONFIRMED alerts. These two alert flags could be implemented by IceCube in the future.

- For at least two of the experiments involved in the coincidence, the rate of GOOD alarms for several past time intervals T_i = 10 minutes, 1 hour, 10 hours, 1 day, 3 days, 1 week, 1 month preceding the first alarm of the coincidence candidate, must be consistent with the $\lambda_{\max} = 1/10$ days requirement (in other words, the observed rate must have a reasonably high Poisson probability). The precise condition is defined as follows: if an experiment sent n_i alarms in each of the last intervals T_i before the first event of the coincidence, then the Poisson probabilities P_i for n_i or more alarms in T_i, $P_i = \sum_{n=n_i}^{\inf} (\lambda_{max} T_i)^n e^{-\lambda_{max} T_i}/n!$ for each interval T_i, must each be greater than $P_{\text{thr}} = 0.4\%$. This corresponds to the condition that each n_i must be be less than {1, 2, 2, 3, 3, 5, 9} for the preceding intervals T_i.

When the first of the above listed criteria is satisfied, but at least one of the other criteria is not satisfied, the generated coincidence alert is only circulated amongst the SNEWS participants. In this case, the alert has to be checked by the individual experiment collaborations before any public announcement. No alert will be sent to the community by SNEWS until (and if) the individual alerts have been reflagged to satisfy all four criteria.

3.6 SnDaq improvements and new features

This section describes further improvements or developments of components of the SnDaq system that were introduced in the framework of this thesis. The main goals are higher uptime through stability improvements, lower downtime through improved logging and error descriptions and training of future on-site personnel and (much) faster alert channels including preview datasets. A multiple-alert-structure has been developed which is capable of sending up to four different datasets ranging from $\mathcal{O}$(100 bytes) to $\mathcal{O}$(10 Gb) with latencies from seconds to days, overall maximising the amount of transmitted information across all available delayed channels.

3.6.1 SMS and e-mail alerts

All alert messages are now being transparently sent via I3Live which takes care of and ensures delivery. This procedure allows for the data transfer channels to be centrally maintained within I3Live and enables additional functionality. The southern I3Live server receives alert information from SnDaq which are tagged with a transmission priority and forwards them to the northern I3Live server through the appropriate channel. Once they arrive, the alert data is either being stored in the database, displayed on the I3Live webpages or forwarded by email to specified targets.

As an example, we will discuss the changes to the delivery of the supernova working group (sn-wg) email list notifications which are sent for every alert exceeding 6 sigma. These e-mail messages contain the following information:

- alert time in UTC[21],
- significance of the alert and its error,
- the analysis binning which caused the trigger,
- run information such as run- and candidate-number,
- a todo-list based on the sn alert scheme, and
- χ^2 value of the alert significance and number of active channels.

These e-mail messages used to be sent directly from SnDaq to the working group e-mail list using the Iridium *icms* based e-mail system. In a first step, SnDaq was modified to send the alert information to the southern I3Live server tagged with a priority of "2". Based on this priority, I3Live itself would use *icms* in order to transfer this information to its northern mirror server which would then issue a regular email to the sn-wg email-list. The priority "2" channel has recently been transparently upgraded within I3Live from using *icms* to using icecube's own *Rudics* system. This enables users to send larger prio 2 messages at lower latencies.

A new feature is the implementation of alert SMS messages. It is now possible to also use the ITS system through I3Live in order to trigger an e-mail to be sent from the northern server to any specified target. As SMS messages only support up to 160 characters, this fits well into the size limit of the ITS stream of 1800 characters. SnDaq sends a < 160 character messages to I3Live containing the following information:

- alert time in UTC,
- significance of the alert and its error, and
- the χ^2 value of the alert significance.

The message is flagged with a priority of "1" and also flagged to generate an email in the north. The target E-Mail address is specified in the alert message JSON and points to a commercial email2sms gateway[22]. This gateway forwards the subject line of the e-mail as SMS messages to recipients as specified in the body of the incoming email as shown here for a specific example:

[21] Coordinated Universal Time, see Chap. 3.6.5.
[22] http://www.sms77.de/

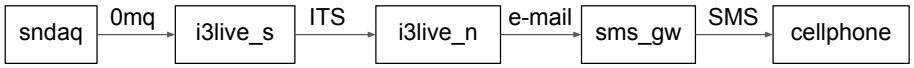

Figure 3.11: SnDaq can now instruct the I3Live server in the south to trigger an E-Mail to be sent from its northern counterpart. Communication between SnDaq and I3Live is performed using the 0mq data transport protocol. The instruction contains a target e-mail adress, an e-mail subject and header as well as a satellite priority flag. The priority flag for this message is "1" which instructs the souther I3Live server to transmit it to the northern server using the ITS channel. The northern I3Live server then generates an e-mail based on the instructions it received which is sent to a commercial sms gateway server. A list of recipient phone numbers is stored on the e-mail2sms gateway server; the subject line of the e-mail is then forwarded to all recipients.

- email subject line: 9.29537 signi[23] SN cand triggered on sps at 2015-11-26 17:08:05 in run #127170, Chi2: 5043.38
- email body: <key>#<recipients>#<sms-type>#<sender>

The e-mail api of the sms provider allows for an access key to be set. Preconfigured receipient lists can be referenced by name. The gateway provides two different SMS delivery channels at two different prices called basic and quality. We are using the quality channel. The sender name can be a short string which we set to "icecube", which shows up as the sender of the SMS on the cellphone.

The full data transport chain of the sms alert channel is shown in Fig. 3.11. It has a latency of mostly below 1 min to reach the user phone after the alert was issued at Pole.

3.6.2 Fast analysis data export and onset-time fit

SnDaq collects its analysis data per 8 h run in root data files. These files are $\mathcal{O}$(100 MB) in size and have a typical satellite transfer delay time of $\mathcal{O}$(d) through the *JADE*'s SPTR channel. In case of a high significance, supernova alert experts would have to wait this long to investigate this data. To shorten this time, using a higher priority *JADE* channel (see Chap. 3.5.4), a very condensed dataset surrounding the alert time is sent north within only minutes for investigation. The current threshold for this to happen is set to 7.3 sigma.

The duration of a supernova signal is expected to be on the order of 10 s [12]. In case of a high significant supernova alert, SnDaq therefore extracts 30 s of supernova scaler data before the alert and 60 s after the alert. In order to minimize the size of the condensed dataset, only the sum of the noise rates of all channels is exported but in the finest available time binning of 2 ms. To further reduce the number of characters in the datafile, the mean value of all bin entries is derived and subtracted from each bin. The resulting dataset is then sent

[23] This high significance supernova candidate alert from Nov 2015 was caused by a malfunction in one of the optical modules. It was chosen as an exemplary alert message here, as it also shows the importance of fast data access. Experts need to check the validity of the alert data as soon as possible after the alert message arrives. Due to satellite availability and bandwidth quota, supernova data has a delay of $\mathcal{O}$(d). One solution to remedy this situation is described in the next section.

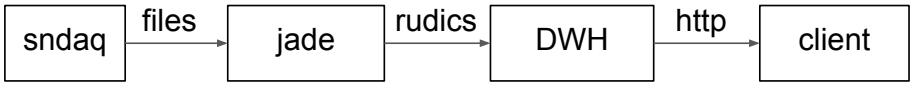

Figure 3.12: In case of a supernova alert, the corresponding light curve and all detailed analysis data will only become available to the North after $\mathcal{O}$(d). The data has to queue in for satellite transfer will as other large chunks of science data. In order to allow northern experts to view a condensed preview of the light curve, SnDaq extracts 90 s of scaler from around the alert time into separate files. These files are then put into a high priority dropbox of the satellite queing system *JADE* which transfers them to the northern data warehouse using *Rudics*. An automated fast analysis script checks for new data in the warehouse and displays the results on a web page [95].

through gzip which produces a final output file of approximately 60 kB in size. This method keeps the fast analysis data size well below the configured limit of 350 kB for *JADE*'s *Rudics* datastream.

The data transport chain is outlined in Fig. 3.12. The data is organised into the main IceCube data warehouse by *JADE* where it is then picked up by the fast analysis tool performing an automated analysis and display. Recent development of the I3Live system enables services in the south to transmit labeled messages to the southern I3Live server using 0mq. An additonal priority flag would determine the satellite channel to be used for the transfer. A subscriber to the I3Live message stream in the north could then be triggered to process the messages once they arrive. This method would significantly reduce the complexity of the current fast analysis data transfer mechanism and is currently under development.

Using different parametrisations, the light curve can be fitted and the onset time (and other features) be determined with millisecond precision. The method for doing this will be described in the following paragraph.

Fitting Methods

Based on the relation between detector hitrate and neutrino luminosity as described in Chapter A.1, the fast analysis data can be fitted to obtain physical properties of the supernova event. The data is first fitted based on the parameterized antineutrino flux from [96] (Pagliaroli-Fit):

$$\Phi_{\bar{\nu}_e}(t) = f_r(t)\Phi_a(t) + (1 - j_k(t)) \times \Phi_c(t - \tau_a) \quad . \tag{3.5}$$

This function contains two parts, one for the accretion ($_a$) phase of the neutrino emission and the cooling ($_c$) phase. The function $j_k(t)$ is used to interpolate between the two. An additional function $f_r(t)$ was added in [97] to describe the onset of the flux.

First we start with the antineutrino flux during the accretion phase in absence of oscillations (Φ_a^0)

$$\begin{aligned}\Phi_a^0(t, E_\nu) =& \frac{1}{4\pi D^2}\frac{8\pi c}{(hc)^3} \\ & \times [N_n(t)\sigma_{e^+n}(E - \nu)g_{e^+}(\bar{E}_{e^+}(E_\nu), T_a(t))]\cdot,\end{aligned} \tag{3.6}$$

where $N_n(t)$ is the number of target neutrons in the star, assumed to be at rest. Values for the thermal flux of positrons $g_{e^+}(\bar{E}_{e^+}(E_\nu), T_a(t))$ and for the cross section for positron interaction $\sigma_{e^+n}(E-\nu)$ have been taken from the paper.

The antineutrino flux during the cooling phase in absence of oscillations (Φ_c^0) is taken into account as follows:

$$\Phi_c^0(t, E_\nu) = \frac{1}{4\pi D^2} \frac{\pi c}{(hc)^3} [4\pi R_c^2 g_{\bar{\nu}_e}(E_\nu, T_c(t))], \tag{3.7}$$

where the Fermi-Dirac spectrum of the antineutrino is given by

$$g_{\bar{\nu}_e}(E_\nu, T_c(t)) = \frac{E_\nu^2}{1 + \exp[E_\nu / T_c(t)]} \tag{3.8}$$

and the timescale of the process is

$$T_c(t) = T_c \exp[-t/(4\tau_c)]. \tag{3.9}$$

The above mentioned time dependent factor

$$j_k(t) = exp[-(t/\tau_a)^k] \tag{3.10}$$

terminates the accretion phase around $t \approx \tau_a$ with $k = 2$ which leads to a smooth, continouous luminosity curve as found in numerical simulations. In order to take neutrino osciallations into account, $\Phi_{\bar{\nu}_e}$ can be described as

$$\Phi_{\bar{\nu}_e} = P\Phi^0_{\bar{\nu}_e} + (1-P)\Phi^0_{\bar{\nu}_\mu} \tag{3.11}$$

assuming that

$$\Phi^0_{\bar{\nu}_\mu} = \Phi^0_{\bar{\nu}_\tau} \tag{3.12}$$

and

$$P = P_{\mathrm{NH}} = U^2_{\mathrm{e1}} \tag{3.13}$$

for the assumed case of normal neutrino hierarchy. The corresponding formula for IH can be found in [96] Eq. 19.

An example plot is illustrated in Fig. 3.13, where the parameterized fit has been applied to 1 ms[24] binned hitspool data based on a 10 kpc distance Lawrence Livermore model [38]. In order to prepare the data for fitting, a signal region is defined as ±15 s around the signal. The mean value of the remaining sidebands is then subtracted from all data.

The *Pagliaroli fit* is performed on the flux/ luminosity at the experiment given in $1/(\mathrm{MeV{\cdot}s{\cdot}cm^2})$ and allows one to determine the following properties of the star and the neutrinos:

- E_ν: neutrino energy in MeV

[24] This particular dataset has been produced using hitspool data which offers an increased resolution over the *fast analysis* data of up to 1 ns, however, at the cost of an increased transmission latency of $\mathcal{O}$(d). An additional automated fit procedure based on hitspool data could be realised on-site which would eliminate the transmission time. Another example of a simulated neutrino lightvurve fitted based on *fast analysis* data is shown in A.1.

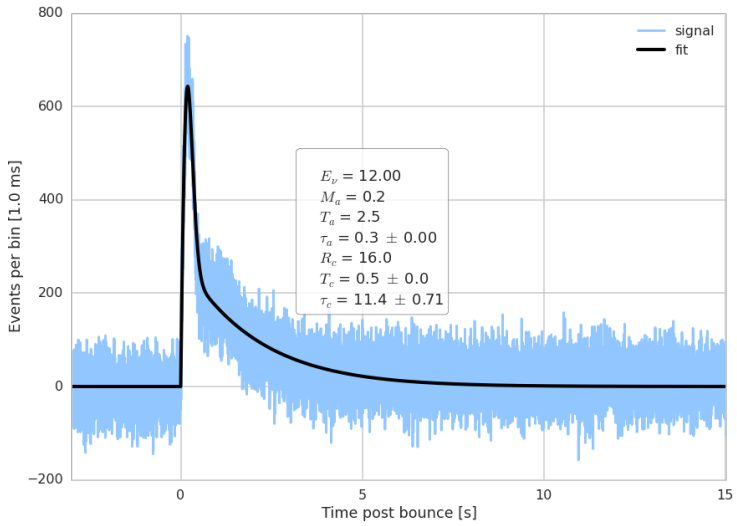

Figure 3.13: Simulated Lawrence Livermore signal at 10 kpc distance, including a complete fit after Pagliaroli et al.

- M_a: mass of neutrons exposed to positron flux in solar masses
- T_a: initial accretion temperature in MeV
- τ_a: time of accretion process in sec
- R_c: radius of the NS in km
- T_c: initial cooling temperature in MeV
- τ_c: time of cooling process in sec
- τ_r: risetime (50-300 ms)

This fit method proved to be unreliable and depended on careful starting parameter tuning for the fit to succeed. The method does not seem to be suitable for an automated fit of the light curve features.

In addition to the ten parameter fit of Pagliaroli et al., a two parameter fit is performed for the starting phase of the outburst. This signal onset fit is separated in order to extract the two parameters more reliably, the signal onset time t_r and the rise-time τ_r. The result is shown in Fig. 3.14. The fit function as described in [98] is

$$\Phi_{\bar{\nu}_e} = \Phi^{\max}_{\bar{\nu}_e}\ \Theta(t, t_\tau)\ (1 - \exp[-(t - t_\tau)/\tau_r]) \quad . \tag{3.14}$$

Using the two parameter fit, the onset time can be reconstructed with single millisecond precison. Given that at least two more neutrino detectors would provide the signal onset time with similar precision, this would allow for example for an inter-experiment directional reconstruction of the supernova explosion as shown in [99].

For a supernova at 10 kpc, the uncertainty of the onset time determination is ≈5 ms based on the 2 ms binned data. This has been investigated in detail in

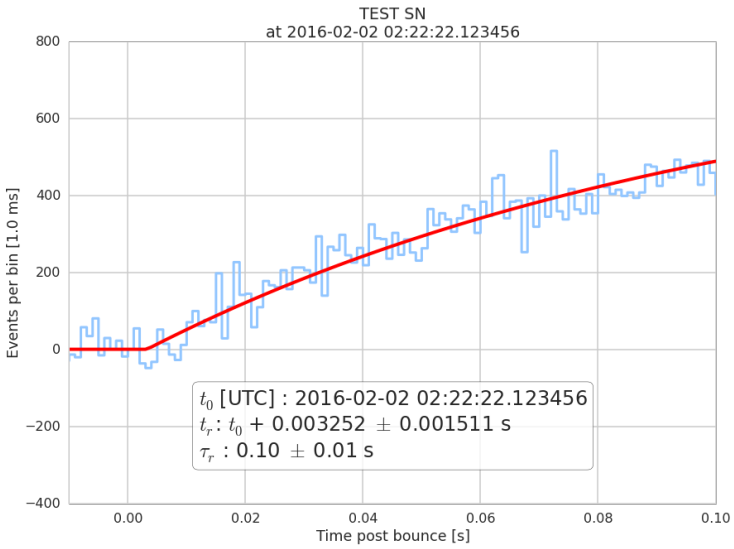

Figure 3.14: Fit of the onset and risetime of a simulated Lawrence Livermore signal at 10 kpc distance based on the fit function by Halzen et al. [98].

[91] based on simulations and the application of the Halzen fit. The *fast analysis* method now allows this fit to be performed manually within minutes after the alert. It has to be noted that the uncertainty was found to depend on the supernova distance which can not be determined by neutrino experiments and needs optical follow up. As the main purpose of direction determination with neutrino experiments is to pre-warn optical follow up, the distance dependent uncertainty remains at this point.

In order to provide the signal onset time to an automated inter-experiment triangulation service, the fit needs to be performed automatically. An automated fit can be performed on-site, hence skipping satellite data transmission of the data. The onset time can then be dervied based on hitspool data offering increased resolution. The result would then basically be a single number and qualify for the fastest transmission link.

3.6.3 Test systems

Developing, installing and running software on the South Pole system is a very delicate task. Software malfunctions might result in data aquisition downtime and data loss. Scarse satellite access can delay repair attempts from the North and make matters worse. The station personnel is usually well trained to react to known problems which are detected by the software and registered in its logfiles. They cannot be expected to fix software bugs.

In order to prevent malfunctions from happening, extensive tests are performed whenever changes are to be made on the South Pole system. A test system is provided by the University of Wisconsin which aims at being an exact replica of the South Pole computing system. All servers and components described in Chap. 3.4 and 3.5.3 also exist in the South Pole Test System (SPTS). This includes satellite modems as well as real data taking equipment such as

IceCube optical modules and GPS timing units. As SnDaq is concerned, the SPTS system has four test-modes to simulate the data taking and processing chain on SPS:

- In scaler data mode, the test-SnDaq is being fed with supernova scaler data which have been saved and extracted from SPS and hand carried to SPTS using hard drives. This is the standard mode for testing new SnDaq features. In the course of this work, 4 TB ($\approx$ 10 d) of test-data have been carried and the test-datasets have been categorized. Different features, such as high significant alerts, and also known problems such as time gaps and corrupted information were highlighted in a wiki table. SnDaq has then been adapted to properly recognize these problems.

- Additionally, in simulation mode, a simulated supernova signal can be injected into the running SnDaq. This mode is a pure sub-function of SnDaq itself. In the course of this work, SnDaq has been modified in order to use this simulation feature to instantly test SnDaq's alert chain.

- Replay mode is very similar to the scaler data mode. Using the new hitspool feature, a 24 h dataset of hitspool data, containing three full runs, has been saved on SPS and made available on the test-system. Using this data, the whole of IceCube's data aquisition system can be run. This mode is used in order to test the interoperability and data handover between IceCube's main data aquisition and SnDaq.

- In full data taking mode, the behaviour of the whole detector can be tested. A combination of real optical modules and simulated optical modules provide data to IceCube's main data aquisition which then provides secondary data to SnDaq. In the course of this work, this method has been tested and established as one of the testing methods for SnDaq.

Using the test system, the following improvements were made to the supernova data aquisition:

- Reproducibility: The SnDaq software differences between SPS and SPTS have been removed. The same SnDaq software package can now be installed on either system using a newly developed installer. All differences between the real- and the test-system are being reflected in a single configuration file which is loaded respectively. This defines e.g. different alert targets, so that supernova alerts that are detected on the test system are sent to a developer e-mail list instead of the supernova working group or snews.

- Stability: First, an automatic restart feature was developed and tested using the IceCube live experiment control infrastructure. Secondly, using the scaler data test-mode, all cases of data induced instability have been removed and are now properly detected by SnDaq. This reduced the number of SnDaq crashes to about one per year, almost rendering the automatic restart feature obsolete.

3.6.4 Logging and control

IceCube is mainly operated by two people who are staying at the South Pole for one year at a time. In the austral winter, there is no access to the South Pole due to temperatures ranging down to -80 °C which makes it too dangerous for planes to start and land. The personnel on site are therefore called winterovers. In case of a subsystem failure IceCube winter personnel can only get limited help from the north due to very scarse satellite connectivity throughout the day.

As I3Live is integrated into the station's paging, telefone and email system, there now is an easy way to notify winter personnel about a subsytem failure. Whenever one of SnDaq's monitored variables deviates from a given range a specific alert is raised and predefined notifications are being sent automatically.

However, not all problems can be covered in this way for the winterovers. There is the need for clear instructions in case of failures. As a second step, SnDaq's logging system has therefore been completely revised including different loglevels and timestamped logging information. The most common problem occurs e.g. due to data gaps or data corruption in SnDaq's input scaler data. The new logging system makes it easy for operators to identify which file is currently being processed and at which step in the analysis chain the error occurred.

A wiki page has been created which lists every alert predefined in I3Live, presents examples from the SnDaq log file and appropriate solutions. Whever an error occurs operators can check the logfile against the wiki and will be guided step by step through the solution process. This procedure is also trained in advance during the winterover training session.

3.6.5 Time and leap seconds

In 1967, the SI second was redefined based on atomic properties rather than the earth's movement around the sun. This allows for more precise timekeeping and measurements but also decouples human timekeeping from earth's slightly irregular motion. The two timekeeping methods, however, can run out of synchronisation.

Atomic clock time systems are based on the international atomic time TAI[25]. Time systems like UT1[26] or UT2[27], which are successors of GMT[28], are related to the length of the mean solar day and therefore depend on the motion of the earth. As during the past centuries earth's rotation speed has slowed down the time difference between UT1 and TAI is now about 36 s since their definition.

In order to keep SI timekeeping synchronised with the length of the mean solar day, the coordinated universal time UTC is introduced which corrects TAI to match UT1. The correction happens in form of seconds being added to the TAI system. Due to the irregularities of the deviations, the NIST[29] committee decides on the addition of the next leap second insertion only six months in advance. A plot of the remaining subsecond time difference between UTC and UT1 is shown in Fig. 3.15.

[25] Temps Atomique International
[26] Solar time at 0° longitude
[27] Smoothed version of UT1, filtering out periodic seasonal variations
[28] Greenwich Mean Time
[29] National Institute of Standards and Technology

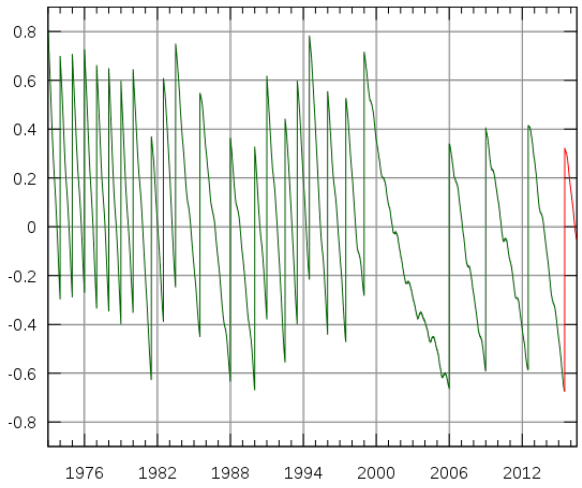

Figure 3.15: Time difference in seconds between UT1 and UTC between 1972 and 2016. Vertical segments correspond to the insertion of leap seconds. Human timekeeping today is based on an average of a network of more than 400 atomic clocks. Earths rotation time on the other hand is irregular and slowly decreasing over the past centuries. UT1 is a time system which is based on the movement of the earth, UTC is an atomic clock based system which is irregularly corrected in order to stay close to UT1. The plot was taken from the UTC wikipedia article[30].

All of IceCubes data aquisition systems count time from the beginning of the current year. The last run of the year is stopped a couple of seconds before the end of the year and the next run ist started a couple of seconds into the new year, after the time counter has been reset. Therefore IceCube does not have to deal with leap seconds which are inserted by NIST as the last second of a calendar year. There are, however, also leap second insertions on July 1st in some years.

As time is being counted as true nanoseconds from the beginning of the year (SnDaq time), SnDaq does not have to worry about leap seconds for its data processing at all as leap seconds are only inserted into the coordinated universal time system UTC. In case of a supernova alert, the information is sent to various email lists and further automatic processing systems (such as SNEWS) which do not understand SnDaq time. At this point, SnDaq has to convert all the signal time information which it provides into UTC thus taking into account extra leap seconds.

Due to the 2012 mid-year leap second insertion, SnDaq's time class had to be updated and was completely rewritten. The core variables, which are stored in SnDaq's time handling class are the current year and the number of nanoseconds since its start which itself is defined by a an external GPS time clock. Multiple getter and setter functions enable to create instances of the class using different time formats or extracting time into different formats such as UTC, various epoch time based systems or modified julian time.

[30] https://en.wikipedia.org/wiki/Coordinated_Universal_Time

Table 3.1: The NIST leapsecond file contains one line per leapsecond, stating the time of the insertion in seconds since 1900 in the first row and the total number of leapseconds added so far in the second row.

seconds since epoch 1900	#ls	ls insertion date (UTC)
3439756800	34	1 Jan 2009
3550089600	35	1 Jul 2012
3644697600	36	1 Jul 2015

Table 3.2: This example shows a conversion from the SnDaq nanosecond counter for the year 2012 into UTC time with and without taking into account the NIST leapsecond insertion on July 1st.

DAQ time (ns)	UTC 2012 /wo ls	UTC 2012 /w ls
15724799999999999	6/30 23:59:59.999999999	6/30 23:59:59.999999999
15724800000000000	7/1 00:00:00.000000000	6/30 23:59:60.000000000
15724801000000000	7/1 00:00:01.000000000	7/1 00:00:00.000000000

The functions, which convert SnDaq time to and from UTC, are based on the leap second database file[31] which is regularly published by NIST at least 6 months prior to a leap second insertion. The file contains one line per leap second, stating the time of the insertion in seconds since 1900 in the first row and the total number of leap seconds added so far in the second row. It also contains an expiry date until which it contains a complete list of leap seconds. Whenever the file is about to expire, SnDaq raises an alert through I3Live in order for operators or northern experts to update its leap second database file from the NIST website.

The process of converting between different time systems in SnDaq is performed by the C++ Boost library[32] which itself does not support leap second handling. The leap second correction is additionally performed after the conversion. The NIST file lists all past leap second insertions by time of insertion and number of accumulated leap seconds as shown in table 3.1. SnDaq then determines the number of accumulated leap seconds at the beginning of the current year and at the requested time. If there is a difference in the determined amount of leap seconds, this number is subtracted from the current conversion as determined by the Boost library.

An example of the leap second conversion from daq time to UTC is shown in tab. 3.2 for the 2012 leap second insertion. The algorithm first uses the Boost library to add the requested amount of nanoseconds to the start of the year and saves the result as a UTC variable. In a second step, the algorithm consults the NIST database file and determines the leapsecond offset as of Jan 1st 2012 (34) and the leapsecond offset on July 1st 2012 (35). Calculating the difference between these two values and subtracting them from the previously determined UTC value will ensure that the UTC time value will be correct no matter how many leap seconds have been added since the start of SnDaq's nanosecond time counter. Please note that the UTC value of "23:59:60" is the offical value of the inserted leapsecond, whereas the described algorithm will simply make the

[31] published e.g. by the ietf https://www.ietf.org/timezones/data/leap-seconds.list
[32] http://www.boost.org/

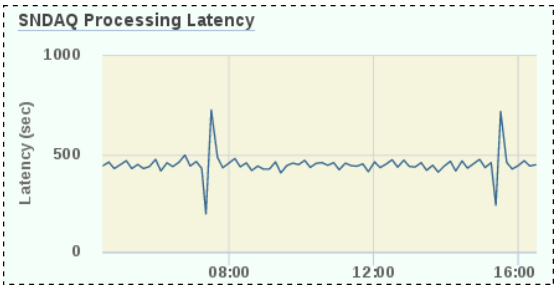

Figure 3.16: SnDaq processing delay as presented on the I3Live webpage. The delay value is roughly 7 to 8 minutes and mainly caused by SnDaq's 5 minute wide sideband buffer and datafile copy operations. The drops and peaks in SnDaq's processing time at regular intervals are the result of SnDaq emptying and filling its analysis buffer at the end and start of every 8h IceCube DAQ run. This latency information is one of six surveilance quantities being transmitted to I3Live.

UTC clock stop for one second on "23:59:59".

SnDaq now supports the multiple time systems for different purposes. A list including a short description is given here:

- SnDaq time - for data processing,
- UTC - for communication with experts and further automated processing systems (e.g. SNEWS),
- Epoch 1900 - seconds since Jan 1st 1900 - for parsing the NIST database,
- Epoch 1970 / unix time - for message delay measurements with northern data servers, and
- JD and MJD - for corellation studies with astronomical data.

3.6.6 Processing delay and message latency

Due to the nature of the SnDaq analysis algorithm as presented in chapter 3.2, SnDaq has a minimal data processing delay of 5 min which is the size of the data buffer it uses to determine the average background rate. In addition, the dataflow experiences some additional delay in the processing chain e.g. due to file copy operations as described in chapter 3.4. In order to better understand and monitor the data processing delay, SnDaq now regularly compares the data time to the current system time and reports the total current delay to I3Live as shown in Fig. 3.16. Whenever the data processing delay rises above a given threshold, I3Live issues a predefined alert, notifying the winterover personnel as described in chapter 3.5.3.

When SnDaq detects a high significant rate change in one of its analyses, multiple sn-alerts are now being generated containing different sets of information. In an attempt to minimize overall message delay between SnDaq at the South Pole and northern experts, different satellite channels are being used for different purposes. Available communication channels were described in chapter 3.5.2.

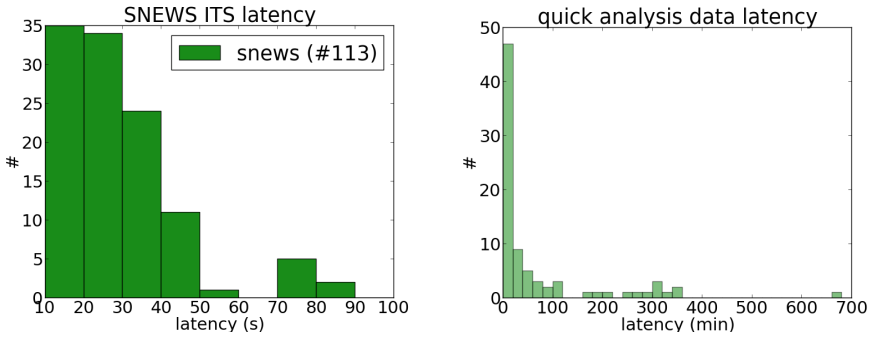

Figure 3.17: The left plot shows the latency between ITS transmission time and message reception on the snews server. The latency of the ITS channel is on the order of tens of seconds. The right plot shows the time difference between the alert time and the e-mail reception of the fast analysis data on the northern analysis server. These values therefore contain the SnDaq processing latency. Approximately 10 % of the messages have a delay time of more than 300 min.

The most time critical alert message is the one sent to the snews system which was presented in chapter 3.5.5. The snews alert message only contains a few characters describing the most important variables of the alert such as the alert time and significance. The snews alert therefore qualifies for the most low bandwith and low latency satellite link through the dedicated IceCube Iridium modem. SnDaq is now setup to not communicate directly with the Iridium modem anymore but to use I3Live to forward its messages. This additional step added a couple of seconds to the message latency but enables a centralised way of handling satellite communication channels which may change over time. The snews message as well as the newly implemented sms alerts have a similar typical message delay of $\mathcal{O}(1\text{ min})$ and a total delay time since the alert of $<$10 min.

Due to its $\mathcal{O}(100\text{ MB/run})$ filesize, the bulk of analysed sn-data only qualifies for the high bandwith high latency satellite stream which has a delay of $\mathcal{O}(\text{d})$. This transfer is handled by *JADE* (chap 3.5.4) which places it in the appropriate satellite queue.

In case of a supernova alert, SnDaq extracts 90 s of its fine binned 2 ms scaler data as described in 3.6.2. This so-called fast analysis data was initially sent north as an email-attachment from the SnDaq server at SPS. In a second step, this condensed dataset is now being tranparently transferred using the *JADE* service. *JADE* recently switched its delivery channel to support Iridium *Rudics* which provides a 24 h service for larger datasets up to 350 kB. These messages are now typically being delivered with a total delay of $<$1 h.

Typical delay times of snews and fast analysis information are shown in Fig. 3.17. Delay times for all 2015 hitspool datasets and all 2011 to 2017 alert sms messages[33] are shown in Fig. 3.18. The hitspool data delay is approximately 24 hours on average. The typical alert sms is delivered within 10 s.

For a high significance supernova alert the chain of events concerning automated information and data transfer now looks as follows. Supernova experts

[33]The database extract of all icecube sms delay times was kindly provided by the operators of sms77.io

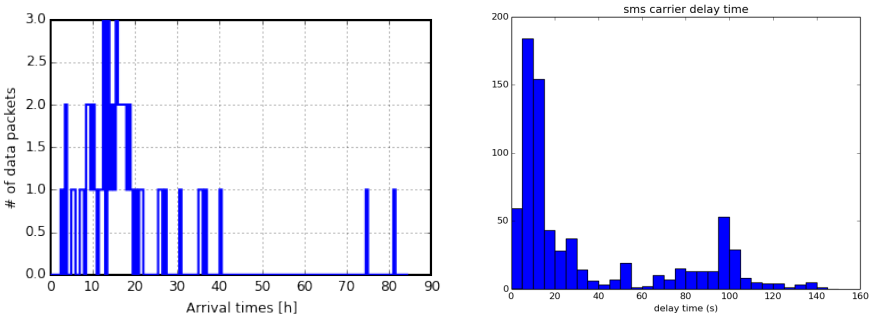

Figure 3.18: Latency of all 2015 HitSpool datasets (left). Time differences are measured between the alert time as determined by SnDaq and the timestamp at which the data has been written onto the data warehouse server. As HitSpool datasets contain multiple files, the last file to be written determines the total latency. The right figure illustrates the delay time introduced by the sms service provider. The time is effectively measured between reception of the alert email by the sms gateway and its reception of the sms delivery confirmation. The actual delivery time is therfore shorter. The peak at 100 s is not fully understood and is caused by either the carrier network or by the receiving cellphone temporarily loosing reception. Only 7.5 % of the messages have reported arrival confirmation times of more than 150 s.

receive an alert sms on their cell phone within seconds after the event has been triggered at South Pole. Within minutes a detailed alert description follows via e-mail. Within one hour a preview dataset is available for verification and a first analysis. Within one day hitspool data is available for a detailed analysis. The delay times may vary due to current bandwidth usage, data backlogs and link outages which are not uncommon.

3.6.7 Summary and outlook

A variety of measures has been taken to improve uptime, stability and maintainability of IceCube's supernova data acquisition. The internal time management has been revised in order to reliably eliminate leap-second related errors in inter-experiment data analyses and in the UTC-based propagation of supernova alert timestamps. A data transport scheme has been developed which adapts to the limited connectivity and bandwith of the South Pole based experiment. After a high alert (e.g. false alert Nov 2015), supernova experts will no longer have to wait days, but rather minutes, to obtain the first preview dataset. The data transmission time to the SNEWS coincidence network has been reduced to less than one minute on average.

The system has been integrated into a new generation of run monitoring and almost all message and data handling has been adapted to be handled by experiment-wide standardised and centralised systems. This process however is ongoing. The supernova related monitoring in IceCube still consists of five different monitoring and offline analysis systems running at different sites and using different technologies:

- Technical monitoring (I3Live)[34],
- Run Monitoring (I3Live, moni2.0)[35]
- Physics monitoring (Mainz)[36],
- Snews monitoring (Mainz)[37], and
- Fast analysis and HitSpool analysis (Madison)[38].

Efforts should continue to transfer all monitoring and fast analysis data transparently through IceCube-Live. The monitoring systems should be combined and all monitoring quantities be displayed within the new IceCube live and moni2.0 systems.

A scheme has been developed which would enable IceCube to save hitspool data based on external alert sources. In order to implement this reliably we would need this source to additionally send periodic test messages. This has not been the case until very recently.

External hitspool requests

Here we assume the case that IceCube's SnDaq misses a supernova signal, however, a signal was observed by at least two other neutrino observatories. In this case, a snews alert message is sent out and could be captured by IceCube. The message could be delivered to the Hitspool system as outlined in Fig. 3.19. Hitspool data covering the time of the alert can then be put aside to enable detailed analysis.

The SNEWS system now sends periodic test messages. A system still needs to be developed that parses these messages and forwards them south as shown in Fig. 3.19. This would also enable the system for a periodic checks of sucessfull transmission. Hitspool data saving, however, should only occur in case of a real alert for bandwith reasons.

[34] https://live.icecube.wisc.edu/details/sndaq/
[35] e.g. https://live.icecube.wisc.edu/run/129689/
[36] http://butler.physik.uni-mainz.de/icecube-sn-monitoring/
[37] http://butler.physik.uni-mainz.de/icecube-snews-monitoring/index.html
[38] http://convey.icecube.wisc.edu/data/ana/Supernova/

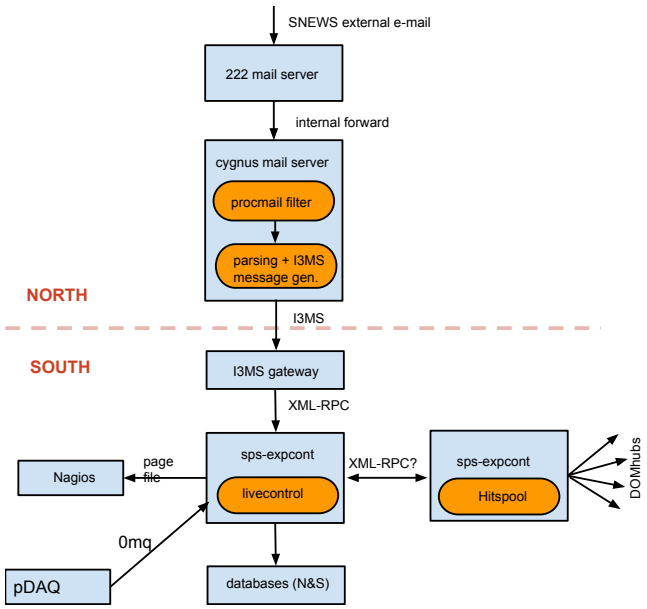

Figure 3.19: Schematic view of the implementation for an external hitspool trigger based on an SNEWS alert. The system captures an alert e-mail issued by the SNEWS network and forwards it to the South Pole using the new bi-directional IceCube messaging system. The South Pole servers then in turn save hitspool data of the specified time region for a subsequent manual analysis. Scheme made by [100].

Chapter 4

Analysis

The analysis is geared towards obtaining additonal information from supernova neutrinos such as the average neutrino energy and the direction of the supernova. Such information has recently become accessible to IceCube due to the new HitSpooling [1] data acquisition technique which provides new physics opportunities (see chapter 3).

The standard supernova daq system performs its analysis based on 2 ms binned hit rates. In case of a supernova alert issued by SnDaq, the HitSpooling system provides access to a predefined time window of untriggered and unfiltered detector raw hit data with sub nanosecond resolution per single hit. These new datasets allow one to apply $\mathcal{O}$(ns) coincidence criteria on consecutive hits or to analyse the hit pattern of supernova neutrinos passing through the detector.

Correspondingly, a new supernova simulation framework has been developed [75] which provides simulated detector hits with comparable time resolution. This analysis is a first attempt to use and combine these new datasources for analysis, merging simulated signal hits with real hitspool datasets taken in 2015 as background. As this is not a standard IceCube analysis all tools had to be developed from scratch. Numerous ideas have been fed back and contributed to the development of the hitspool interface.

4.1 Supernova direction reconstruction

The early warning of a supernova and its location might allow for greatly improved astronomical observations [101]. Generally, two options can be considered to reconstruct the direction of a supernova based on the neutrino channel:

- The directionality of the individual neutrino interactions, mainly neutrino-electron forward scattering, and
- inter-experiment triangulation based on varying arrival times.

The first option is not accessible in IceCube due its very low sensitivity to electron neutrinos. It has been proposed in [102] that also inverse beta decay has a small directional component which could be accessible using high resolution hitspool data, exploiting the directional dependent sensitivity of the IceCube DOMs, but this has not yet been investigated. We want at first to explore

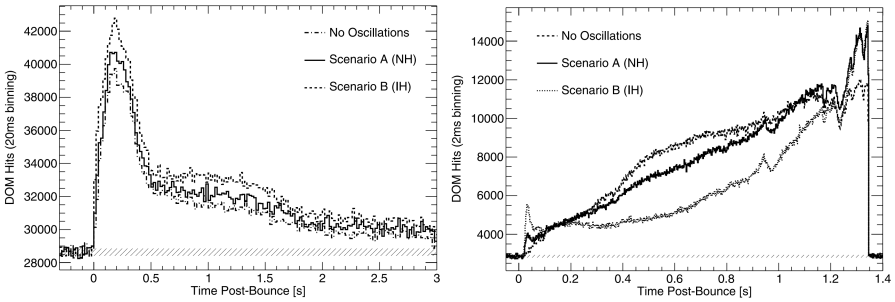

Figure 4.1: Left: Expected rates for a supernova at 10 kpc following the Lawrence-Livermore model. Right: Expected neutrino signal from the gravitational collapse of a non rotating massive star of 40 solar masses into a black hole at 10 kpc distance following Sumiyoshi et al. [12] and [56].

IceCube direction reconstruction capabilities based on a new approach and secondly show how IceCube could contribute to inter experiment triangulation.

Due to the kilometer-scale size of the IceCube detector, neutrinos travelling at the speed of light will take at least 2.5 μs to traverse it. The propagation of an incoming supernova-neutrino wavefront may therefore be observed by causing rate changes on the same timescale and could effectively be triangulated within the volume of IceCube. (See also [103].)

Figure 4.1 presents an example of a typical rise time of the neutrino light curve of $\mathcal{O}(10$ ms). Consequently, the signal rate change of a typical supernova signal is a few orders of magnitude slower than required. An alternative would be to observe the signal drop of the black hole formation of a heavy star. The rate drop at black hole formation time (see Fig. 4.1) is expected to be on the order of $\mathcal{O}(100\ \mu$s) [49, 104].

A likelihood analysis has been established in order to investigate the capabilities of IceCube to perform a directional analysis of supernova events based on a black hole formation signal drop. Note that one has to identify the wavefront in the presence of a dominant dark rate background. Signal and background rates are taken from [12] as illustrated in Fig. 4.1. In a first analysis, the black hole formation is assumed to happen instantaneously. Thus, in order to simulate the neutrino flux at the star, a heavyside function is assumed.

4.1.1 Likelihood method

The neutrino energy spectrum is assumed to follow the probability density [40] (Eqn. 14)

$$f_\alpha(\epsilon) = \left(\frac{\epsilon}{\bar{\epsilon}}\right)^\alpha e^{-(\alpha+1)\epsilon/\bar{\epsilon}} \quad , \tag{4.1}$$

with an average neutrino energy of $\bar{\epsilon} = \langle\epsilon\rangle = 22.93$ MeV and a shape parameter of $\alpha = 2.03$, based on data from the supernova simulations published in [56].

The neutrino cross section in the ice is proportional to ϵ^2 (Eqn. (1.2)) and the length of the track in the detector is proportional to ϵ (Eq. (1.5)). In order to obtain the signal rate, the spectrum is therefore weighted by ϵ^3 and integrated to the upper neutrino energy limit [104]:

$$r(m_\nu, \bar{\epsilon}, t) = \frac{1}{n} \int_0^{E_{\max}} \epsilon^3 f_\alpha(\epsilon)\, \mathrm{d}\epsilon \quad , \tag{4.2}$$

with the normalisation

$$n(\bar{\epsilon}) = \int_0^{\infty} f_\alpha(\epsilon)\, \mathrm{d}\epsilon \quad . \tag{4.3}$$

The upper neutrino energy limit can be derived by solving

$$E^2 = \gamma^2 m^2 c^4 = \frac{1}{1-\beta^2} m^2 c^4 \tag{4.4}$$

for β^2:

$$\beta^2 = \frac{v^2}{c^2} = 1 - \frac{m^2 c^4}{E^2} \tag{4.5}$$

$$\Rightarrow \quad v = \frac{D}{t} = c\sqrt{1 - \frac{m^2 c^4}{E^2}} \quad , \tag{4.6}$$

where D is the distance to the supernova and t, m and E are the travel time, mass and energy of the neutrino. Using $(1+x)^n \approx 1 + nx$ for $x \ll 1$ leads to a travel time of the neutrino of

$$t \approx \frac{D}{c}\left(1 + \frac{m^2 c^4}{2E^2}\right) \quad . \tag{4.7}$$

Subtraction of the travel time of the photon leads to the neutrino's arrival time dispersion due to its mass and energy:

$$\Delta t = \frac{D}{c}\left(1 + \frac{m^2 c^4}{2E^2}\right) - \frac{D}{c} = \frac{m^2 c^3 D}{2E^2} \quad . \tag{4.8}$$

There is an upper limit on the neutrino energy, which must be small enough for the neutrino to be delayed the time Δt after the black hole formation time

$$E_{\max} = m_\nu \sqrt{\frac{0.515 D}{t - t_0}} \quad , \tag{4.9}$$

where D is the distance of the supernova (in 10 kpc, scaled to the distance to the Milky Way center), t_0 is the reference time of the black hole formation, t is the arrival time of the signal hit at the detector center (both in seconds) and m_ν is the neutrino mass (in eV).

The analytic integration results in the so-called upper incomplete gamma function:

$$p_{\mathrm{signal}}(\phi, \theta, t) = 1 - \Gamma\left(4 + \alpha, \frac{0.72(1+\alpha) m_\nu}{\bar{\epsilon}} \sqrt{\frac{D}{t_m(\phi,\theta) + t - t_0}}\right) \quad . \tag{4.10}$$

Here $t + t_m(\phi, \theta)$ is the arrival time of the signal hit at a specific detector module. The additional time value $t_m(\phi, \theta)$ is the dot product of the module's position in the detector and the assumed direction of the incoming neutrino wave.

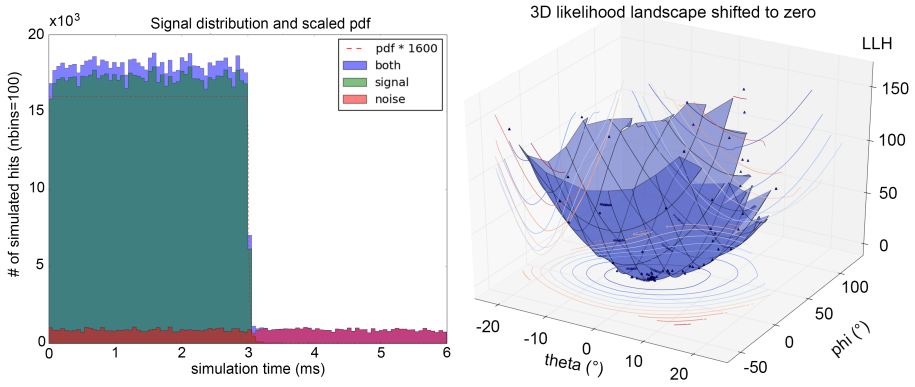

Figure 4.2: The left figure shows randomly distributed hits following Eq. (4.10), with the signal drawn in purple and the noise background drawn in magenta. The right plot shows an example 3D representation of the 2D likelihood following Eq. (4.11) onto which the minimizers are applied.

The unbinned likelihood per angle under which the supernova is observed is derived as follows as the product over all registred hits:

$$\mathrm{P}(\phi,\theta) = \prod_{j=1}^{m_{\mathrm{hit}}} \left(N_{\mathrm{signal}} \cdot p_{\mathrm{signal}}(\phi,\theta,t_j) + \frac{N_{\mathrm{noise}}}{T} \right) / (N_{\mathrm{signal}} + N_{\mathrm{noise}}) \quad . \tag{4.11}$$

As the likelihood function cannot be easily derived a python minimizer is later used to reconstruct the direction of simulated signals.

4.1.2 Signal simulation

Signal hits are randomly generated per optical module based on expected rates and following a heavyside function which imitates the signal drop at black hole formation time. The simulation timespan is 6 ms. For the first 3 ms, the signal function is set to unity. Afterwards the signal function follows Eq. (4.10) as illustrated in Fig. 4.2. This scenario assumes that the neutrino signal ends abruptly at the star and is only delayed by the travelling time of the neutrino due to its mass. Noise hits are also being randomly generated per dom based on the expected rates. All hits are then time shifted by $t_m(\phi_{\mathrm{real}}, \theta_{\mathrm{real}})$.

In order to reconstruct ϕ and θ, a set of minimizers is then applied to the likelihood landscape spanned by $\log(\mathrm{P}(\phi,\theta))$ (see Fig. 4.2 and 4.3). This step is repeated n-times for an unchanged set of parameters (D, m_ν, α, $\bar{\epsilon}$) but different randomly generated hits. The achievable resolution for a given set of parameters is then defined as the standard deviation σ of the list of n reconstructed angle values for θ and ϕ.

The uncertainty of this resolution is defined as:

$$\mathrm{Var}\left[\sigma^2\right] = \left[\frac{\mu_4}{4\mu_2 n} - \frac{n-3}{(n-1)^2} \frac{\mu_2}{4} \right] \quad , \tag{4.12}$$

where μ_2 and μ_4 are the 2nd and 4th central moment of the distribution of reconstructed angle values.

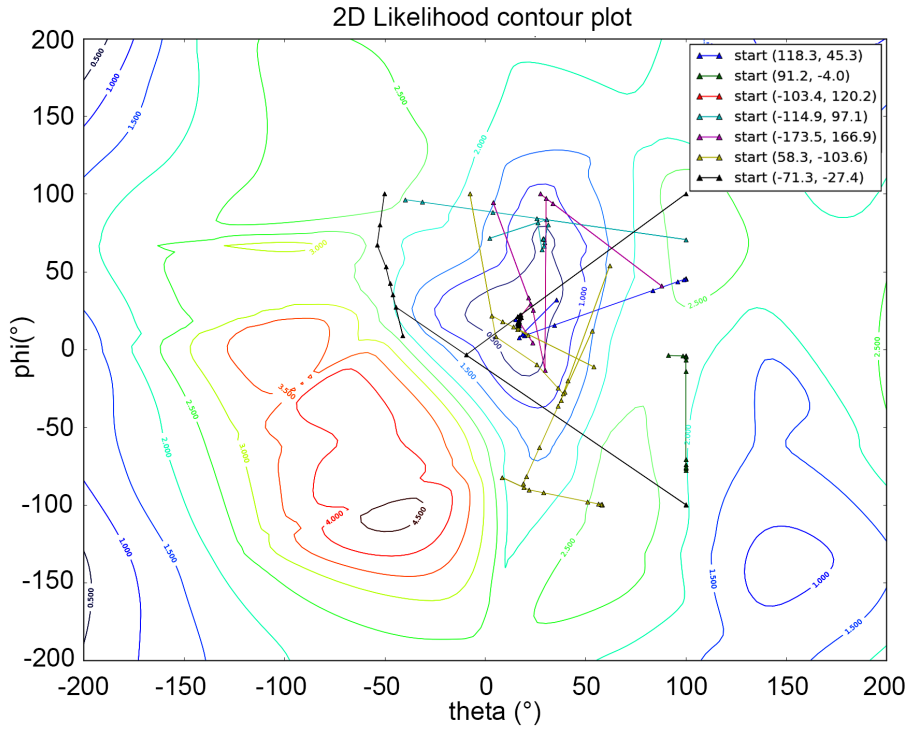

Figure 4.3: 2D likelihood map of different zenith and azimuth angles covering a full sphere. Seven minimizers have been positioned randomly to the right hemisphere of the logarithmic likelihood landscape. Multiple minimizers are started to reduce the chance of being trapped in a local minimum. The number of started minimizers depends on the difficulty of the terrain, the number is increased if previous minimizers continued to find lower minima.

The results are displayed in Fig. 4.4 and 4.5. For very small neutrino masses < 0.01 eV, the achievable resolution is $<= 20°$ for supernova events at the center of the Milky Way (d <= 8 kpc). The resolution saturates at $360/\sqrt{12} \approx 109°$ as this is approximately the standard deviation of a 360° uniform distribution of individual results.

4.1.3 Detector configuration scenarios

In order to increase the resolution, different theoretical detector configurations have been tested. As an example, three additional IceCube strings with 60 optical modules each, have been added at different distances, equally distributed at 120° from each other. The resolution to reconstruct the direction of a galactic supernova increases to below 5° when adding 3 strings e.g. at a distance of 70 km each.

When looking at the globe, different possibilities for even more distant IceCube satellite stations arise. The US Antarctic research stations McMurdo and Palmer for example are each several hundres of kilometers away from IceCube.

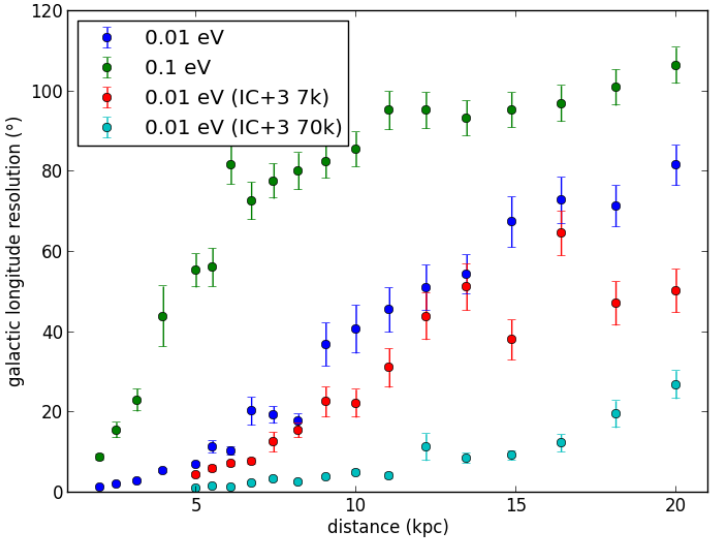

Figure 4.4: IceCube supernova direction resolution capabilities based on two different neutrino masses and theoretical IceCube extensions with three additonal strings in 7 and 70 km distance. Every datapoint is a mean of 60 minimisation reconstructions. For a supernova at the center of the galaxy (distance ≈8 kpc), the uncertainty of the resolution is ≈20 degree, if the effect of neutrino masses can be neglected. The resolution increases drastically if satellite detectors are added in large distances.

A possible third location could be established in Alaska or Greenland. All of these could probably be ice or water based. As the development of optical modules continues toward a new generation neutrino telescope, their signal to noise ratio and photon acceptance increases. Several proposed designs include the wavelength shifting module [105] and the multi-pmt module [106]. Each of the global satellite stations would eventually only need to house a small number of advanced optical modules. The amount of data needed to be exchanged between these remote locations (in near-realtime) would, however, be quite high.

4.1.4 Non-instantaneous black hole formation

Due to the non vanishing size of the black hole forming object it can be assumed that the neutrino emission does not cease absolutely instantaneously. For a massive core object the size of approx 10 km information would need $\mathcal{O}(10\ \mu s)$ to traverse it.

In [49], a delayed black hole formation is simulated until the final stage. It is proposed that the neutrino flux at the star does not cease instantaneously but continuing over a timespan of $\approx$ 500 μs (see also Fig. 4.6). Additionally [56] estimate in their simulation of non-rotating failed supernovae that: “It is to be noted that the computations of neutrino burst are terminated at the formation of apparent horizon in this study. After this moment, the neutrinosphere will

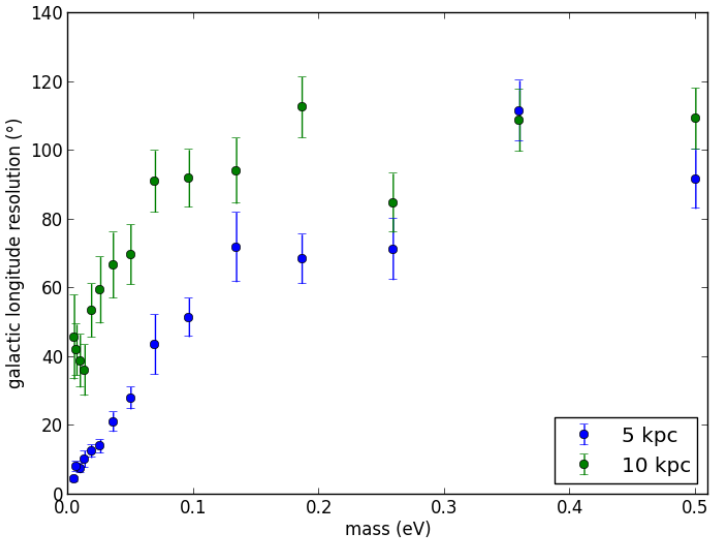

Figure 4.5: IceCube supernova direction resolution capabilities in dependence of the neutrino mass for two different supernova distances at 5 and 10 kpc. Every datapoint is a mean of 60 minimisation reconstructions.

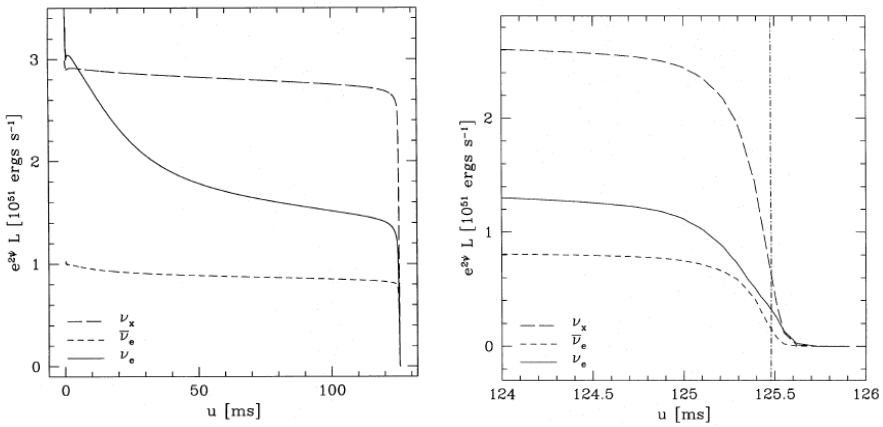

Figure 4.6: Neutrino luminosities as a function of observer time u based on a simulation from [49]. The ν_x flux represents the sum of the contributions from all heavy-lepton neutrinos. A phase of quasi-stationary neutrino emission is followed by the suppression of the fluxes in the final gravitational collapse to a black hole. The vertical line on the right marks the time at which the surface of the star crosses the photon sphere at radius $R = 3GM/c^2$.

be swallowed by the horizon in a fraction of millisecond and the major neutrino emissions cease at this point."

If a gradual decrease of the neutrino flux on the order of 100 μs is considered at the star, the previously described IceCube internal triangulation method did not offer any usable result for distances larger than 5 kpc. For closer distances and the smallest investigated neutrino mass of 0.01 MeV the method enabled at least to point to the right hemisphere.

As an attempt to improve these results, the Milky Way constraint has been adapted to this simulation. A relation between galactic coordinates and detector coordinates has been implemented and a supernova coming from the centre of the galaxy has been assumed. Likelihood values with a galactic latitude of $>$ 2.5° have been quadratically supressed. This procedure was found to increase the speed of the minimisation process, basically reducing it to a 1D minimizer problem. It did however not increase the precision of the resolution.

4.1.5 Triangulation of the supernova direction

At large distances between detecting sites, another triangulation approach becomes favourable. Equipped with a GPS timing unit and a stand-alone data aquisition, high statistics neutrino detectors can autonomously determine either the onset-time of a supernova signal or, with even higher precision, the signal-drop-time of a failed supernova. This would reduce the amount of data needed to be exchanged to a minimum. Timestamps per station can be delivered within seconds to a central direction reconstruction service using the internet, or Iridium satellite communications services. The timestap based triangulation method using multiple stations is outlined in [99]. The cited paper shows that for four contributing sites, the achievable resolution is below 10° if the uncertainties of the respective timstamps is on the order of 2 ms. Reconstruction is possible with a lower number of contributing sites when using the Milky Way band as a geometric constraint.

IceCube can already determine the signal onset time with the required precision, as shown in Chap. 3.6.2 and [91]. The authors of [101] show that the signal uncertainties for Super-K (30 ms) and SNO (150 ms) are too large for triangulation. Both experiments are better suited to exploit the directionality of the neutrino interactions to achieve individual direction reconstruction on the order of 10°. Due to its large volume, IceCube is currently the only experiment which can collect enough statistics to determine the arrival time of the neutrino wave with sufficient precision. It is estimated in [99] that the proposed Hyper-Kamiokande and LAGUNA [107] detectors will provide sufficient statistics for triangulation. A fourth candidate could be the Km3Net detector [81] which is being built in the Mediterranean and will be comparable to IceCube in volume.

The fast analysis method in Chap. 3.6.2 could be run online on-site and configured to attempt an automated fit of different signal features e.g. signal onset and signal drop (if applicable). The determined timestamps can then be transmitted to a central agent with a combined delay of $\approx$7 min as outlined in previous chapters. The SNEWS service would be an ideal candidate for triangulation as it already collects supernova signal onset timestamps from every participating experiment. The current precision requirement for the mere coincidence criterium of two alerts in 10 min is very low. IceCube currently sends its timestamps with an analysis dependent precision of 0.5 to 10 s.

If a sufficient number (>=3) of (current and future) experiments were to send millisecond precision timestamps of (multiple) signal features to SNEWS, triangulation would basically come "free of charge". SNEWS is already a central database (and distributor) of supernova direction information as it already collects individual direction reconstruction results alongs with the experiment alert notifications. The expansion of SNEWS into a triangulation service would be the next logical step along with the current construction and planning of high statistics neutrino detectors.

4.2 Average supernova neutrino energy

We assume the neutrino differential flux at distance d from the supernova to follow [12]

$$\frac{d\Phi^{\nu}_{\mathrm{Earth}}(t)}{dE_{\nu}} = \frac{L^{\nu}_{\mathrm{SN}}(t)}{4\pi d^2 \overline{E_{\nu}}} f^{\nu}(E_{\nu}, \overline{E_{\nu}}, t) \quad . \tag{4.13}$$

In order to determine the luminosity, measuring the average supernova neutrino energy therefore is a key factor.

IceCube was mainly constructed to measure the most high energetic cosmic neutrinos. Its inter-string and inter optical-module distances are by design too large to measure the energy of a single supernova neutrino event. It is therefore impossible to reconstruct the supernova neutrino flux in the detector based on the number of detected photons for individual events. For example, the same number of detector hits can be produced by a rather large number of low energetic neutrinos or by a smaller number of neutrinos with a higher energy. The only handle on measuring the neutrino energy is to statistically investigate coincident hits at a very close range of one or two optical module distance and at very short time differences of tens of nanoseconds.

Fig. 4.7 shows the spatial hit distribution of a simulated supernova signal following a model similar to Totani et al. [38] ("Lawrence Livermore") with a mean energy of 18.7 MeV and a shape parameter [40] of $\alpha = 3$ (see Fig. 4.8). The simulation assumes that the neutrino energy is constant over time. Only coincident hits originating from the same neutrino have been drawn. Red dots symbol neutrino events of which hits have been detected by the same module, blue dots illustrate neutrino events of which hits have been detected by different modules. The right plot in Fig. 4.7 shows the distance distribution for both cases. Coincident hits which registered on the same module show a steep decrease depending on the distance to the detecting module. In case of coincident hits registered on different modules, a maximum is observable at a distance of ≈17 m, which corresponds to the distance between two modules. With increasing distance, the number of hits decreases roughly exponentially.

4.2.1 Coincidence rates

The average neutrino energy can be estimated by comparing the rate of multiple coincidences to the single hit rate, as described in [108] and [102, 109]. The time and spatial distribution of hit-time-differences can be analysed using a two dimensional histogram.

The analysis is based on a set of $\approx 5 \cdot 10^6$ simulated supernova neutrino induced hits as seen by the IceCube optical modules, that were tracked with a

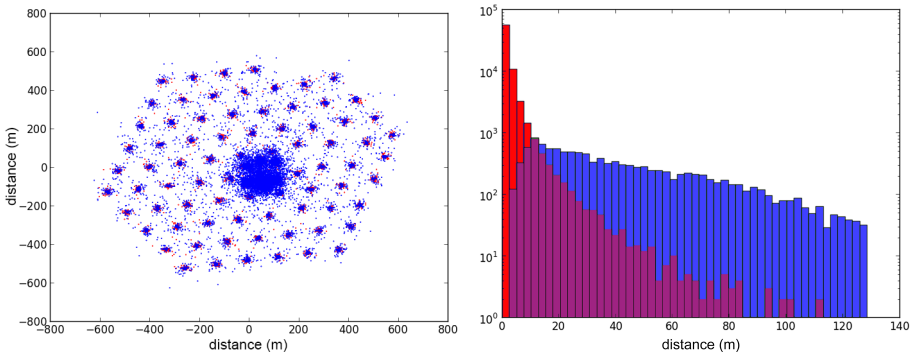

Figure 4.7: 2D top view of IceCube illustrating neutrino interaction points in the ice (left). Only simulated coincident signal events are shown which have produced at least two hits. Red dots indicate interactions which have produced multiple hits on *one* module. Blue dots illustrate interactions which have produced two or more hits on *different* modules. On the right, the distance distribution for both cases is shown. The red (blue) curve illustrates coincident hits that have registered on the same (different) optical module(s), 90% of the registered coincident interactions take place within 2.6 m (82 m) of the respective module(s). All scales are in meters. Distances larger than 130 m have not been investigated.

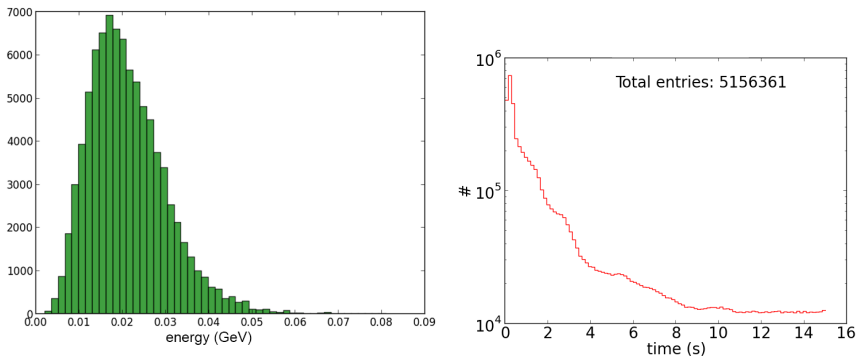

Figure 4.8: Neutrino energy distribution (in GeV, left) and number of hits as a function of time (right) for a simulated dataset. The simulation was run based on the Lawrence-Livermore model with an average neutrino energy of 18.7 MeV and a shape parameter of $\alpha = 3$.

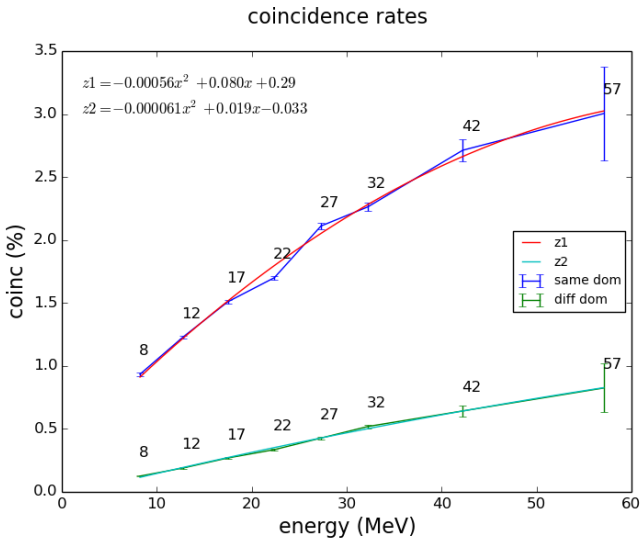

Figure 4.9: Fraction of coincident simulated hits created by the same neutrino and all detected hits as a function of the energy. The hits were categorized into 5 MeV bins depending on the neutrino's energy. The blue (green) curve contains coincident hits which were detected by the same (different) optical module(s). The average energy of events contributing to a bin is also given.

Geant based Monte Carlo [75]. The neutrino-energy and hit-time distribution is illustrated in Fig. 4.8. The hits are additionally categorized into 5 MeV bins depending on the neutrino energy. Low statistics bins were combined.

Coincident hits arising from the same neutrino within a coincidence time window of 500 ns are identified and counted. Fig. 4.9 shows the fraction of coincident simulated hits created by the same neutrino and all detected hits as a function of the energy. The average energy of the bin is also given as numbers. The blue curve contains coincident hits which were detected by the same optical module, the green curve counts hits which were detected by different sensors.

The error in coincidence rate is determined as:

$$\sigma_y = \frac{m}{N}\sqrt{m(1-\frac{m}{N})}, \tag{4.14}$$

where m is the number of coincidences and N is the total number of hits.

Both rate curves are rising with increasing energy. They are flattened as compared to a linear incrase by a negative quadratic term due to the finite detector size (See also [110]).

Most of the coincident hits arrive at the same module as also shown in Fig. 4.7. The IceCube DOM unfortunately has a built in deadtime of 2.5 μs [69] which makes it necessary to look at the accumulated charge for overlapping signals. Waveforms are only stored with 300 MHz resolution if neighbouring modules have detected a coincident signal within 1 μs. This is rarely the case for neutrino signals from supernovae. We therefore concentrate on an investigation of coincident hits between different neighbouring modules at the cost of a lower coincident rate.

The major background affecting the analysis is the influence of atmospheric muons which can also cause coincidences with comparable time signatures. The hitspool/ background datasets for this analysis have therefore undergone a very intense, state of the art filtering process [1] which allows one to identify and flag most of the hits that have been caused by atmospheric muons.

4.2.2 Energy measurement using time and position information

The energy measurement analysis is based on the combination of two previous investigations, which each provide a table of detector response hits:

- Pure unfiltered (hitspool) data which have been extracted from IceCube in 2015. Hits that were induced by muons were identified and flagged using a set of various techniques and up to date algorithms [1]. This dataset will serve as a background sample.

- Simulated neutrino induced hits based on the Lawrence Livermore model of a supernova at a distance of ≈3 kpc (5 million simulated hits). This dataset provides the signal which is later merged with the hitspool data. This is the minimum distance (maximum number of hits) available from the simulation and will be fully exploited as a test of the method.

The table containing hits of the simulated signal is modified before being merged with the background table by:

- Matching the table column names to match the hitspool names and adding a boolean field, which indicates every hit as a simulation hit.

- Converting the simulation timestamps into single nanosecond counters based on the begnning of the UTC year.

- Cleaning out simulation artifacts by removing hits with identical production parameters (majorID and particle position)[1].

- Compensating further for simulation time periodicity effects by time-shifting hits from the same neutrino by a random integer between 0 to 10 μs.

- Adding a column wich represents the neutrino's energy in a binning of 5 MeV. This binning is applied to 80 % of the hits. This data will serve as a reference to a specific average energy. The remaining data are flagged as a full energy spectrum data and will serve as the test signal (at approx. 7 kpc) to be evaluated.

- Time sorting the resulting table.

[1] The simulation contained ≈10% of duplicated data. This data had been produced by different simulation nodes but sometimes its particle properties were identical. Every simulated event is uniquely identified by its major- and minorID [75]. The majorID is composed by characteristics of the computing node. The minorID is a local (per node) increasing event counter. The particles three dimensional coordinates were used to identify and remove duplicated hits produced by different nodes.

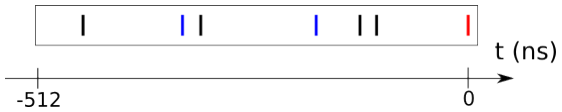

Figure 4.10: Lookback analysis method and sliding time window. A 512 ns sliding time window is shifted hit by hit over the time sorted table. The time and spatial difference between between the current hit (red) and the previous hits (black, blue) in the window is derived. Different colors indicate different types of hits (e.g. muon, simulation, background). Based in the time window illustration it can be seen that the number of coincidences of a combined dataset (black + blue) is larger than the sum of the individual dataset's coincidences. The number of pair-coincidences of n hits is given by the binomial coefficient of C(n,2). Assuming that the current hit is a blue hit, we have three blue hits, four black hits and seven hits in combination. The number of excess coincidences thus derives as C(7,2)-C(4,2)-C(3,2)=21-6-3=12.

The first step of the analysis procedure is to merge all hits of both time sorted background and signal tables. This is done by time shifting the simulation data to the start of the hitspool dataset. Different coincidence counters are then implemented, each processing only a specific subset of the whole table:

- Hitspool data (without hits flagged as induced by muons) combined with simulation hits (this is done for the 7 kpc test signal and for each of the 5 MeV energy binnings).
- Pure hitspool data without muon flagged hits.
- Pure simulation hits (test signal and one for each energy bin).
- Hitspool data with muon flagged hits (all background hits).

In order to improve the signal to noise ratio, we restrict ourselves to the strongest part of the signal. According to Fig. 4.8, the first 0.6 s are therefore evaluated in the following manner.

Every hit in the combined time sorted table is compared to its successor in time with respect to its category. A sliding time window, as shown in Fig. 4.10, is shifted over the data to enable investigation of all hit combinations in a specific time-space region.

The spatial distance (dx) of the modules registering a hit pair is determined by using the detector geometry. The time difference (dt) between two hit times is also derived and combined with an additional geometric information as follows. As IceCube's optical modules have a downward opening angle of ≈60 °, it is possible to distinguish partly between down- and upgoing events. Photons, that can only arrive at the sensor through scattering in the ice, arrive later. Hit pairs of which the first hit has registered on a spatially higher DOM has a higher probability to be a downgoing event and likely to be caused by muons. The time difference between these two hits is multiplied by (-1) in order to encode this information for later use.

As a next step, the resulting value pairs (dt, dx) are sorted into 2D histograms per category. Nine spatial bins are derived from Fig. 4.11 as such as that the first bin contains hits detected by the same module, its six neighbours

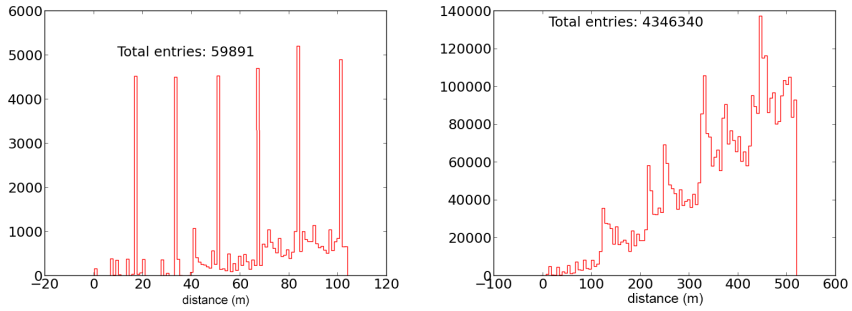

Figure 4.11: Distances between all optical modules within IceCube. The first six neighbours of an optical module are clearly distinguishable in the distance distribution (left). The smaller distances in between the large peaks are caused by DeepCore modules which are spaced more finely. At approximately 120 m, the first neighbouring string appears (right).

and the two neighbouring strings. The spatially denser *DeepCore* subdetector of IceCube contributes to the analysis by increasing the coincidences in the first bins. The time binning is divided equally into 32 ms bins. This binning was chosen to smoothen out remaining simulation time artifacts.

The resulting 2D histograms are shown in Fig. 4.12 in four different exemplary combinations containing only background with- and without muon subtraction, signal, and signal combined with muon reduced background. It can be seen that the muon induced hits are mainly downgoing (negative times) as they travel from the atmosphere downwards into the detector. It can also be seen that their influence can almost entirely be removed due to muon hit detection mechanism in the hitspool data processing chain. The signal induced hit pairs are equally distributed and do not favour any direction. They do though mainly populate the upward going region of the histogram due to the downward opening angle of the optical modules. This enables us to further distinguish between signal and muon induced background.

An additional background histogram is generated with higher statistics based on a separate 100 s hitspool dataset. In order to extract the simulated supernova signal, this high statistics background, properly scaled, is then subtracted from all combined background+signal histograms for every energy.

4.2.3 Hit coincidences

As a first step, the number of coincidences on directly neighbouring modules is investigated and displayed in Fig. 4.13. It is a 1D representation of the second bin of the respective 2D histogram in Fig. 4.12. The signal is extracted from the coincidence values of the combined signal plus background datasets by subtracting the coincidences obtained from a separate 100 s high statistics background sample (b_{100}).

As illustrated in Fig. 4.10, it has to be taken into account that the coincidence rate of the combined background (hs) plus signal (ll) dataset is higher than the sum of the coincidences for the individual datasets:

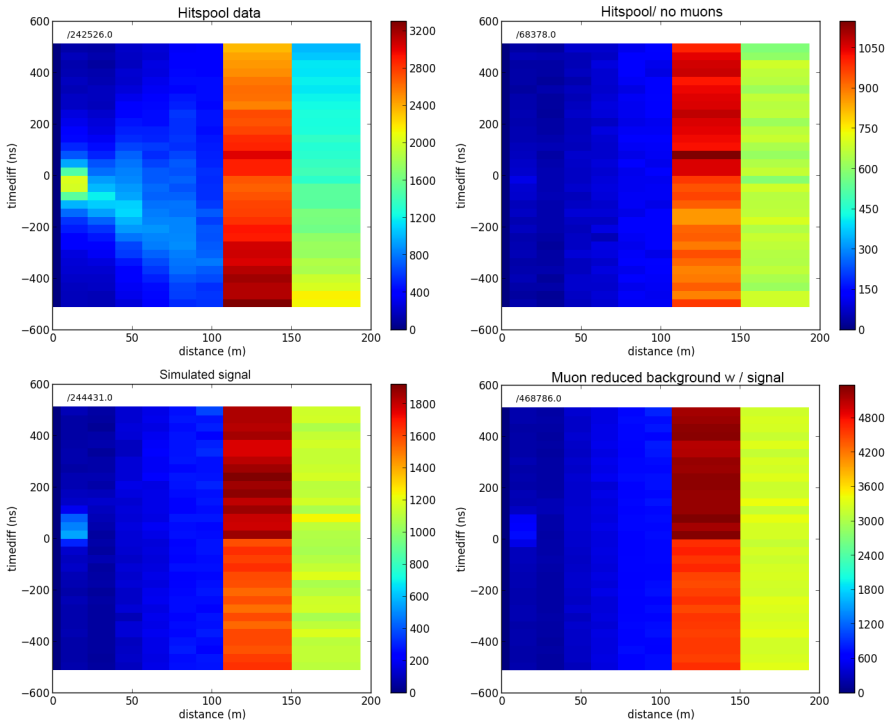

Figure 4.12: Hit-time difference over distance of the detecting optical modules for time differences between 0 and 512 ns and distances up to 180 m. Negative times indicate downward going events. The following datasets are being displayed: Full Hitspool background (upper left), hitspool data/ background with cosmic ray muon hits suppressed (upper right), simulated signal without taking noise into account (lower left) and simulated signal with measured noise added (lower right). Note that the intensity scales are different. It can be seen that the muon hits polluting the close region of neighbouring modules can be effecively cleaned from the hitspool data, strongly improving the signal to background ratio in this area.

$$\text{coinc(hs+ll)} = \text{coinc(hs)} + \text{coinc(ll)} + \text{excess(hits(hs+ll))} \quad . \tag{4.15}$$

The excess amount of coincident hits in the combined background plus signal (hs+ll) dataset depends effectively linear[2] on the total amount of hits in the combined dataset and can be fitted through all test-energy datapoints. The number of coincident signal hits per energy can then be derived from the combined test-datasets as

$$\text{coinc(ll)} = \text{coinc(hs+ll)} - \text{coinc(hs}_{100}\text{)}\frac{0.6\text{s}}{100\text{s}} - \text{excess(hits(hs+ll))} \quad . \tag{4.16}$$

[2]It has been found that the number of excess hit-time-differences due to the combination of background and signal hits depends effectively linearly on the measured time difference. For more details see Chapter A.2.

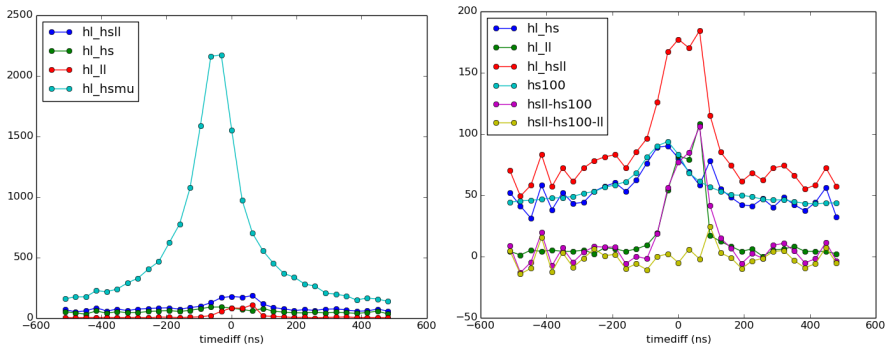

Figure 4.13: Histogram of hit time differences for neighbouring optical modules from 0 to 512 ns based on an average neutrino energy of ≈17.5 MeV. Negative times indicate a downward going hit sequence. The plots are 1D histograms extracted from the 1-DOM-distance bin of the 2D histograms in Fig. 4.12. The hitspool data before muon subtraction curve is displayed on the left side in order to demonstrate the effectiveness of the muon subtraction. For visibility reasons, it has been left out in the right plot. The following datasets are shown: Hitspool data with reduced muon background (hs), simulated signal (ll), hitspool data and simulated signal combined with muon reduced background (hsll), high statistics hitspool background (hs100) and simulated signal with background, reduced by the high statistics background and an excess offset (hsll-hs100). As an additional curve, the known signal has been subtracted from the reconstructed signal (hsll-hs100-ll). It can be seen that the hitspool datasets favour hits to accumulate on the downward going side which is being caused by remaining coincident muon hits, whereas the signal data mainly populates the positive region of the histogram.

Table 4.1: Signal to noise ratio of coincident hits depending on different time-space-cuts on the histograms shown in Fig. 4.12. The total amount (100%) of hits consists of ≈ 1.75 million hitspool hits (of which ≈ 2.8% were identified as muon hits) and 0.37 million signal hits based on the 0.6 s dataset. The last two lines show that approximately 40% of the coincident signal hits are distributed between the first six neighbouring modules and between direct neighbouring strings. These are mainly accidental coincidences not originating from the same event.

timecut (ns)	spatial cut	sig (%)	noise (%)
0:128	direct neighbour	5.4	0.4
-32:128	direct neighbour	6.3	0.5
0:128	next neighbour	0.5	0.3
0:128	next string	5.7	6.3
-512:512	all 6 neighbours	34	23
-512:512	next string	41	47

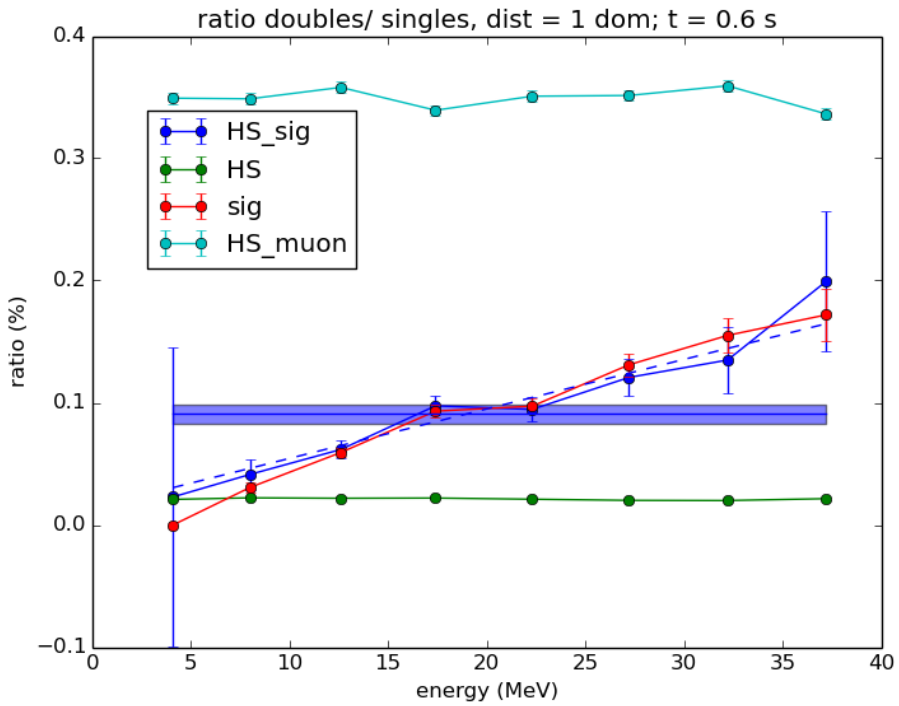

Figure 4.14: The ratio of coincident hits to single hits is displayed depending on the average energy of a subset of the simulated neutrino events. The *sig*-curve (red) is based on the pure signal, wheras the *hs_sig*-curve (blue) is derived from a combination of simulated signal hits and a hitspool background sample. The *hs* (green) and *hsmu* curves (cyan) do not contain any signal but illustrate the coincident hit ratio for the background dataset with- and without subtraction of hits identified as muon induced hits. The ratio of coincident hits to single hits of the full simulated neutrino energy spectrum including background is shown as the horizontal blue line including errorband. The intersection of the full spectrum result with the *hs_sig*-curve shows that the neutrino energy can be determined with an uncertainty of approximately 2 MeV for 7 kpc distance.

In order to extract the highest number of coincident signal hits with the lowest background, different time-space-cuts were applied to the 2D datasets displayed in Fig. 4.12. The results are summarized in Tab. 4.1. It can be seen that the best cut is obtained when only looking at neighbouring modules and time differences between -32 ns and 128 ns (compare to Fig. 4.13). The remaining noise rate after this cut is 2.8 Hz per DOM.

4.2.4 Coincidences on the neighbouring module

As outlined in the previous section, we restrict ourselves to coincidences between direct neighbouring modules and time differences between -32 and 128 ns. Fig. 4.14 shows the ratio of these coincidences by the number of single hits. This is performed for every test-energy with background and also for the Lawrence Livermore spectrum signal data at 7 kpc with background, which is displayed

as a blue line with an errorband.

It can be seen that, under the assumptions made, the 7 kpc signal can be well extracted from the background. The combined curve (blue) represents the pure signal (red) within its statistical error boundaries. The uncertainties of the combined curve propagate from the uncertainties of the signal, the hitspool background sample and the subtracted high statistics hitspool sample. Please note that the uncertainties are smallest around the average energy region as the test energy datasets were derived based on an energy distribution as shown in Fig. 4.8. The number of signal hits therefore decreases towards lower and higher energies.

The coincident- to single-hit ratio of the 7 kpc Lawrence Livermore spectrum data intersects the test-energy curve at ≈ 18.9 MeV with an uncertainty of 1.9 MeV. The average energy of the simulated neutrinos of 18.7 MeV can therefore be very well reconstructed within the given uncertainties.

With the access to hitspool data, tools to greatly reduce muon background and a new Geant based supernova neutrino hit simulation framework it is now possible to measure the mean energy of supernova neutrinos with IceCube within the distance to the galactic centre, which is where the next supernova is most likely to occur. The result is compatible with previous energy resolution simulations [108, 111] which have, however, not included real background datasets. In the following section we show that the uncertainty could in principle be decreased by observing coincidences on the same optical module, which, however is presently severely limited by the capabilities of the IceCube data acquisition setup.

4.2.5 Coincidences on the same module

The rate of supernova signal coincidences is approximately four times higher on average on the same module as on neighbouring modules as shown in Fig. 4.9. IceCube's data acquisition system on the other hand is optimized towards detecting inter module coincidences and discards certain information which would be needed to investigate short time coincidences per optical module.

Due to the internal 2.5 μs deadtime of the IceCube DOM, the hitspool data does not provide hit sequences on the same module in the $\mathcal{O}(100\,\text{ns})$ region. One option to access this data would be to investigate charge over time of the fADC and ATWD waveform digitizers (see Chap. 2.4). Due to coincidence criteria, each DOM unfortunately discards these waveform informations before sending them to the surface if the criterion with its neighbours is not met. The minimum information to always be transmitted with each hit is the peak charge value of the slow sampling fADC.

The deadtime limitation applies to all registered hits on one module. While the fADC in principle could sample up to 6.4 μs of PMT output, only the information related to the first hit is kept if no neighbouring DOM saw a photon within 1 μs. This was done in order to save bandwidth. By investigating the hit pattern of coincident simulated hits on the same module in Fig. 4.15 (right), one can see that the majority of the correlated coincidences caused by a neutrino interaction happen within the first 25 ns. As the sampling rate of the fADC is 40 MHz, these registered coincidences are unresolvable and are kept and transmitted with every hit.

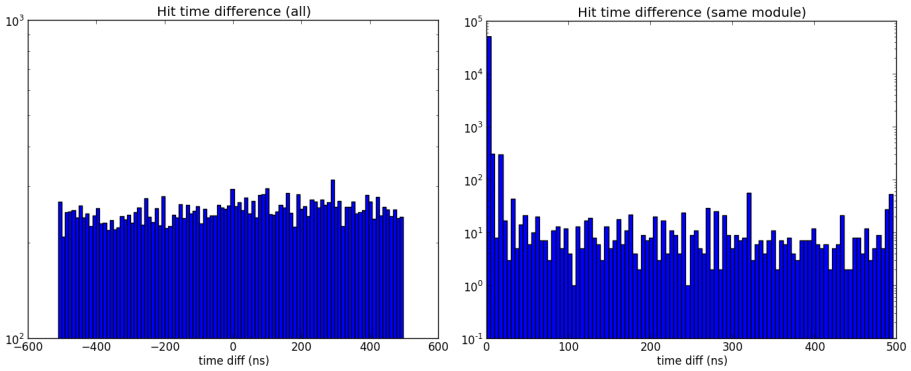

Figure 4.15: The left figure shows the hit time differences between all hitspool hits in the detector, excluding hit time differences on the same optical module due to module deadtime. The right plot shows simulated signal hit time differences on the same optical module. Coincident hits from the same neutrino event arrive mostly within one 25 ns cycle of the fADC sample rate.

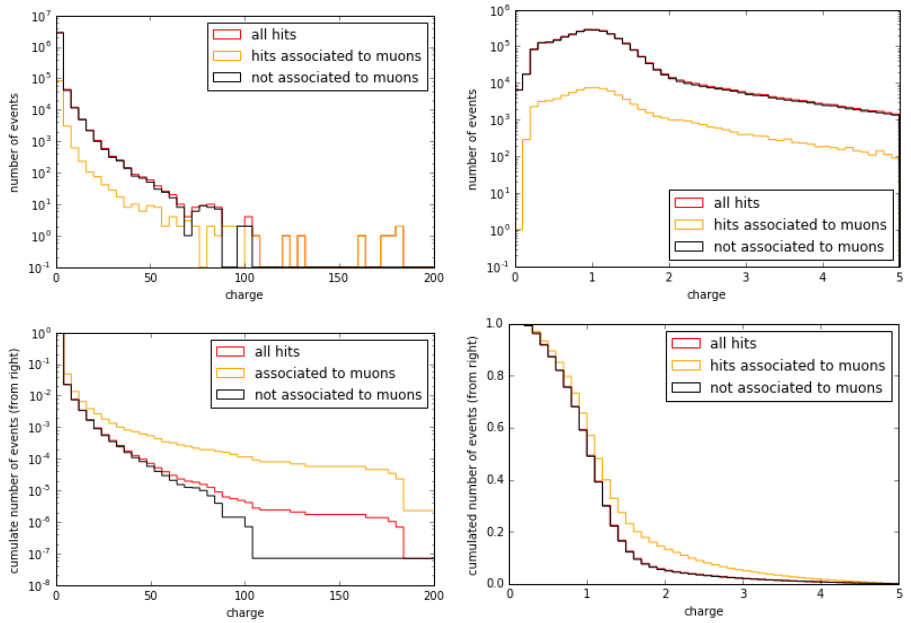

Figure 4.16: Dark rate background as function of pulse height (upper left) for the hitspool data sample. The lower plot shows a cumulative version. On the right side, zoomed in versions from 0 to 5 pe are shown in order to identify the best cut for the single photon distributuon. A charge cut at 1.5 pe eliminates most of the very broad single photon peak but leaves 18 % of the background.

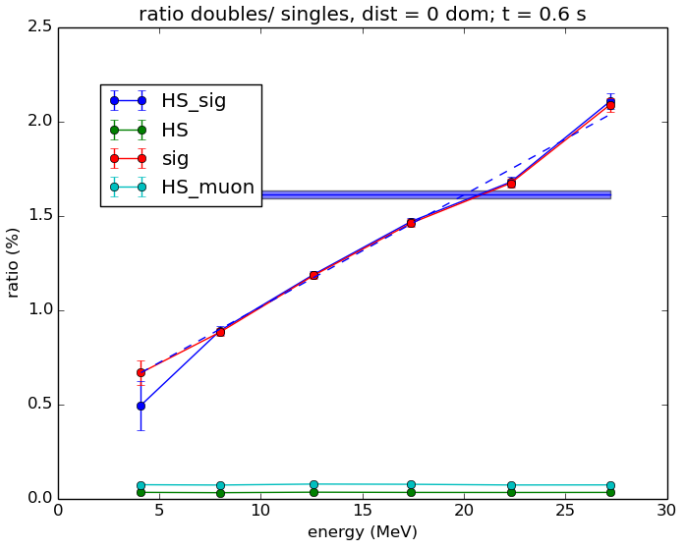

Figure 4.17: Ratio of coincident hits to single hits depending on the average energy of a subset of the simulated neutrino events. The coincident hits are collected by an assumed ideal optical module with no deadtime and no PE cut. All features in the plot are identical to Fig. 4.14.

A realistic approach would therefore be to restrict oneself to hits that can not be distinguished by the fADC as two hits separated in time and to exploit the peak photo-electron charge information which is registered by the optical module and is also available in the hitspool data. Only the first photoelectron (pe) peak is digitized by the 40 MHz fADC. A charge cut of e.g. 1.5 pe can then be applied to reduce single hit background as shown in Fig. 4.16.

Preliminary research has shown that it should possible to exploit the higher signal on the same module by investigating the charge information. This method though involves a substantially higher background influence due to a very broad charge distribution of the hitspool background hits as shown in Fig. 4.16. A relatively high cut of 1.5 pe is necessary to partially remove the 1 pe charge peak which still leaves 18 % of the background. This translates to a background rate of $\approx$ 102 Hz which is $\approx$ 40 times higher than the rate which can be obtained when applying time and spatial cuts as shown in Chap. 4.2.3.

4.2.6 Coincidences on future Gen2 modules

An intriguing option to explore the previous method on coincident hits on the same optical module is to assume an ideal detector with no deadtime. This might be possible in the future for the Gen2-extension [8] by using alternative optical modules like the multi-PMT module [106].

For the current hitspool noise datasets we assume that the background of coincident hits per multi-PMT module would be similar to the hit time distribution between two IceCube optical modules as shown in Fig. 4.15 (left). We also assume that the simulated signal data does not have a deadtime limitation. The simulated signal coincidences on the same module are shown in Fig. 4.15

Table 4.2: Systematic Uncertainties on the simulated signal rates.

Systematical uncertainty	Estimate (%)	Source
Effective photon volume	~ 12	[22, 91]
Ice properties	~ 5	[75]
$e^{\pm}$ track length	~ 5	[91]
Cross section for ν and $\bar{\nu}$	~ 1	[91]
Oscillation scenario in the star	~ 25	[12]
Earth matter oscillations	-8	[11]

(right). The result of this combined method can be seen in Fig. 4.17. The reconstructed energy is 20.0 ± 0.37 MeV and would carry a substancially lower statistical error due to the increased signal coincidence rate.

4.3 Systematic uncertainties

The analysis uses real noise data from the actual detector which does not carry a systematic error. This reduces overall systematic effects as compared to using simulated background hits. For the energy measurement procedure, the obtained coincidence rates are normalized against the single hit rates, hence further reducing systematic uncertainties [108].

Supernova model, energy distribution and width cannot be specified, but need to be determined from the measurement. The Lawrence Livermore model provides an optimistic number of supernova neutrinos and is currently the only model to be reliably supported by the new Geant based Monte Carlo system. There is a broad range of models coressponding to an order of magnitude variation in expected signal hits [12]. If the distance to the supernova is not known, the model dependence can be canceled out.

Systematic effects have still to be considered as simulated events are used in both investigations. Such effects arise from various sources, e.g. the modeling of the optical modules and the Antarctic ice as well as neutrino interaction and oscillation and are presented in table 4.2.

The ice properties within IceCube are very complex and vary throughout the detector. This effects both the absorption and the scattering (delay) of the photon signal hence modifying the hit rate. For the low energy supernova neutrinos, however, an average over the whole 1 km^3 cube can be assumed. The effective photon volume combines the uncertainties of the ice model ($\sim$5%), the optical module sensitivity ($\sim$10%) and the positron track length ($\sim$5%).

A normal hierarchy but no collective scattering effects of neutrinos are assumed, which may offset the effect of matter oscillation. The relative systematic effect on the hit rate reaches $\pm$25% depending on the oscillation scenario assumed. Earth matter oscillation effects have not been considered and yield another systematic effect of -8%.

Drilling the holes for the IceCube strings and the re-freezing process of the drilling water chages the ice structure in the hole and causes former impurities in the ice to settle on the module. Further effects are caused by cable shadows which are estimated to be as large as 3%. Understanding the hole ice is subject to recent studies [112].

Chapter 5

Conclusion and outlook

Due to its unmatched effective volume IceCube can currently provide the highest statistics light curve of a supernova explosion. IceCube's supernova data acquisition software therefore continuously monitors the dark noise rate of all optical modules. Technical restrictions like bandwidth and processing power limit this to a time binning of 2 ms. With the development of additional, high resolution data extraction and supernova signal simulation tools, the next step is to fully explore IceCube's capabilities in the supernova low-energy regime.

Improved stability and maintainability of the IceCube supernova data acquistion system has lead to a current record up-time of 99.7% on average, thus maximising the detection capability of these rare events. Several automated and manual alert response actions have been explored in order to most efficiently use the opportunity time window to alert the astronomical community. Different communication channels have been investigated and combined, transporting carefully selected messages and datasets, in order to reduce overall delay time of important information from the order of days to minutes or even seconds.

In order to achieve an uptime of 100% in supernova detection, IceCube already contributes to an inter-experiment coincidence system, providing a rather coarse timestamp of the determined signal onset time. This Supernova Early Warning System combines various information from every participating experiment such as e.g. the supernova direction. Different options have been explored to improve the information provided by IceCube. Investigations on IceCube internal triangulation show that the direction of a supernova up to the center of the Milky Way can be determined with ≈20 degree uncertainty if the effect of neutrino masses can be neglected and the neutrino flux ceases sufficiently fast at the black hole forming star. By expanding its online analysis to include a simple, two-parameter fit IceCube could also contribute the supernova signal onset-time with a precision on the order of milliseconds. At least two more neutrino detectors offering comparable precision will become operational within the next 10 years which would enable for a ≈10 ° resolution of supernova direction reconstruction based on inter-experiment triangulation.

The method of exploiting nanosecond scale coincidences on optical modules to obtain information about the neutrino energy has been tested for the first time based on new high resolution post-alert data extraction and high resolution simulation data. In the current IceCube configuration, including the current low energy extension, it was found that the average neutrino energy can be

determined with MeV-precision at a distance close to the galactic centre, by exploiting the strongest part of the neutrino light curve. Future low energy detector extensions with smaller inter module distances and improved module deadtime would enable to improve this result and allow to track the neutrino energy development throughout the cooling phase.

Appendix A

Appendix

A.1 Neutrino flux in IceCube

As the IceCube detector counts photon hits and not neutrinos a relation between the two is needed in order to combine theoretical models and measurements. An example is shown in Fig. A.1 for a sample supernova neutrino light curve. The left axis displays detector hits and the right axis shows the corresponding neutrino luminosity depending on the average neutrino energy. With additional knowledge of the neutrino energy spectrum the neutrino luminosity can be derived based on the number of observed hits.

The dependence of the hit rate on the luminosity can be simplified as follows. We start off with the basic expression of the time dependent hit rate R(t) in the detector [12]:

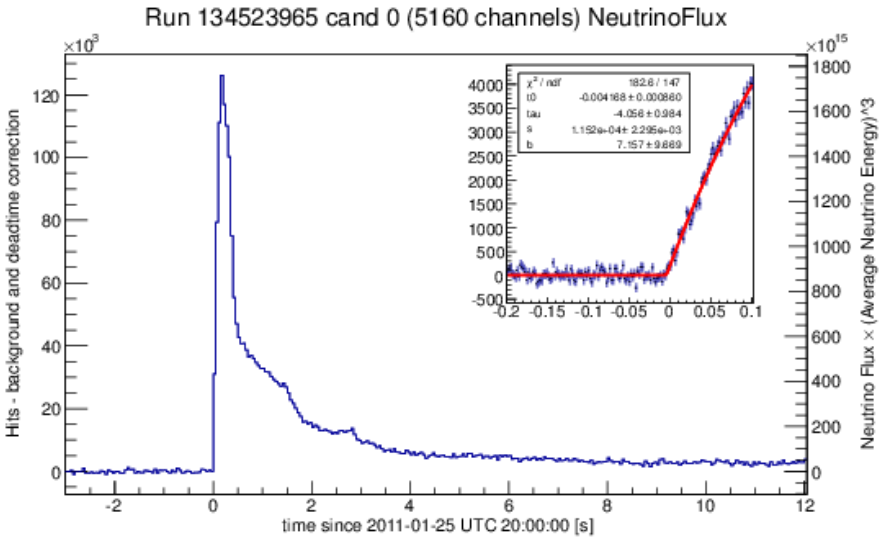

Figure A.1: Relation between hitrate and neutrino luminosity shown for a simulated signal in a 2 ms binning with subtracted average background. The total luminosity can be derived if the average neutrino energy is known.

$$\begin{aligned} R(t) =& \epsilon_{\text{deadtime}} \frac{n_{\text{target}}\, L^{\nu}_{\text{SN}}(t)}{4\pi d^2 \overline{E_\nu}(t)} \int_0^\infty dE_{\text{e}} \int_0^\infty dE_\nu \\ & \times \frac{d\sigma}{dE_{\text{e}}}(E_{\text{e}}, E_\nu) V^{\text{eff}}_{\text{e}^+} f(E_\nu, \overline{E_\nu}, \alpha_\nu, t) \quad . \end{aligned} \tag{A.1}$$

An approximate expression for $\frac{d\sigma}{dE_e}(E_e, E_v)$ is given by:

$$\frac{d\sigma}{dE_e} = \sigma(E_\nu) \cdot \delta(E_e - E_\nu + \Delta) \tag{A.2}$$

with [13]:

$$\sigma(E_\nu) \approx 10^{-43}\text{cm}^2 \cdot p_e \cdot E_e \cdot E_\nu^{-0.07+0.02 \ln E_\nu - 0.002 (ln E_\nu)^3} \quad . \tag{A.3}$$

Note that the latter is only valid in the coarse approximation

$$E_e = E_\nu - \Delta \tag{A.4}$$

with

$$\Delta = m_n - m_p \approx 1.293 \text{ MeV} \tag{A.5}$$

and [12]

$$p_e = \sqrt{E_e^2 - m_e^2} \quad . \tag{A.6}$$

Simulations of the detector in the ice yield

$$V^{\text{eff}}_{\text{e}^+} = 29.0 \pm 3.8 \text{ m}^3 \cdot E_e \tag{A.7}$$

and the deadtime leads to a loss of

$$\epsilon_{\text{deadtime}} \approx 0.87/(1 + R(t) \cdot \tau), \tag{A.8}$$

with an artificial deadtime [22] of

$$\tau = 250 \times 10^{-6} s \tag{A.9}$$

and a target density of

$$n_{\text{target}} = 2 \cdot (916.6 \pm 1.6) \text{ kg/m}^3 \cdot N_A/(0.018 \text{ kg/mol}) \tag{A.10}$$

$$N_A = 6.022 \times 10^{23}. \tag{A.11}$$

$$R(t) = \epsilon_{\text{deadtime}} \frac{n_{\text{target}}\, L^{\nu}_{\text{SN}}(t)}{4\pi d^2 \overline{E_\nu}(t)} \int_0^\infty dE_\nu \times \sigma(E_\nu)\; V^{\text{eff}}_{\text{e}^+}\; f(E_\nu, \overline{E_\nu}, \alpha_\nu, t) \tag{A.12}$$

$$\begin{aligned} R(t) =& 29.0 \cdot 10^{-43} \epsilon_{\text{deadtime}} \frac{n_{\text{target}} L^{\nu}_{\text{SN}}(t)}{4\pi d^2 \overline{E_\nu}(t)} \int_0^\infty dE_\nu \\ & \times \sqrt{(E_\nu - \Delta)^2 - m_e^2} \cdot E_\nu^{-0.07+0.02 \ln E_\nu - 0.002 (ln E_\nu)^3} \\ & \cdot (E_\nu - \Delta)^2 f(E_\nu, \overline{E_\nu}, \alpha_\nu, t) \end{aligned} \tag{A.13}$$

or in the more naive approximation:

$$\sigma \approx 9.52 \times 10^{-44} \frac{p_e E_e}{\mathrm{MeV}^2} cm^2 \tag{A.14}$$

$$\begin{aligned} R(t) =& 29.0 \cdot 9.52 \cdot 10^{-44} \epsilon_{\mathrm{deadtime}} \frac{n_{\mathrm{target}} L^{\nu}_{\mathrm{SN}}(t)}{4\pi d^2 \overline{E_\nu}(t)} \int_0^\infty dE_\nu \\ & \times \sqrt{(E_\nu - \Delta)^2 - m_e^2} \cdot (E_\nu - \Delta)^2 \, f(E_\nu, \overline{E_\nu}, \alpha_\nu, t) \end{aligned} \tag{A.15}$$

for

$$E_e \approx E_\nu \approx p_\nu : \tag{A.16}$$

$$\begin{aligned} R(t) \approx& 0.276 \cdot 10^{-41} \epsilon_{\mathrm{deadtime}} \frac{n_{\mathrm{target}} L^{\nu}_{\mathrm{SN}}(t)}{4\pi d^2 \overline{E_\nu}(t)} \int_0^\infty dE_\nu \\ & \times E_\nu^3 f(E_\nu, \overline{E_\nu}, \alpha_\nu, t) \\ \approx& 0.276 \cdot 10^{-41} \epsilon_{\mathrm{deadtime}} \frac{n_{\mathrm{target}} \, L^{\nu}_{\mathrm{SN}}(t)}{4\pi d^2} \overline{E_\nu^3} / \overline{E_\nu}(t) \end{aligned} \tag{A.17}$$

solving for the luminosity $L^{\nu}_{\mathrm{SN}}(t)$:

$$\begin{aligned} L^{\nu}_{\mathrm{SN}}(t) \approx& 4.165 \times 10^{41} \frac{R(t) \cdot (1 + R(t) \cdot 0.00025) \cdot 4\pi \cdot d^2 \cdot \overline{E_\nu}}{n_{\mathrm{target}} \cdot \overline{E_\nu^3}(t)} \\ \approx& 8.9 \times 10^{14} \frac{R(t) \cdot (1 + R(t) \cdot 0.00025) \cdot d^2 \cdot \overline{E_\nu}}{\overline{E_\nu^3}(t)} \end{aligned} \tag{A.18}$$

$$\longrightarrow R(t) \cdot (1 + R(t) \cdot 0.00025) = \frac{L^{\nu}_{\mathrm{SN}}(t)}{d^2} \frac{\overline{E_\nu^3}(t)}{\overline{E_\nu}} \cdot 1.11 \times 10^{-14} \quad . \tag{A.19}$$

This quadratic formula needs to be solved for R(t). When working with Hitspool[1] data, the deadtime related coefficient is zero simplifying the hit rate to luminosity relation to

$$R(t) = \frac{L^{\nu}_{\mathrm{SN}}(t)}{d^2} \frac{\overline{E_\nu^3}(t)}{\overline{E_\nu}} \cdot 1.11 \times 10^{-14} \quad . \tag{A.20}$$

The derived rate is given for one standard IceCube DOM. The luminosity has to be provided in MeV/s, and the distance[2] in cm.

An alternative approach to derive the hit rate depending on the average neutrino energy and the α-Parameter (see Chap. 1.5.3) of the neutrino energy spectrum can be found in [113]. When using a pinching factor α, one can eliminate the $\overline{E_\nu^3}$ dependence by the relation of

$$\frac{\overline{E_\nu^3}}{\overline{E_\nu}} = \overline{E_\nu}^2 \frac{(1+\alpha)^2}{(2+\alpha)(3+\alpha)} \quad . \tag{A.21}$$

[1] As discussed in the detector chapter, hitspool data has no artificial deadtime but, due to its large size, is only available with a delay on the order of days. Hitspool based analyses could be performed on-site to remedy this situation.

[2] 1 kpc = $3.086 \cdot 10^{21}$ cm

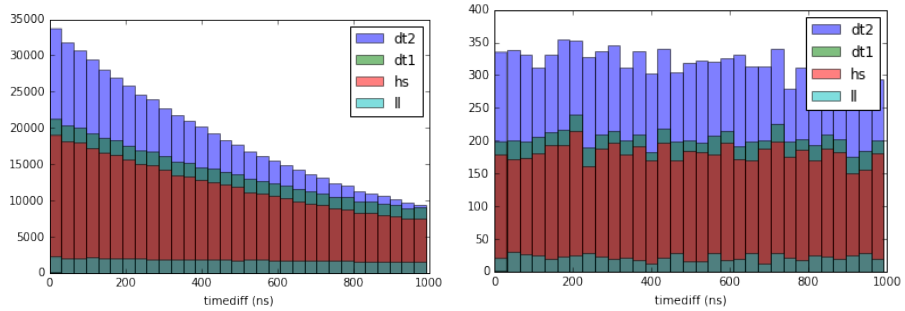

Figure A.2: The histograms show the time difference distributions between 0 and 1000 ns of two Poissonian hit datasets (hs and ll) of 0.6 s length at a very high hit rate (left) and a lower hit rate (right). The ratio of hs to ll hits is 3:1. The $dt1$ histogram sums the number of hit time differences whereas the $dt2$ histogram illustrates the hit time differences in the combined hs and ll datasets. When looking at the difference $dt = dt2 - dt1$ it can be seen that the combined dataset shows an increased number of time difference entries in the range of the histogram. In the low rate histogram the time difference distribution is approximately linear.

A.2 Excess hit time differences

Details on describing the time difference distribution of combined (or subtracted) Poissonian hit datasets in a binned histogram are given in this appendix. Generally, the normalized likelihood distribution for time differences is given by

$$f(\Delta t) = R\exp(-R\Delta t) = \frac{N}{T}\exp(-\frac{N}{T}\Delta t) \quad , \tag{A.22}$$

where $R = N/T$ is the rate and N the number of events measured in the time T. If the number of events is small, then the exponential function becomes approximately linear. Fig A.2 shows two cases for a large number of hits and a smaller number of hits which is on the order of the coincident hit rate of the analysis.

When adding two Poissonian datasets, the density of hits increases favouring shorter hit time differences and suppressing longer ones. In order to subtract the background ($_2$) from a combined signal and background hit dataset ($_1$), the likelihood distribution can be written as

$$\begin{aligned} f(\Delta t_1) - f(\Delta t_2) &= R_1\exp(-R_1\Delta t) - R_2\exp(-R_2\Delta t) \\ &= (R_1 - R_2) + (-R_1^2 + R_2^2)\Delta t + \mathcal{O}(\Delta t^2) \end{aligned} \tag{A.23}$$

as illustrated in Fig. A.3. For a low rate of coincident hits, such as shown in Fig. A.2 (right), the excess of small hit time differences within the range of the histogram is approximately equally distributed over every bin. The number of excess hits in bin i, and a total number of bins N_B, can then be approximated as

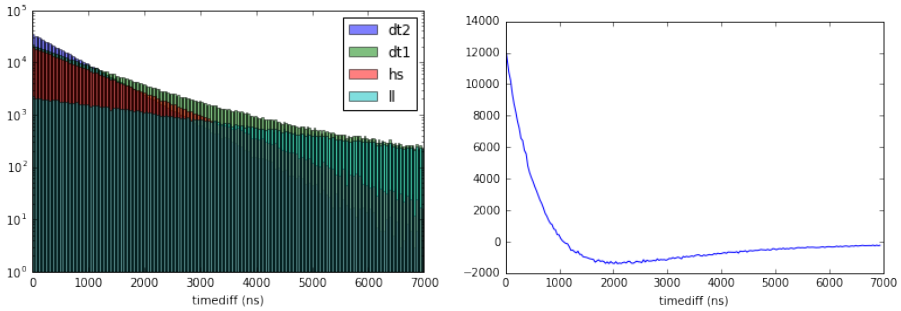

Figure A.3: A longer timeframe illustration of Fig. A.2 (left) between 0 and 7 μs (left) and the corresponding distribution of dt (right). It can be seen that the combination of two Poissonian datasets favours shorter hit time differences and suppresses longer ones.

$$n_i \approx \frac{N_1 - N_2}{N_B} \quad . \tag{A.24}$$

A.3 Automatic SnDaq alerts

An IceCube wiki page[3] explains the different SnDaq I3Live alerts, what they mean and how to respond. They are meant to be used as an on site reference manual additional to prior training. Only two alert conditions require human intervention. The numbers given are the real I3Live alert numbers for SnDaq at the South Pole system. This appendix is an extract of the on-site operator's wiki and is meant to be understood as a list of instructions the winter over personnel.

- SnDaq is set up to be automatically restarted by I3Live in case of problems which can be cured by a restart. In case of a page[4] a simple restart will not help.
- In case of a page caused by the following alerts please have a look at SnDaq's logfile[5], follow the step by step instructions listed below and report to logbook.
- Manually restarting SnDaq will not solve any of the alerts mentioned on this page. It will only cure the symptoms for another 15 minutes or so and probably make things worse.
- Do not restart SnDaq before having looked at its logfile and having followed the instructions listed below. It will reduce SnDaq uptime and not solve the problem.

[3] https://wiki.icecube.wisc.edu/index.php/Sndaq -> What to do in case of an I3Live alert or page
[4] A page is an immediate notification the pager device of the IceCube winter over on shift.
[5] pdaq@2ndbuild:/usr/local/pdaq/stage/sndaq/current_build/log/sndaq.log

A.3.1 List of alerts

All experiment specific alerts are shown on the IceCube-Live status page as shown in Fig. 3.7. They usually appear green and can turn red in case their alert condition is triggered. Every alert is clickable and then presents its alert definition, a short description and a historical summary of when it was triggered. A corresponding wiki page provides further information on how to react to each individual alert.

Time since SnDaq reported its latency to I3Live

- Alert number: 122[6]
- Paging: **This alert generates pages to the winter-overs**
- I3live alert definition: maxdt_sndaq_latency=900

This alert is based on the time that has passed since SnDaq hast last reported its latency to i3live. This can be caused by different reasons and further investigation based on SnDaq's logfile is necessary. The threshold for this alert is 900 s or 15 min.

- SnDaq is still running but having trouble to understand the data it receives from pDaq. Hence restarting SnDaq will not help but just reset the alert.
- A corrupt raw data file (tmp/sn*.dat) which causes SnDaq to repeatedly crash or freeze while trying to process it (then this corrupt data file has to be manually (re)moved)
- Global detector downtime (in this case no action has to be performed, the alert should clear itself once pDaq is up and running again)
- Many corrupt data files coming in from pDaq in a row which are recognized as corrupt by SnDaq. This is not counted as "sucessfully processing data" and therefore creates an alert after 15 minutes. No action is to be performed either except maybe to keep an eye on the logfiles until "normal" sn-raw data starts to be processed again. If a large number of raw-data files are affected then it is best to stop SnDaq, wait until the next run starts, move all bad raw files of the old run into a separate directory for later investigation and then start SnDaq so that it will start processing the new run.
- pDaq is running but not properly providing sn raw data (this has happened for example in Jan 15 as data was accidentally flowing to pdaq2 instead of 2ndbuild). This problem has to be solved on pDaq side.

Solutions can be found in the Winterover training guide. Usually the SnDaq log file should be very conclusive and allow to identfy easily e.g. a corrupted datafile which can then manually put aside. Please inform the operations logbook and experts about the steps that have been performed.

[6] https://live.icecube.wisc.edu/live_alert/122/

Max SnDaq latency

- Alert number: 136[7]
- Paging: This alert does not generate pages to the winter-overs
- I3Live alert definition: max_sndaq_latency=900,800

This alert is based on the current time difference between data time that SnDaq is currently processing and realtime. SnDaq has a intrinsic delay of about 5 mín, a larger value might point to data having piled up on 2ndbuild. If nothing obvious shows up in the logfile this should not be a problem to worry about. If SnDaq is properly processing this backlog should catch up approximately four times faster than realtime. The threshold for this alert is 900 s, deactivating if dropping below 800 s.

Max time between SnDaq alerts

- Alert number: 135[8]
- Paging: This alert does not generate pages to the winter-overs
- I3Live alert definition: maxdt_sndaq_alert=86400

Usually there are SnDaq alerts at about every 4-6 hrs depending on the season. If this alert triggers it might be due to connection problems to I3Live. This should be obvious in the logfile. If there is nothing to be found it might be that there has not been an alert. Please keep having an eye on the log file if there is an alert coming up which cannot be transmitted to I3Live and contact the coressponding experts. This alert triggers if no supernova alert has been registered within 24 h.

SERIOUS SN alert triggered!

- Alert number: 111[9]
- Paging: **This alert generates pages to the winter-overs**
- I3Live alert definition: max_sndaq_significance=10.0,5.0

This alert has been caused by:

- The latest sn significance observed by SnDaq has been > 10

Solution:

- Please follow the supernova alert escalation scheme as shown in Fig. 3.2 and perform the following technical operations[10].
- After the current run is finished please put aside a hardlink copy of the sn-raw data from the sn-raw data backup ring:

[7] https://live.icecube.wisc.edu/live_alert/136/
[8] https://live.icecube.wisc.edu/live_alert/135/
[9] https://live.icecube.wisc.edu/live_alert/111/
[10] https://wiki.icecube.wisc.edu/index.php/What_to_do_in_case_of_a_high_SN_alert

  - From within pdaq@2ndbuild:/software/stage/sndaq/current_build/ create backup folder for sn-raw (tmp) files, e.g.

    ```
    mkdir tmp/tmp_119362
    ```

    .

  - Create hardlink copy of sn-raw files of the whole run, e.g.

    ```
    cp -l tmp/backup/sn_119362_*.dat* tmp/tmp_119362/
    ```

    .

- Put aside PFFilt DST data corresponding to the run, at least the three files around the trigger timestamp. Currently the only way to retrieve these files would be to get them from the sattx machines.

- Make sure, that hitspool data has been sucessfully put aside (if already available).

- Check for interference sources with the detector and inform the e-mail lists run-coordination and sn-wg.

- Read instructions in the coressponding sn-alert email to sn-wg when available.

- The I3Live alert condition can be cleared by performing the following command from within the SnDaq current_build directory:

  ```
  ./bin/sni3ctl reset10sigmaAlert
  ```

Supernova DAQ state check

- Alert number: 78[11]

- Paging: This alert does not generate pages to the winter-overs

- I3Live alert definition: sndaq_state_is_not=RUNNING

This alert has been caused by:

- SnDaq has crashed

- LSD.py has crashed

Solution:

- I3Live should automatically take care of restarting SnDaq.

- If restarting fails, alert #122 will eventually trigger.

[11] https://live.icecube.wisc.edu/live_alert/78/

Exceeding unpacked temporary file count

- Alert number: 11[12]
- Paging: This alert does not generate pages to the winter-overs
- I3Live alert definition: max_sndaq_tmpFileCount=2,1

This alert has been caused by:

- The number of sn-raw files created by pDaq and moved into SnDaq's processing directory by process_files.pl has increased over 2. They are found here: 2ndbuild:/usr/local/pdaq/sndaq/tmp*.dat
- Usually SnDaq processes these files much faster than they appear so that their number should never be >1
- The SnDaq LSD component counts these files and sends it as a monitoring quantity (sndaq_tmpFileCount) to I3Live based on which the alert is created.
- For the sdaq dataflow please refer to Fig. 3.4.

Solution:

- The data backlog should automatically decrease if SnDaq is running properly.
- If processing fails, alert #122 will eventually trigger.

Exceeding secondary temporary file count

- Alert number: 97[13]
- Paging: This alert does not generate pages to the winter-overs
- I3Live alert definition: max_sndaq_dataFileCount=10,3

This alert has been caused by:

- The number of sn-raw files created by pDaq has increased over 10. They are found here: 2ndbuild:/mnt/data/pdaqlocal/SPS*sn.tar
- The SnDaq LSD component counts these files and sends it as a monitoring quantity (sndaq_dataFileCount) to I3Live based on which the alert is created.
- For the sdaq dataflow please refer to Fig. 3.4.

Solution:

- Check if the process_files.pl cronjob is active.
- Check if process_files.pl can be called without returning an error. Process_files.pl output can usually be found in sndaq.log.
- If process_files.pl continously fails to operate eventually alert #122 will trigger. If sndaq.log in inconclusive please contact the experts.

[12] https://live.icecube.wisc.edu/live_alert/11/
[13] https://live.icecube.wisc.edu/live_alert/97/

Bibliography

[1] D. Heereman. "HitSpooling: An Improvement for the Supernova Neutrino Detection System in IceCube". PhD thesis. Université Libre de Bruxelles, 2015. URL: http://w3.iihe.ac.be/~dheereman/thesis/PhD_dheereman_submitted_version.pdf (cit. on pp. 1, 12, 33, 35, 37, 44, 71, 82).

[2] Wikipedia. *Standard Model*. https://en.wikipedia.org/wiki/Standard_Model. [Online; accessed 07-July-2017]. 2017 (cit. on p. 4).

[3] Francis Halzen. "Status of Neutrino Astronomy: The Quest for Kilometer Scale Instruments". In: *arXiv preprint astro-ph/9701029* (1997). arXiv: astro-ph/9701029 (cit. on p. 4).

[4] Wolfgang Wagner. "Design and realisation of a new AMANDA data acquisition system with transient waveform recorders". PhD thesis. Universität Dortmund, 2005 (cit. on p. 5).

[5] Ulrich F Katz and Ch Spiering. "High-energy neutrino astrophysics: Status and perspectives". In: *Progress in Particle and Nuclear Physics* 67.3 (2012), pp. 651–704 (cit. on p. 6).

[6] F Halzen. "The Case for a Kilometer-Scale High-Energy Neutrino Detector: 1996". In: *arXiv preprint astro-ph/9605014* (1996) (cit. on p. 4).

[7] IceCube Collaboration et al. "Evidence for high-energy extraterrestrial neutrinos at the IceCube detector". In: *Science* 342.6161 (2013), p. 1242856 (cit. on pp. 4, 20, 28).

[8] MG Aartsen et al. "IceCube-Gen2: a vision for the future of neutrino astronomy in Antarctica". In: *arXiv* (2014). arXiv: 1412.5106 (cit. on pp. 4, 90).

[9] Joseph A Formaggio and GP Zeller. "From eV to EeV: Neutrino cross sections across energy scales". In: *Reviews of Modern Physics* 84.3 (2012), p. 1307 (cit. on p. 4).

[10] Raj Gandhi et al. "Neutrino interactions at ultrahigh energies". In: *Physical Review D* 58.9 (1998), p. 093009 (cit. on p. 5).

[11] A. Piégsa. "Supernova-Detektion mit d. IceCube-Neutrinoteleskop". PhD thesis. Johannes Gutenberg Universität Mainz, 2009. URL: http://ubm.opus.hbz-nrw.de/volltexte/2010/2166/pdf/diss.pdf (cit. on pp. 7–9, 35, 51, 91).

[12] R Abbasi et al. “IceCube sensitivity for low-energy neutrinos from nearby supernovae”. In: *Astronomy & astrophysics* 535 (2011), A109. DOI: 10.1051/0004-6361/201117810 (cit. on pp. 5, 27, 33, 37, 56, 72, 79, 91, 95, 96).

[13] A. Strumia and F. Vissani. “Precise quasielastic neutrino/nucleon cross-section”. In: *Physics Letters B* 564.1 (2003), pp. 42–54. DOI: 10.1016/S0370-2693(03)00616-6 (cit. on pp. 6, 96).

[14] Juerg Beringer et al. “Review of particle physics particle data group”. In: *Physical Review D (Particles, Fields, Gravitation and Cosmology)* 86.1 (2012) (cit. on p. 7).

[15] T. Feser. “Echtzeit-Suche nach Neutrinoausbrüchen von Supernovae mit dem AMANDA-II Detektor”. PhD thesis. Johannes Gutenberg Universität Mainz, 2004. URL: http://ubm.opus.hbz-nrw.de/volltexte/2005/678/pdf/diss.pdf (cit. on p. 7).

[16] Kei Kotake, Katsuhiko Sato, and Keitaro Takahashi. “Explosion mechanism, neutrino burst and gravitational wave in core-collapse supernovae”. In: *Reports on Progress in Physics* 69.4 (2006), p. 971 (cit. on pp. 8, 21).

[17] Carlo Giunti and Chung W Kim. *Fundamentals of neutrino physics and astrophysics*. Oxford university press, 2007 (cit. on p. 9).

[18] Amol S Dighe, Mathias Th Keil, and Georg G Raffelt. “Detecting the neutrino mass hierarchy with a supernova at IceCube”. In: *Journal of Cosmology and Astroparticle Physics* 2003.06 (2003), p. 005 (cit. on p. 9).

[19] Fritz Zwicky. “Die rotverschiebung von extragalaktischen nebeln”. In: *Helvetica Physica Acta* 6 (1933), pp. 110–127 (cit. on p. 10).

[20] NC Santos et al. “Star Formation in Bok Globules: Near-Infrared Survey of a Southern Sky Sample”. In: *The Astronomical Journal* 116.3 (1998), p. 1376 (cit. on p. 10).

[21] AGW Cameron. “The first ten million years in the solar nebula”. In: *Meteoritics* 30.2 (1995), pp. 133–161 (cit. on p. 10).

[22] T. Griesel. “Optimierung des Nachweises von Supernovae in IceCube”. PhD thesis. Johannes Gutenberg Universität Mainz, 2010. URL: http://ubm.opus.hbz-nrw.de/volltexte/2010/2479/pdf/doc.pdf (cit. on pp. 12, 17, 24, 33, 91, 96).

[23] Alexander Heger et al. “How massive single stars end their life”. In: *The Astrophysical Journal* 591.1 (2003), p. 288 (cit. on pp. 11, 13).

[24] Stanford E Woosley, Alex Heger, and Thomas A Weaver. “The evolution and explosion of massive stars”. In: *Reviews of modern physics* 74.4 (2002), p. 1015 (cit. on p. 11).

[25] Rudolph Minkowski. “Spectra of supernovae”. In: *Publications of the Astronomical Society of the Pacific* 53 (1941), p. 224 (cit. on p. 11).

[26] Alexei V Filippenko. “Optical spectra of supernovae”. In: *Annual Review of Astronomy and Astrophysics* 35.1 (1997), pp. 309–355 (cit. on p. 12).

[27] David Branch and GA Tammann. “Type Ia supernovae as standard candles”. In: *Annual review of astronomy and astrophysics* 30.1 (1992), pp. 359–389 (cit. on p. 12).

[28] Bruno Leibundgut. “Type Ia Supernovae”. In: *Astronomy and Astrophysics Review* 10.3 (2000), pp. 179–209 (cit. on p. 12).

[29] Subrahmanyan Chandrasekhar. “The maximum mass of ideal white dwarfs”. In: *The Astrophysical Journal* 74 (1931), p. 81 (cit. on p. 12).

[30] Stan Woosley and Thomas Janka. “The physics of core-collapse supernovae”. In: *Nature Physics* 1.3 (2005), pp. 147–154 (cit. on p. 13).

[31] H-Th Janka et al. “Theory of core-collapse supernovae”. In: *Physics Reports* 442.1 (2007), pp. 38–74 (cit. on p. 14).

[32] Hans-Thomas Janka and Ewald Müller. “Wenn Sterne explodieren: Die Theorie von Supernovae”. In: *Physik in unserer Zeit* 32.5 (2001), pp. 202–211 (cit. on p. 15).

[33] Adam Burrows. “Towards a synthesis of core-collapse supernova theory”. In: *Nuclear Physics A* 606.1-2 (1996), pp. 151–166 (cit. on p. 15).

[34] Mathias Th Keil. “Supernova neutrino spectra and applications to flavor oscillations”. PhD thesis. 2003. arXiv: astro-ph/0308228 (cit. on p. 15).

[35] Hans-Thomas Janka and Ewald Müller. *Supernovaexplosionen massereicher Sterne*. 2001 (cit. on pp. 16, 19).

[36] T Foglizzo, L Scheck, and H-Th Janka. “Neutrino-driven convection versus advection in core-collapse supernovae”. In: *The Astrophysical Journal* 652.2 (2006), p. 1436 (cit. on p. 16).

[37] K-L Kratz et al. “Nucleosynthesis modes in the high-entropy-wind of type II supernovae”. In: *New Astronomy Reviews* 52.7 (2008), pp. 390–395 (cit. on p. 16).

[38] T Totani et al. “Future detection of supernova neutrino burst and explosion mechanism”. In: *The Astrophysical Journal* 496.1 (1998), p. 216. DOI: 10.1086/305364 (cit. on pp. 17, 21, 58, 79).

[39] Jorge I Zuluaga. “Study of core collapse neutrino signals and constraints on neutrino masses from a future Galactic Supernova”. PhD thesis. 2005 (cit. on p. 18).

[40] Mathias Th Keil, Georg G Raffelt, and Hans-Thomas Janka. “Monte Carlo study of supernova neutrino spectra formation”. In: *The Astrophysical Journal* 590.2 (2003), p. 971. DOI: 10.1086/375130 (cit. on pp. 18, 19, 72, 79).

[41] J Robert Oppenheimer and George M Volkoff. “On massive neutron cores”. In: *Physical Review* 55.4 (1939), p. 374 (cit. on p. 19).

[42] I Bombaci. “The maximum mass of a neutron star.” In: *Astronomy and Astrophysics* 305 (1996), p. 871 (cit. on p. 19).

[43] John Antoniadis et al. “A massive pulsar in a compact relativistic binary”. In: *Science* 340.6131 (2013), p. 1233232 (cit. on p. 19).

[44] K Sumiyoshi et al. “The fate of a neutron star just below the minimum mass: does it explode?” In: *arXiv preprint astro-ph/9707230* (1997) (cit. on p. 19).

[45] Bülent Kiziltan et al. “The neutron star mass distribution”. In: *The Astrophysical Journal* 778.1 (2013), p. 66 (cit. on pp. 19, 20).

[46] Dipankar Bhattacharya and Edeard Peter Jacobus van den Heuvel. “Formation and evolution of binary and millisecond radio pulsars”. In: *Physics Reports* 203.1-2 (1991), pp. 1–124 (cit. on p. 19).

[47] DD Ivanenko and DF Kurdgelaidze. “Hypothesis concerning quark stars”. In: *Astrophysics* 1.4 (1965), pp. 251–252 (cit. on p. 20).

[48] F Weber et al. *Strange-matter stars*. Tech. rep. SCAN-9503155, 1994 (cit. on p. 20).

[49] Thomas W Baumgarte et al. “Delayed collapse of hot neutron stars to black holes via hadronic phase transitions”. In: *The Astrophysical Journal* 468 (1996), p. 823. DOI: 10.1086/177738 (cit. on pp. 20, 72, 76, 77).

[50] ESA/Hubble & NASA. *Hubble revisits an old friend*. Oct. 2011. URL: http://www.spacetelescope.org/images/potw1142a/ (visited on 05/20/2017) (cit. on p. 21).

[51] Nino Panagia. “Distance to SN 1987A and the LMC”. In: *Symposium-International Astronomical Union*. Vol. 190. Cambridge Univ Press. 1999, pp. 549–554 (cit. on p. 20).

[52] Philipp Podsiadlowski. “The progenitor of SN 1987A”. In: *Publications of the Astronomical Society of the Pacific* 104.679 (1992), p. 717 (cit. on p. 20).

[53] RM Bionta et al. “Observation of a neutrino burst in coincidence with supernova 1987A in the Large Magellanic Cloud”. In: *Physical Review Letters* 58.14 (1987), p. 1494 (cit. on p. 21).

[54] K Hirata et al. “Observation of a neutrino burst from the supernova SN1987A”. In: *Physical Review Letters* 58.14 (1987), p. 1490 (cit. on p. 21).

[55] GE Brown, SW Bruenn, and JC Wheeler. “Is There a Black-Hole in Supernova 1987A”. In: *Comments on Astrophysics* 16 (1992), p. 153 (cit. on p. 22).

[56] K Sumiyoshi, S Yamada, and H Suzuki. “Dynamics and neutrino signal of black hole formation in nonrotating failed supernovae. I. Equation of state dependence”. In: *The Astrophysical Journal* 667.1 (2007), p. 382. DOI: 10.1086/520876 (cit. on pp. 22, 23, 72, 76).

[57] Thomas M Reynolds, Morgan Fraser, and Gerard Gilmore. “Gone without a bang: an archival HST survey for disappearing massive stars”. In: *Monthly Notices of the Royal Astronomical Society* 453.3 (2015), pp. 2885–2900 (cit. on p. 22).

[58] SM Adams et al. “The search for failed supernovae with the Large Binocular Telescope: confirmation of a disappearing star”. In: *arXiv preprint arXiv:1609.01283* (2016) (cit. on p. 22).

[59] Central Bureau for Astronomical Telegrams. *List of Supernovae*. Feb. 2015. URL: http://cbat.eps.harvard.edu/lists/Supernovae.html (visited on 05/23/2017) (cit. on p. 22).

[60] X-ray: NASA/CXC/MSSL/R.Soria et al, Optical: AURA/Gemini OBs. *NGC 6946*. Nov. 2013. URL: https://www.nasa.gov/mission_pages/chandra/multimedia/fireworks-galaxy-ngc6946.html (visited on 05/23/2017) (cit. on p. 22).

[61] Georg G Raffelt. "Supernova neutrino observations: What can we learn?" In: *Nuclear Physics B-Proceedings Supplements* 221 (2011), pp. 218–229 (cit. on p. 23).

[62] Pavel Kroupa. "On the variation of the initial mass function". In: *Monthly Notices of the Royal Astronomical Society* 322.2 (2001), pp. 231–246 (cit. on p. 23).

[63] Gilles Chabrier. "Galactic Stellar and Substellar Initial Mass Function-The page charges for this Review were partially covered by a generous gift from a PASP supporter." In: *Publications of the Astronomical Society of the Pacific* 115.809 (2003), p. 763 (cit. on p. 23).

[64] Georg G Raffelt. "Physics with supernovae". In: *Nuclear Physics B-Proceedings Supplements* 110 (2002), pp. 254–267 (cit. on p. 23).

[65] Hans-Thomas Janka. *Supernovae und kosmische Gammablitze: Ursachen und Folgen von Sternexplosionen*. Spektrum Akademischer Verlag, 2011 (cit. on p. 24).

[66] NASA/ESA. *A Giant Hubble Mosaic of the Crab Nebula*. Jan. 2005. URL: http://hubblesite.org/image/1823/news_release/2005-37 (visited on 04/26/2017) (cit. on p. 24).

[67] David W Pankenier. "Notes on translations of the East Asian records relating to the supernova of AD 1054". In: *Journal of Astronomical History and Heritage* 9 (2006), pp. 77–82 (cit. on p. 24).

[68] F Mannucci et al. "The supernova rate per unit mass". In: *Astronomy & Astrophysics* 433.3 (2005), pp. 807–814 (cit. on p. 24).

[69] M.G. Aartsen et al. "The IceCube Neutrino Observatory: instrumentation and online systems". In: *Journal of Instrumentation* 12.03 (2017), P03012. DOI: 10.1088/1748-0221/12/03/P03012 (cit. on pp. 25, 26, 28, 31, 46, 81).

[70] The IceCube Collaboration. *Docushare and public webpage* (cit. on p. 28).

[71] MG Aartsen et al. "Observation of high-energy astrophysical neutrinos in three years of IceCube data". In: *Physical review letters* 113.10 (2014), p. 101101 (cit. on p. 28).

[72] Rasha Abbasi et al. "The IceCube data acquisition system: Signal capture, digitization, and timestamping". In: *Nuclear Instruments and Methods in Physics Research Section A: Accelerators, Spectrometers, Detectors and Associated Equipment* 601.3 (2009), pp. 294–316. DOI: 10.1016/j.nima.2009.01.001 (cit. on pp. 29, 30).

[73] Harry Nyquist. "Thermal agitation of electric charge in conductors". In: *Physical review* 32.1 (1928), p. 110 (cit. on p. 33).

[74] Peter V Hobbs. *Ice physics*. Oxford university press, 2010 (cit. on p. 33).

[75] B. Riedel. "Modeling and Understanding Supernova Signals in the IceCube Neutrino Observatory". PhD thesis. University of Wisconsin Madison, 2015. URL: http://icecube.wisc.edu/~briedel/thesis/thesis_final.pdf (cit. on pp. 33, 41, 71, 81, 82, 91).

[76] HO Meyer. "Dark Rate of a Photomultiplier at Cryogenic Temperatures". In: *arXiv preprint arXiv:0805.0771* (2008) (cit. on p. 33).

[77] HO Meyer. “Spontaneous electron emission from a cold surface”. In: *EPL (Europhysics Letters)* 89.5 (2010), p. 58001 (cit. on p. 33).

[78] V. Baum. “Verbesserung der Supernova-Detektion mit dem IceCube-Neutrinoteleskop”. MA thesis. Johannes Gutenberg Universität Mainz, 2011. URL: http://butler.physik.uni-mainz.de/icecube/thesis/dipl_volker.pdf (cit. on p. 35).

[79] V. Baum. “Search for Low Energetic Neutrino Signals from Galactic Supernovae and Collisionally Heated Gamma-Ray Bursts with the IceCube Neutrino Observatory”. PhD thesis. Johannes Gutenberg Universität Mainz, 2017. URL: http://butler.physik.uni-mainz.de/icecube/thesis/phd_baum.pdf (cit. on pp. 35, 37, 39).

[80] Kate Scholberg. “Supernova neutrino detection”. In: *Annual Review of Nuclear and Particle Science* 62 (2012), pp. 81–103 (cit. on p. 35).

[81] Silvia Adrian-Martinez et al. “Letter of intent for KM3NeT 2.0”. In: *Journal of Physics G: Nuclear and Particle Physics* 43.8 (2016), p. 084001 (cit. on pp. 35, 78).

[82] Annarita Margiotta, KM3NeT Collaboration, et al. “The KM3NeT deep-sea neutrino telescope”. In: *Nuclear Instruments and Methods in Physics Research Section A: Accelerators, Spectrometers, Detectors and Associated Equipment* 766 (2014), pp. 83–87 (cit. on p. 35).

[83] Ricard Tomas et al. “Supernova pointing with low-and high-energy neutrino detectors”. In: *Physical Review D* 68.9 (2003), p. 093013 (cit. on p. 36).

[84] Kirk Bays, Super-Kamiokande Collaboration, et al. “Supernova relic neutrinos at Super-Kamiokande”. In: *Journal of Physics: Conference Series*. Vol. 375. 4. IOP Publishing. 2012, p. 042037 (cit. on p. 36).

[85] N Yu Agafonova et al. “On-line recognition of supernova neutrino bursts in the LVD”. In: *Astroparticle Physics* 28.6 (2008), pp. 516–522 (cit. on p. 36).

[86] M Aglietta et al. “Effects of neutrino oscillations on the supernova signal in LVD”. In: *Nuclear Physics B-Proceedings Supplements* 110 (2002), pp. 410–413 (cit. on p. 36).

[87] G Bruno et al. “The core collapse supernova rate from 24 years of data of the Large Volume Detector”. In: *arXiv preprint arXiv:1701.06765* (2017) (cit. on p. 36).

[88] Basudeb Dasgupta and John F Beacom. “Reconstruction of supernova $\nu\ \mu$, $\nu\ \tau$, $\nu^-\ \mu$, and $\nu^-\ \tau$ neutrino spectra at scintillator detectors”. In: *Physical Review D* 83.11 (2011), p. 113006 (cit. on p. 36).

[89] CA Duba et al. “HALO–the helium and lead observatory for supernova neutrinos”. In: *Journal of Physics: Conference Series*. Vol. 136. 4. IOP Publishing. 2008, p. 042077 (cit. on p. 36).

[90] C Rubbia et al. “Underground operation of the ICARUS T600 LAr-TPC: first results”. In: *Journal of Instrumentation* 6.07 (2011), P07011 (cit. on p. 36).

[91] T. Kowarik. “Supernova neutrinos in AMANDA and IceCube - Monte Carlo development and data analysis”. PhD thesis. Johannes Gutenberg Universität Mainz, 2010. URL: http://ubm.opus.hbz-nrw.de/volltexte/2010/2466/pdf/doc.pdf (cit. on pp. 39, 60, 78, 91).

[92] MG Aartsen et al. “The IceCube Neutrino Observatory-Contributions to ICRC 2015 Part V: Neutrino Oscillations and Supernova Searches”. In: *arXiv preprint arXiv:1510.05227* (2015) (cit. on p. 39).

[93] D. Laitsch and the Supernova working group. *Supernova escalation scheme v5*. 2013 (cit. on p. 40).

[94] Pietro Antonioli et al. “Snews: The supernova early warning system”. In: *New Journal of Physics* 6.1 (2004), p. 114 (cit. on p. 53).

[95] Heereman, D. *Multi Purpose HitSpool Analysis Suite*. June 2016. URL: http://icecube.wisc.edu:/~hitspool/main/main.html (visited on 06/10/2016) (cit. on p. 57).

[96] G Pagliaroli et al. “Improved analysis of SN1987A antineutrino events”. In: *Astroparticle Physics* 31.3 (2009), pp. 163–176. DOI: 10.1016/j.astropartphys.2008.12.010 (cit. on pp. 57, 58).

[97] G Pagliaroli et al. “Neutrinos from supernovae as a trigger for gravitational wave search”. In: *Physical review letters* 103.3 (2009), p. 031102. DOI: 10.1103/PhysRevLett.103.031102 (cit. on p. 57).

[98] F Halzen and Georg G Raffelt. “Reconstructing the supernova bounce time with neutrinos in IceCube”. In: *Physical Review D* 80.8 (2009), p. 087301. DOI: 10.1103/PhysRevD.80.087301 (cit. on pp. 59, 60).

[99] T Mühlbeier, H Nunokawa, and R Zukanovich Funchal. “Revisiting the triangulation method for pointing to supernova and failed supernova with neutrinos”. In: *Physical Review D* 88.8 (2013), p. 085010. DOI: 10.1103/PhysRevD.88.085010 (cit. on pp. 59, 78).

[100] J. Jacobsen. *External SNEWS alerts*. 2013 (cit. on p. 69).

[101] John F Beacom and P Vogel. “Can a supernova be located by its neutrinos?” In: *Physical Review D* 60.3 (1999), p. 033007 (cit. on pp. 71, 78).

[102] M. Salathe. “Novel Search Methodology for Supernovae with IceCube”. MA thesis. Ecole Polytechnique Fédérale de Lausanne, 2011. URL: http://lphe.epfl.ch/publications/diplomas/ms.master.pdf (cit. on pp. 71, 79).

[103] E. Lohfink. “PMT noise and supernova direction determination in IceCube”. BA thesis. Johannes Gutenberg Universität Mainz, 2014. URL: http://butler.physik.uni-mainz.de/icecube/thesis/bachelor_elisa.pdf (cit. on p. 72).

[104] John F Beacom, RN Boyd, and A Mezzacappa. “Black hole formation in core-collapse supernovae and time-of-flight measurements of the neutrino masses”. In: *Physical Review D* 63.7 (2001), p. 073011. DOI: 10.1103/PhysRevD.63.073011. arXiv: astro-ph/0010398 (cit. on p. 72).

[105] Dustin Hebecker et al. “A Wavelength-shifting Optical Module (WOM) for in-ice neutrino detectors”. In: *EPJ Web of Conferences*. Vol. 116. EDP Sciences. 2016, p. 01006. DOI: 10.1051/epjconf/201611601006 (cit. on p. 76).

[106] Alexander Kappes. “Multi-PMT Optical Module Designs for IceCube-Gen2”. In: *EPJ Web Conferences*. Vol. 116. EDP Sciences. 2016, p. 01001. DOI: 10.1051/epjconf/201611601001 (cit. on pp. 76, 90).

[107] T Patzak, LAGUNA–LBNO Collab., et al. “LAGUNA and LAGUNA–LBNO: Future megaton neutrino detectors in Europe”. In: *Nuclear Instruments and Methods in Physics Research Section A: Accelerators, Spectrometers, Detectors and Associated Equipment* 695 (2012), pp. 184–187 (cit. on p. 78).

[108] Ronald Bruijn, IceCube Collaboration, et al. “Supernova Detection in IceCube: Status and Future”. In: *Nuclear Physics B-Proceedings Supplements* 237 (2013), pp. 94–97. DOI: 10.1016/j.nuclphysbps.2013.04.065 (cit. on pp. 79, 88, 91).

[109] M Salathe, M Ribordy, and L Demiroers. “Novel technique for supernova detection with IceCube”. In: *Astroparticle Physics* 35.8 (2012), pp. 485–494 (cit. on p. 79).

[110] L. Schulte. “Supernova Detection in a future Extension of the IceCube Neutrino Telescope”. MA thesis. Johannes Gutenberg Universität Mainz, 2011. URL: http://butler.physik.uni-mainz.de/icecube/thesis/dipl_lukas.pdf (cit. on p. 81).

[111] MG Aartsen et al. “The IceCube neutrino observatory part V: neutrino oscillations and supernova searches”. In: *arXiv preprint arXiv:1309.7008* (2013) (cit. on p. 88).

[112] MG Aartsen et al. “Measurement of South Pole ice transparency with the IceCube LED calibration system”. In: *Nuclear Instruments and Methods in Physics Research Section A: Accelerators, Spectrometers, Detectors and Associated Equipment* 711 (2013), pp. 73–89 (cit. on p. 91).

[113] A. Fritz. “Supernova-Signaturen im IceCube-Neutrino- und aLIGO-Gravitationswellendetektor”. MA thesis. Johannes Gutenberg Universität Mainz, 2017. URL: http://butler.physik.uni-mainz.de/icecube/thesis/master_Alexander_Fritz.pdf (cit. on p. 97).

List of Figures

List of Tables

Index